

DEVELOPMENT OF CAST AND HEAT TREATED 7075 ALLOY RIFLE
RECEIVER

A THESIS SUBMITTED TO
THE GRADUATE SCHOOL OF NATURAL AND APPLIED SCIENCES
OF
MIDDLE EAST TECHNICAL UNIVERSITY

BY

AHMET UMUR GÜNGÖR

IN PARTIAL FULFILLMENT OF THE REQUIREMENTS
FOR
THE DEGREE OF MASTER OF SCIENCE
IN
METALLURGICAL AND MATERIALS ENGINEERING

MAY 2015

Approval of the thesis:

**DEVELOPMENT OF CAST AND HEAT TREATED 7075 ALLOY RIFLE
RECEIVER**

submitted by **AHMET UMUR GÜNGÖR** in partial fulfillment of the requirements
for the degree of **Master of Science in Metallurgical and Materials Engineering**
Department, Middle East Technical University by,

Prof. Dr. Gülbin Dural Ünver

Dean, Graduate School of **Natural and Applied Sciences**

Prof. Dr. Hakan Gür

Head of Department, **Metallurgical and Materials Engineering**

Prof. Dr. Ali Kalkanlı

Supervisor, **Metallurgical and Materials Eng. Dept., METU**

Examining Committee Members:

Prof. Dr. Bilgehan Ögel

Metallurgical and Materials Eng. Dept., METU

Prof. Dr. Ali Kalkanlı

Metallurgical and Materials Eng. Dept., METU

Prof. Dr. Rıza Gürbüz

Metallurgical and Materials Eng. Dept., METU

Prof. Dr. A. Tamer Özdemir

Metallurgical and Materials Eng. Dept., Gazi University

Asst. Prof. Dr. Mert Efe

Metallurgical and Materials Eng. Dept., METU

Date: 06.05.2015

I hereby declare that all information in this document has been obtained and presented in accordance with academic rules and ethical conduct. I also declare that, as required by these rules and conduct, I have fully cited and referenced all material and results that are not original to this work.

Name, Last name: AHMET UMUR GÜNGÖR

Signature:

ABSTRACT

DEVELOPMENT OF CAST AND HEAT TREATED 7075 ALLOY RIFLE RECEIVER

Güngör, Ahmet Umur

M.S. Department of Metallurgical and Materials Engineering

Supervisor: Prof. Dr. Ali Kalkanlı

May 2015, 146 pages

Developing technology in the world makes products lighter and have higher strength values. That's why, aluminum and titanium alloys start to be used instead of steel. It can be seen that 7075 aluminum alloy is one of the highest strength amongst the aluminum alloys. This alloy has a close tensile strength value to some steels, with help of the heat treatment applications and developing production technologies. Generally, industrial usage of 7075 alloy is machining of 7075 alloy extrusion slab into desired shape. However, it becomes costly and time wasting as making complicated and hollow products. Therefore, near net shape methods like thixoforming and squeeze casting are vital for these conditions.

This work aimed to replace production method of rifle receiver part which is machined into a hollow structure from extruded T6 heat treated 7075 alloy slab which cause heavy raw material lost with casted and T6 heat treated preform which has close tensile properties and needs very little machining to turn into receiver part. In order to achieve this purpose, squeeze casting, thixoforming, sand casting, gravity die casting, SIMA and high pressure die casting experiments were conducted.

In order to investigate mechanical properties of samples, tensile and hardness tests were performed. X-Ray Diffraction analysis (XRD) and Scanning Electron Microscopy analysis (SEM) were conducted to determine the intermetallics inside of samples after heat treatment. Moreover, average grain size of samples was obtained by optical microscopy technique. Newtonian thermal analysis method was used to compute solid fraction values with respect to temperature and time.

Target mechanical values were determined as mechanical properties of extruded 7075-T6 alloy which are 150 HB hardness, 505 MPa yield strength and 11% elongation. Hardness target was reached after T6 heat treatment with squeeze casting method as 150 HB, die casting with vacuum support method as 160 HB and thixoforming method as 173 HB. Other methods could not reach the target hardness and has hardness values between 100 HB and 130 HB. 505 MPa yield strength target was achieved only by thixoforming method with 0.67 solid fraction as 526 MPa. Other close results were 429 MPa with squeeze casting method and 365 MPa with SIMA method. Elongation target was reached by semi-solid injection molding method as 11.5% but its other mechanical properties were poor. Elongation results of other methods were found to be between 4% and 5%.

Keywords: 7075-T6, aluminum, thixoforming, squeeze casting.

ÖZ

DÖKÜM VE ISIL İŞLEMLİ 7075 ALAŞIMLI TÜFEK GÖVDESİ GELİŞTİRİLMESİ

Güngör, Ahmet Umur

Yüksek Lisans, Metalurji ve Malzeme Mühendisliği Bölümü

Tez Yöneticisi: Prof. Dr. Ali Kalkanlı

Mayıs 2015, 146 sayfa

Dünyada gelişen teknoloji ile beraber, üretilen ürünler artık daha hafif ve dayanıklı olmaya başlamıştır. Bu sebeple alüminyum ve titanyum alaşımları yavaş yavaş çeliğin yerine kullanılmaya başlanmıştır. Alüminyum alaşımları içinde ise dayanım gücüyle 7075 alaşımı dikkat çekmektedir. Bu alaşım kullanılan üretim yöntemleri ve ısıl işlemlerle birlikte bazı çeliklerin dayanım gücüne yaklaşmıştır. Genellikle, 7075 alaşımının endüstriyel kullanımı, 7075 ekstrüzyon kütüğünün talaş kaldırma yöntemi ile istenilen haline getirilmesi şeklindedir. Fakat bu yöntem karmaşık ve içi boş ürünler yaparken zaman kaybına ve yüksek maliyete sebep olur. Bu sebeple, bu gibi durumlar için tikso-şekillendirme ve sıkıştırma döküm gibi son hale yakın biçimdeki üretim yöntemleri önem taşımaktadır.

Bu çalışmanın amacı, ekstrüzyon 7075-T6 kütüğünden çok fazla hammadde kaybı ile işlenen içi boş yapıya sahip tüfek gövde parçasının üretim yönteminin, son ürüne yakın döküm yöntemi ile çok az işleme gerektiren, T6 ısıl işleme sahip bir ön şekil değiştirilmesidir. Bu amaca ulaşmak için, sıkıştırma döküm, kısmi katı şekillendirme, kum döküm, kokil döküm, SIMA ve yüksek basınçlı döküm yöntemleri denenmiştir.

Numunelerin mekanik özelliklerini arařtırmak için çekme testi ve sertlik testi uygulanmıřtır. Isıl iřlem sonrasında, numune yapısındaki metallere arası bileřiklerin belirlenmesi için x iřını kırınım analizi (XRD) ve taramalı elektron mikroskobu analizleri (SEM) yapılmıřtır. Ayrıca, ortalama tane boyutları ise optik mikroskopi yöntemi ile belirlenmiřtir. Newtonian termal analiz yöntemi ise sıcaklıęa ve zamana baęlı katı fraksiyon deęerlerini hesaplamakta kullanılmıřtır.

Hedef mekanik deęerler, ekstrüzyon 7075-T6 alařımının mekanik deęerleri olarak belirlenmiřtir. Bu deęerler, 150 HB sertlik, 505 MPa akma dayancı ve %11 uzamadır. T6 ısıl iřlemi sonrasında sertlik hedefine, 150 HB olarak sıkıřtırma döküm yönteminde, 160 HB olarak vakum destekli kokil döküm yönteminde ve 173 HB olarak tikso-řekillendirme yönteminde ulařılmıřtır. Dięer yöntemler hedef sertlik deęerine ulařamayıp 100 HB ile 130 HB arasında deęerlere sahiptirler. 505 MPa olan akma dayancı hedefine 526MPa olarak sadece 0.67 katı oranına sahip tikso-řekillendirme yönteminde ulařılmıřtır. Dięer yakın sonuçlar ise 429 MPa ile sıkıřtırma döküm yöntemi ve 365 MPa ile SIMA yöntemidir. Yüzde uzama hedefine ise yarı-katı enjeksiyon döküm yönteminde ulařıldı fakat bu numunenin dięer mekanik özellikleri düřüktü. Dięer yöntemlerin yüzde uzama deęerleri ise %4 ile %5 arasında bulunmuřtur.

Anahtar kelimeler: 7075-T6, alüminyum, kısmi katı řekillendirme, sıkıřtırma döküm.

To My Dear Family,

ACKNOWLEDGEMENTS

This thesis would not have been submitted without the help and contribution of several individuals who provided their valuable supports.

Firstly, I would like to express my utmost gratitude to my supervisor dear Prof. Dr. Ali KALKANLI for his guidance, support and tolerance.

I would like to thank to the technical staff of the Department of Metallurgical and Materials Engineering, METU and especially Salih TÜRE, Cemal YANARDAĞ, Önder ŞAHİN and Serkan YILMAZ for their contributions to this study.

This study was supported by SARSILMAZ SİLAH SAN. A.Ş. I would like to thank them for their belief in me and this study especially Mahmut Naci İNCİ, Nuri KIZILTAN and Öner ÖZYILMAZ. Also, many thanks to Furkan KELEŞTİMUR for his friendship and hospitality in Düzce.

I would like to present my sincere thanks to my friends who make this study time tolerable, Onur SAKA, Mehmet DİNCER, Gülten KILIÇ, Seçkin ÇARDAKLI, Tayfun DURMAZ and my other friends from department and also my roommates for their invaluable helps, supports throughout the entire study.

I also would like to thank to my support, life energy and my fiancée Özlem SEVER for her presence, tolerance, love and understanding. Life is much more beautiful and tolerable with you.

Last but not least, I cannot thank enough to my dear parents, Ferhat GÜNGÖR and Nesrin GÜNGÖR whose encouragement, support and presence provide all the success that I have.

TABLE OF CONTENTS

ABSTRACT.....	v
ÖZ.....	vii
ACKNOWLEDGEMENTS	x
TABLE OF CONTENTS	xi
LIST OF FIGURES.....	xiv
LIST OF TABLES	xx
CHAPTERS	
1. INTRODUCTION.....	1
2. LITERATURE REVIEW	3
2.1. 7xxx Series Aluminum Alloy.....	3
2.1.1. 7075 Aluminum Alloy	4
2.1.2. 7085 Aluminum Alloy	5
2.2. Heat Treatment.....	7
2.2.1. Precipitation Heat Treatment	10
2.3. Thermal Analysis	15
2.3.1. Solid Fraction Calculation.....	18
2.4. Production Methods	19
2.4.1. Semi-Solid Metal Casting	19
2.4.2. Squeeze Casting	31
2.4.3. Gravity Die Casting.....	37
2.4.4. Vacuum Assisted Gravity Die Casting	38

2.4.5. Sand Casting.....	38
2.4.6. Grain Refinement in Aluminum Alloys.....	40
3. EXPERIMENTAL PROCEDURE	43
3.1. Squeeze Casting	43
3.2. Vacuum Assisted Gravity Die Casting.....	45
3.3. Gravity Die Casting.....	48
3.4. Sand Casting.....	48
3.5. Vertical Semi Solid Metal Casting.....	50
3.6. Vertical Squeeze Casting	52
3.7. Semi-Solid Metal Casting	53
3.8. Strain Induced Melt Activation (SIMA) Process for Thixocasting.....	55
3.9. Thermal Analysis and Solid Fraction Calculations.....	57
3.10. Characterization	62
3.10.1. Mechanical Testing	62
3.10.2. Metallography	63
3.10.3. Optical Microscopy.....	64
3.10.4. Scanning Electron Microscopy (SEM)	65
3.10.5. X-Ray Diffraction (XRD)	66
3.10.6. Optical Emission Spectrometer Analysis.....	66
4. RESULTS AND DISCUSSION	67
4.1. Squeeze Casting Experiment.....	67
4.2. Gravity Die Casting Experiment.....	70
4.3. Vacuum Assisted Gravity Die Casting Experiment.....	71
4.4. Sand Casting Experiment with/without Al ₅ TiB Additive.....	73

4.5. X-Ray Diffraction (XRD) Results of Casting Experiments.....	78
4.6. Thermal Analysis and Solid Fraction Calculations.....	82
4.6.1. Extrusion Billet of 7075 Aluminum Alloy at 0.25°C/s Cooling Rate.....	83
4.6.2. Modified 7075-1 Aluminum Alloy at 0.04°C/s Cooling Rate.....	85
4.6.3. Modified 7075-1 Aluminum Alloy 0.25°C/s Cooling Rate ...	87
4.6.4. Modified 7075-2 Aluminum Alloy 0.38°C/s Cooling Rate ...	89
4.7. Semi-Solid Casting with Vertical Pressure Die Casting	92
4.8. Pressure Die Casting	96
4.9. Semi-Solid Metal Casting	97
4.10. Strain Induced Melt Activation (SIMA)	100
5. CONCLUSIONS	105
6. SUGGESTED FUTURE WORKS.....	107
REFERENCES.....	109
APPENDICES	
A. TENSILE TEST ANALYSIS	115
B. GRAIN SIZE ANALYSIS	131
C. MATHLAB ALGORITHM	141

LIST OF FIGURES

FIGURES:

Figure 1. Al- Mg-Zn Ternary Phase Diagram (Liquidus projection is on the left and solidus projection is on the right.).....	4
Figure 2. Time-temperature-property curves at 95% of maximum tensile stress for various alloys.....	13
Figure 3. Effects of temperature on the natural aging.....	14
Figure 4. Yield-strength curves for alloy 7075.	14
Figure 5. Zero curve (baseline) differences between Newtonian method and Fourier method of an A356 Al alloy (Al-7%Si).	18
Figure 6. Comparison of Newtonian and Fourier methods on solid fraction for A356 alloy with cooling rate of 0.55 °C/s.....	19
Figure 7. Cooling curves comparison of thixocasting, rheocasting and conventional casting processes. Microstructure comparison of thixocasting, rheocasting and conventional casting processes.....	21
Figure 8. Schematic illustration of the thixo and rheo casting methods.	23
Figure 9. Schematic of SIMA (a) and RAP (b) processes.	25
Figure 10. Schematic illustration of the NRC rheocasting process (UBE).....	27
Figure 11. Schematic illustration of the cooling slope casting process.	28
Figure 12. Schematic illustration of the advanced semisolid casting technology rheocasting process developed by Honda.	29
Figure 13. Schematic illustration of the semisolid rheocasting (SSR) process.....	30
Figure 14. Schematic illustration of direct squeeze die casting.	33
Figure 15. Schematic illustration of indirect squeeze casting.....	34
Figure 16. Vertical squeeze casting machine used in experiments.	44

Figure 17. Squeeze cast 7075 alloy discs. First, second and third from left to right.	44
Figure 18. Squeeze cast 7085 alloy discs.	45
Figure 19. Muffle furnace used for heat treatment in experiments.	45
Figure 20. Vacuum assisted gravity die casting experiment setup. 1. Sprue, 2. Horizontal copper die mold, 3. Vacuum hose-die mold connecter part, 4. Vacuum hose.....	47
Figure 21. Polished and heat treated vacuum assisted gravity die cast sample.	47
Figure 22. Sample that was used for testing in gravity die casting experiment.	48
Figure 23. 7075 aluminum alloy casting after shake out of sand.....	49
Figure 24. Die mold and working principle of vertical squeeze casting press that is used during semi solid experiments in the Foundry laboratory at METU.	50
Figure 25. A prepared sample of extruded 7075 alloy.....	51
Figure 26. Produced disks after T6 heat treatment.....	51
Figure 27. Burst drawing of the mold that produces hollow shaped parts.....	52
Figure 28. Produced hollow shaped parts after T6 heat treatment.	53
Figure 29. The high pressure die casting (HPDC) machine used in semi-solid metal casting.....	54
Figure 30. The die that can produce tensile and bending test specimens.....	54
Figure 31. Cylindrical shaped alloy billets produced (left: ultrasonic stirring, right: mechanical stirring).....	56
Figure 32. Cooling curve of 7075 alloy with 0.04°C/s cooling rate with respect to time.....	58
Figure 33. First derivative of 7075 alloy cooling curve with 0.04°C/s cooling rate with respect to time.	59
Figure 34. Polynomial fits in several degrees for zero curve drawing.....	59
Figure 35. The area between the first derivative and the zero curve is represented as colored.....	60
Figure 36. After integration of the area between the first derivative and the zero curve, solid fraction with respect to temperature graph can be obtained.	60

Figure 37. Data acquisition setup of the thermal analysis and solid fraction calculations experiment and the graphite crucible that was used in experiments (1. Thermocouple, 2. Graphite Crucible, 3. Thermal Blanket, 4. Molten alloy).	61
Figure 38. Mares tensile test machine setup.	62
Figure 39. Instron 5582 Tensile test machine.	63
Figure 40. Metacut-M 250 Cut-Off Machine.....	64
Figure 41. SOIF XJP - 6A Optical Microscope.	65
Figure 42. Foundry Master UV Vacuum CCD optical emission spectrometer.	66
Figure 43. Microstructure of squeeze casting experiment specimen having 37 micron average grain size (100x).	69
Figure 44. SEM image of squeeze casting experiment specimen (100x).	69
Figure 45. Microstructure of gravity die casting experiment specimen with 41 micron average grain size (100x).	70
Figure 46. SEM image of gravity die casting experiment specimen (100x).....	71
Figure 47. Microstructure of vacuum assisted gravity die casting experiment specimen having 38 micron average grain size (100x).	72
Figure 48. SEM image of vacuum assisted gravity die casting experiment specimen (100x).	72
Figure 49. Microstructure of sand cast specimen having 98 micron average grain size (100x).	74
Figure 50. SEM image of sand cast specimen (100x).....	74
Figure 51. Microstructure of sand cast alloy with Al5TiB addition, specimen having 74 micron average grain size (100x).	76
Figure 52. Microstructure of sand cast with Al5TiB addition, specimen SEM analysis (100x).	76
Figure 53. XRD results of casting for Al with indicated planes.	79
Figure 54. XRD results of casting for $Al_{0.403}Zn_{0.597}$ with indicated planes.	79
Figure 55. XRD results of casting for $MgZn_2$ with indicated planes.	80
Figure 56. XRD results of casting for Al_2CuMg with indicated planes.....	80
Figure 57. XRD results of casting for $Mg_{32}(Al, Zn)_{49}$ with indicated planes.	81
Figure 58. XRD results of casting for Fe_3Si with indicated planes.....	81

Figure 59. XRD results of casting for FeV with indicated planes.	82
Figure 60. Temperature vs. time graph of Extrusion billet of 7075 aluminum alloy at 0.25°C/s cooling rate.	83
Figure 61. First derivative $\left(\frac{dT}{dt}\right)_{cc}$ vs. time graph of Extrusion billet of 7075 aluminum alloy at 0.25°C/s cooling rate.	84
Figure 62. Solid fraction vs. temperature and time graph of Extrusion billet of 7075 aluminum alloy at 0.25°C/s cooling rate.	84
Figure 63. Temperature vs. time graph of modified 7075-1 aluminum alloy with 0.04°C/s cooling rate.	85
Figure 64. First derivative $\left(\frac{dT}{dt}\right)_{cc}$ vs. time graph of modified 7075-1 aluminum alloy with 0.04°C/s cooling rate	86
Figure 65. Solid fraction (%) vs. temperature graph of modified 7075-1 aluminum alloy with 0.04°C/s cooling rate.	86
Figure 66. Temperature vs. time graph of modified 7075-1 aluminum alloy with 0.25°C/s cooling rate.	87
Figure 67. First derivative $\left(\frac{dT}{dt}\right)_{cc}$ vs. time graph of modified 7075-1 aluminum alloy with 0.25°C/s cooling rate.	88
Figure 68. Solid fraction (%) vs. temperature graph of modified 7075-1 aluminum alloy with 0.25°C/s cooling rate	88
Figure 69. Temperature vs. time graph of modified 7075-2 aluminum alloy with 0.38°C/s cooling rate.	89
Figure 70. First derivative $\left(\frac{dT}{dt}\right)_{cc}$ vs. time graph of modified 7075-2 aluminum alloy with 0.38°C/s cooling rate.	90
Figure 71. Solid fraction vs. temperature graph of modified 7075-2 aluminum alloy with 0.38°C/s cooling rate.	90
Figure 72. SEM picture of semi-solid casting specimen 1 at 580°C.....	94
Figure 73. SEM picture of semi-solid casting specimen 2 at 595°C.....	94
Figure 74. SEM picture of semi-solid casting specimen 3 at 605°C with 100x magnification.....	95

Figure 75. SEM picture of semi-solid casting specimen 3 at 605°C with 500x magnification.....	95
Figure 76. Pore density vs. solid fraction graph of modified 7075-2 alloy produced by semi solid metal casting.	99
Figure 77. UTS vs. solid fraction graph of modified 7075-2 alloy produced by semi solid metal casting.	99
Figure 78. Microstructure image of ultrasonic stirred specimen (100x).....	101
Figure 79. Microstructure image of mechanical stirred specimen (100x).	102
Figure 80. SEM image of mechanical stirred specimen (100x).	102
Figure 81. SEM image of mechanical stirred specimen (100x).	103
Figure 82. SEM image of mechanical stirred specimen (750x).	103
Figure 83. Designed suggested vertical die.....	107
Figure A.1. Tensile test results of squeeze casting experiment.	115
Figure A.2. Tensile test results of mechanical stirred SIMA sample.....	116
Figure A.3. Tensile test results of ultrasonic stirred SIMA sample.	116
Figure A.4. Tensile test results of semi-solid forming with vertical pressure die casting samples (Specimen 2: 1 st test sample, specimen 3: 2 nd test sample, specimen 4: 3 rd test sample and specimen 1 is a failed sample.).....	117
Figure A.5. Tensile test result of sand casting specimen.	118
Figure A.6. Tensile test result of sand casting with Al5TiB additive specimen. ...	119
Figure A.7. Tensile test result of vacuum assisted gravity die casting experiment specimen.....	120
Figure A.8. Tensile test results of gravity die casting experiment specimen.....	121
Figure A.9. Tensile test results of semi-solid injection molding experiment 1 st of extr. 7075 specimen.....	122
Figure A.10. Tensile test results of semi-solid injection molding experiment 2 nd of extr. 7075 specimen.....	123
Figure A.11. Tensile test results of semi-solid injection molding experiment 6 th of mod. 7075 specimen.....	124
Figure A.12. Tensile test results of semi-solid injection molding experiment 1st of mod. 7075 specimen.....	125

Figure A.13. Tensile test results of semi-solid injection molding experiment 2nd of mod. 7075 specimen.....	126
Figure A.14. Tensile test results of semi-solid injection molding experiment 3rd of mod. 7075 specimen.....	127
Figure A.15. Tensile test results of semi-solid injection molding experiment 4th of mod. 7075 specimen.....	128
Figure A.16. Tensile test results of semi-solid injection molding experiment 5th of mod. 7075 specimen.....	129
Figure B.1. Grain size analysis of squeeze casting sample.....	131
Figure B.2. Grain size analysis of vacuum assisted die casting sample.....	132
Figure B.3. Grain size analysis of gravity die casting sample.	134
Figure B.4. Grain size analysis of sand casting sample.	135
Figure B.5. Grain size analysis of sand casting with Al5TiB additive sample.....	136
Figure B.6. Grain size analysis of mechanical stirred SIMA sample.	138
Figure B.7. Grain size analysis of ultrasonic stirred SIMA sample.....	139

LIST OF TABLES

TABLES

Table 1. Chemical Composition of 7075 aluminum alloy.	5
Table 2. Mechanical properties of 7075 aluminum alloy with respect to various heat treatments.	5
Table 3. Chemical composition of 7085 aluminum alloy.	6
Table 4. Mechanical properties of 7085 aluminum alloy with respect to various heat treatments.	6
Table 5. Soaking Time for Solution Heat Treatment of All Wrought Products.	15
Table 6. Feasibility table of thixocasting, rheocasting and conventional casting processes. (4. Excellent, 3. Good, 2. Somewhat Poor, 1. Poor).....	22
Table 7. The chemical compositions of extruded and modified 7075 alloys produced.	55
Table 8. Experimental parameters of ultrasonic and mechanical stirring.	57
Table 9. Hardness values of 2nd squeeze cast sample.	68
Table 10. Hardness values of gravity die cast samples.	71
Table 11. Hardness values of vacuum assisted gravity die casting experiment.....	73
Table 12. Hardness values of sand casting without Al ₅ TiB additive experiment....	75
Table 13. Hardness values of sand casting with Al ₅ TiB addition.....	77
Table 14. Hardness and average grain size comparison of all casting experiments performed in this study.....	77
Table 15. Literature comparison of chemical compositions of the alloys used at thermal analysis experiments.	91
Table 16. Literature comparison of thermal data obtained during thermal analysis experiments.	92
Table 17. The process data of semi-solid casting with vertical squeeze casting.	93

Table 18. Comparison between values of reduction rates, hardness values and second phase densities.....	93
Table 19. Comparison of chemical compositions of alloys produced during pressure die casting experiments.	96
Table 20. Hardness values of pressure die cast samples.....	97
Table 21. Ultimate tensile strength, elongation at break, pouring temperature and solid fraction values.	98
Table 22. Tensile test results of SIMA experiment.....	101

CHAPTER 1

INTRODUCTION

Aluminum cannot be found in nature as a metal due to its high chemical affinity for oxygen. That's why, it can be found in oxide forms with various purity degrees. Aluminum is the second most abundant metallic element in crust of earth with 8% weight. Furthermore, aluminum has various mechanical and chemical properties. Such as; low density (2.7 g/cm^3) with respect to other popular metals (Steel: 7.83 g/cm^3 and copper: 8.93 g/cm^3), high age-hardening potential, corrosion resistance, weldability and fabrication [1, 2, 3].

Aluminum usage at industrial applications is increasing day by day. Aluminum gets attention because of its low density values and adequate mechanical properties for many industrial applications. 7075 is one of the aluminum alloys that have relatively higher mechanical properties than other aluminum alloys. Extruded 7075-T6 gives higher mechanical properties for 7075 aluminum alloy than other alternative production methods like casting or forging. In production of some complicated parts, extruded 7075-T6 is machined into final shape. If the complicated parts have a hollow shape or need too much machining, this production costs higher prices. Furthermore, it is lost of time and lost of raw materials. That's why, several production methods are tried over years in order to get same mechanical properties with extruded 7075-T6 aluminum alloy. However, since 7075 aluminum alloy is designed for wrought processes, desired mechanical properties cannot be achieved with other production methods [1, 2, 3].

Receiver part of some rifles is made from extruded 7075-T6 aluminum alloy for its durability and lightweight. During its manufacture process, machining and other methods are used. After manufacturing process is completed, it can be seen that nearly 75% of raw material is lost due to the receiver's hollow shape.

Receiver part is the main part of the rifle. It is the part that holds trigger mechanism, stock and barrel. Most rifle receivers have a hollow shape for inserting trigger mechanism. It contains an ejection port which is practically a window for ejecting empty shells on the right side of it. Also, there are rifle types that have an ejection port on the left side for left handed people [4].

Considering the information given, this study is aimed to minimize the loss of raw material during machining. To achieve this goal, mechanical properties of 7075 aluminum alloy with several production methods are investigated. Some of these methods are; thixoforming, pressure die casting, sand casting and permanent mold casting.

CHAPTER 2

LITERATURE REVIEW

2.1. 7xxx Series Aluminum Alloy

7xxx series aluminum alloys are known as having zinc as their main alloying element. Magnesium and copper can also be found in these alloys as other main alloying elements. This alloying group provides high strength to this light-weight alloy. 7xxx series are also heat-treatable by solution treatment and aging. Aging process can be done for various cycles. For example, T6 is done for achieving the maximum strength and T73 is for high stress corrosion resistance. For both instances, alloy must go through solution treatment which dissolves intermetallics or segregated phases into solid solution completely [1].

7xxx series aluminum alloys have dissimilar liquidus and solidus temperatures considering their chemical composition differences. That's why, ternary and binary phase diagrams are used to acquire liquidus and solidus temperatures for required alloy. Al – Mg - Zn ternary phase diagram can be taken as advantage of determining liquidus and solidus temperatures. Liquidus projection of Al-Mg-Zn ternary phase diagram and solidus projection of Al-Mg-Zn ternary phase diagram is shown on Figure 1 [1].

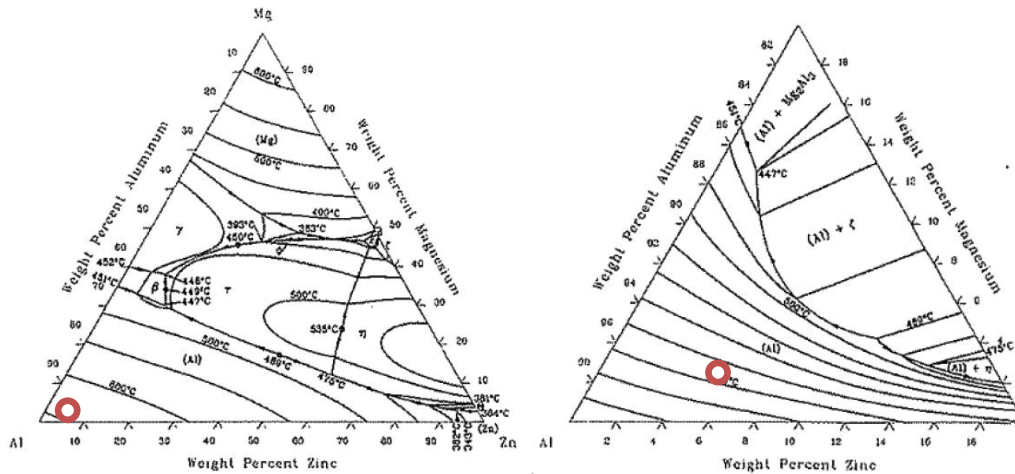


Figure 1. Al- Mg-Zn Ternary Phase Diagram (Liquidus projection is on the left and solidus projection is on the right.) [1].

2.1.1. 7075 Aluminum Alloy

This alloy is a member of 7xxx series aluminum alloy family. It was developed by Sumitomo in 1936 for using in Japanese Fighter Planes. As ISO designation, it can be called as Al Zn5.5MgCu and A97075 for UNS designation. It has 5.1% – 6.1% zinc, 2.1% - 2.9% magnesium, 1.2% - 2.0% copper as main alloying elements.

Chemical composition of 7075 aluminum alloy is given on Table 1. It has relatively higher UTS values with respect to other aluminum alloys. 7075 aluminum alloy may have 570MPa UTS values and 505MPa yield strength after T6 heat treatment [5] Different heat treatments provide various mechanical and chemical properties to 7075 aluminum alloy. Mechanical properties of 7075 aluminum alloy with respect to various heat treatments are given in Table 2 [5].

Table 1. Chemical Composition of 7075 aluminum alloy [5].

Si	Fe	Cu	Mn	Mg	Cr	Zn	Ti	Unspecified other elements		Al minimum
								each	total	
0.40 max	0.50 max	1.2-2.0	0.30 max	2.1-2.9	0.18-0.28	5.1-6.1	0.20 max	0.05 max	0.15 max	Bal.

Table 2. Mechanical properties of 7075 aluminum alloy with respect to various heat treatments [5].

Temper	UTS (MPa)	YS (MPa)	EL (%)	HB
7075-O	230	105	17	60
7075-T6, T651	570	505	11	150
7075-T73, T7351	503	434	13	-

Liquidus temperature and solidus temperature can be determined for 7075 aluminum alloy as 635°C and 477°C, respectively by using Al-Mg-Zn ternary phase diagram (Figure 1). This is also verified by literature [5].

2.1.2. 7085 Aluminum Alloy

This alloy is also a member of 7xxx series aluminum alloy family. 7085 Aluminum Alloy was developed by Alcoa in 2002. This alloy is developed for the aerospace industry and other markets due to the demand of an aluminum alloy with improved thick section properties. It has 7.0% – 8.0% zinc, 1.2% - 1.8% magnesium, 1.3% -

2.0% copper as main alloying elements. Chemical composition of 7085 aluminum alloy is given in Table 3. It has similar mechanical properties with 7075 aluminum alloy except for little differences. However, it has improved fatigue and fracture toughness properties. This alloy is designated and commercialized as plate, sheet and extrusion with various heat treatments. Mechanical properties of 7085 aluminum alloy with respect to various heat treatments are given in Table 4 [6, 7].

Table 3. Chemical composition of 7085 aluminum alloy [6].

Si	Fe	Cu	Mn	Mg	Cr	Zn	Zr	Ti	Unspecified other elements		Al minimum
									each	total	
0.06 max	0.08 max	1.3-2.0	0.04 max	1.2-1.8	0.04 max	7.0-8.0	0.08-0.15	0.06 max	0.05 max	0.15 max	Bal.

Table 4. Mechanical properties of 7085 aluminum alloy with respect to various heat treatments [7].

Temper	Product	Thickness(mm)	UTS(MPa)	YS(MPa)	EL(%)
7085-T711	Plate	12.5-40.0	550	510	10
7085-T721		12.5-40.0	470	415	10
7085-T7451		75-100	505	470	10

Liquidus temperature and solidus temperature is given for 7085 aluminum alloy as 635°C and 552°C, respectively [7]. It is also proved with the help of Al-Mg-Zn ternary phase diagram (Figure 1).

2.2. Heat Treatment

Heat treating is an operation to a metal product with heating and cooling the material so that, its mechanical properties, residual stress state and metallurgical structure can be modified and improved. Heat treatment operations are various and these operations are very broad in the sense of material treatment. However, aluminum heat treatment operations are often limited to hardening and increasing strength for precipitate hardenable wrought and cast alloys. These types of aluminum alloys are called as heat-treatable alloys. Other type of aluminum alloys are called as non-heat treatable alloys due to their inability to advance in mechanical properties with heating and cooling. Non-heat treatable aluminum alloys make little difference when subjected to “heat treatment”. These alloys can enhance their mechanical properties with other methods like cold working [1, 8].

Temper designation is a system that is used for heat-treatable aluminum alloys. It is used for wrought and cast products. This system is used for determine the sequence of the treatment which can be mechanical treatment, thermal treatment or both at the same time. This temper designation system allows us to have information about the heat treatment parameters such as time, temperature and quenching rate that is applied on alloy. Some basic temper designations are as follows [2, 8];

- F, as-fabricated: It defines the alloy have not been heat treated.
- O, annealed: It defines the wrought product is annealed to obtain lowest strength or the cast product is annealed to increase ductility.
- W, solution heat treated: It defines the alloy is unstable and naturally ages after solution treatment.
- H, strain hardened: It defines the wrought product has been strain hardened with or without additional thermal treatment.
- T, heat treated to produce stable tempers other than O: It defines the alloy that has been thermally treated to obtain stability with or without strain hardening [2, 8].

Strain hardened products system:

- H1, strain-hardened only: This defines that the product has been strain hardened without thermal treatment to obtain desired strength. The following digit indicates rate of strain hardening.
- H2, strain-hardened and partially annealed: This defines that the product has been strain hardened more than enough then annealed for decreasing strength to a desired value. The following digit indicates the remaining strain hardening.
- H3, strain-hardened and stabilized: This defines that the product has been strain hardened then mechanical properties of alloy has been stabilized with low temperature thermal treatment. This designation is applied to alloys that soften with time at room temperature. The following digit indicates remaining strain hardening [8].

T temper designation is used for heat treated alloys to produce stable tempers other than W, F and O. T temper designation is followed by a digit that describes the sequence of treatments. The T temper designations are:

- T1, cooled from an elevated-temperature shaping process and naturally aged to substantially stable condition: This defines that the product is not cold worked after high temperature shaping process like casting and extrusion.
- T2, cooled from an elevated-temperature shaping process, cold worked, and naturally aged to a substantially stable condition: This designation defines that product is cold worked than naturally aged at room temperature.
- T3, solution heat treated, cold worked, and naturally aged to a substantially stable condition: This defines the product is solution heat treated then cold worked and naturally aged at room temperature.
- T4, solution heat treated and naturally aged to a substantially stable condition: This defines that the product is applied solution heat treatment then naturally aged at room temperature.

- T5, cooled from an elevated-temperature shaping process and artificially aged: This defines that the product is not cold worked after an elevated temperature shaping process that mechanical properties are improved by precipitation heat treatment.
- T6, solution heat treated and artificially aged: This defines that the product is applied solution heat treatment quenched and artificially aged.
- T7, solution heat treated and over-aged or stabilized: This defines the wrought product has been over aged to obtain properties like resistance to stress corrosion crack.
- T8, solution heat treated, cold worked, and artificially aged: This defines that the product is solution heat treated then cold worked to obtain improved strength. After that, this product is artificially aged.
- T9, solution heat treated, artificially aged, and cold worked: This explains that product is cold worked after precipitation heat treatment.
- T10, cooled from an elevated-temperature shaping process, cold worked, and artificially aged: This pertains that the product is cold worked after a process like casting and extrusion. Then, product is artificially aged [1, 2, 8].

These temper designations are basic temper designations. On the other hand, some other designations are made to fulfill the need for specific heat treatments for other than just strengthening like stress relieving. These temper designations are briefly;

- Tx51, stretched for stress relieving.
- Tx52, compressed for stress relieving.
- Tx54, stretched and compressed for stress relieving.
- T62, solution heat treated and artificially aged from the O or the F temper [1, 5, 8].

2.2.1. Precipitation Heat Treatment

Alloying is a need for strengthening aluminum, since it has very low mechanical properties. Most of the aluminum alloys are created due to developing an alloy with desired mechanical properties. While doing this, most of the inventors considered alloys with particles which impede dislocation motion dispersed in ductile aluminum matrix. If the dispersion is finer, the alloy is stronger [1, 2, 8].

This kind of dispersion can be obtained by selecting an alloy which is single phase at high temperatures but, cooling it will precipitate another phase in the matrix. If hardening is occurred in this precipitation, it is called precipitation hardening or age hardening [2, 8].

The major precipitate hardening aluminum alloys are:

- Al-Cu systems are strengthening from CuAl_2 .
- Al-Cu-Mg systems (precipitation is intensified by magnesium).
- Al-Mg-Si systems are strengthening from Mg_2Si .
- Al-Zn-Mg systems are strengthening from MgZn_2 .
- Al-Zn-Mg-Cu systems [8].

Precipitation strengthening of a super-saturated solid solution needs formation of finely dispersed precipitates by natural aging or artificial aging. The aging must take place below a metastable miscibility gap called the Guinier-Preston (GP) zones. The super saturation of vacancies let zone formation faster than equilibrium diffusion coefficients due to diffusion [8].

Firstly, solute atoms form clusters near vacancies. Coherent precipitates forms after adequate atoms diffused into these vacancies. Solute clusters are surrounded by a strain field due to the mismatch of the solute atoms clusters to the aluminum matrix. Semi-coherent precipitates are formed after an amount of solute atoms diffusion to

the clusters that the matrix can no longer hold. Finally, equilibrium precipitates are formed after semi-coherent precipitates get larger to enough size and the matrix can no longer accommodate the crystallographic mismatch. This is the explanation of precipitation in the most common heat treatable aluminum alloys [2].

2.2.1.1. Al-Zn-Mg-Cu Alloys

As precipitation sequences, there are four sequences in 7xxx series aluminum alloys. The sequences can be seen below [2]:

1. α_{SSS} to S
2. α_{SSS} to T' to T
3. α_{SSS} to VRC to GPZ to η' to η
4. α_{SSS} to η

First precipitation sequence indicates the formation of S phase which is Al_2CuMg . This phase is precipitated from supersaturated solid solution directly. This phase is a coarse inter-metallic which is insoluble in 7xxx alloys at 465°C [2].

Second sequence shows the T phase formation. T' phase is an intermediate phase that occurs in the decomposition of the supersaturated solid solution. Latter, T' phase transforms into the equilibrium T phase which can be called as $\text{Mg}_{32}(\text{Al}, \text{Zn})_{49}$. Also, T phase is incoherent with the aluminum matrix and generally, T phase only precipitates above 200°C [2].

Third sequence consists of vacancy rich cluster formation, Guinier-Preston Zones formation, η' formation and then η formation with respectively. η' phase is formed prior to η formation which is MgZn_2 . Furthermore, GP zones are in sphere form and MgZn_2 is in plate form for this series [9].

Final sequence indicates formation of η directly from supersaturated solid solution [1, 2, 8].

GP zones precipitation and semi-coherent η' phase makes 7XXX alloys stronger. Furthermore, η' precipitates can be formed from existing GP zones which is a unique precipitation behavior of Al-Zn-Mg alloys. Also, deformation does not affect precipitation behavior of this alloy when applied before aging. GP zones can be seen at higher temperatures. Due to copper existence in GP zones, 7XXX alloys have improved stability when compared to Al-Zn-Mg alloys. However, copper do not affect the basic precipitation mechanism on these alloys [10].

This precipitation hardening provides 7xxx series aluminum alloys increase in hardness and improved mechanical properties. Table 2 shows the effects of heat treatment on mechanical properties of 7075 aluminum alloy.

Solution heat treatment is a must for precipitation hardening for 7xxx series aluminum alloys. To obtain a good solution treatment, alloy must be heated over 465°C for dissociation of Al_2CuMg phase and other phases into solid solution. Also, usage of 480°C for solution heat treatment is recommended by ASTM [11]. Alloy should be soaked into this temperature for an enough time for complete formation of super saturated solid solution. On Table 5, solution treatment times for various thicknesses are given. After achieving super saturated solid solution, alloy must be quenched with adequate cooling rate. This quenching procedure is the vital part of having meta-stable super saturated solid solution at room temperature. Otherwise, heat treatment does not provide expected mechanical properties to the alloy. Since precipitates will be formed and super saturated solid solution cannot be obtained. Quenching rate is mentioned as 300°C/s which is a relatively higher than most of other aluminum alloys [8]. Quenched 7xxx series aluminum alloys like 7075 starts aging at room temperature spontaneously. That's why, precipitation heat treatment should be applied to 7xxx series aluminum alloys in less than an hour on room temperature and less than 3 hours for low temperatures after quenching [1, 2, 8]. A

comparison can be made between various alloys for their 95% of maximum tensile stresses in Figure 2. Figure 3 demonstrates the effect of temperature on natural aging of 7075 aluminum alloy after quenching. After this quenching step, artificial aging treatment is applied to quenched 7xxx series aluminum alloy. Different aging times and temperature provide various tempers and mechanical properties. T6 and T73 temper times and temperatures are given in Figure 4 for 7075 aluminum alloy. Also, this figure gives us ability to determine the time and temperature range for desired yield strength. As illustrated in Figure 4, T6 temper, which gives the highest yield strength, can be obtained on 7075 by heating it up to 120°C temperature for 24 hours [8].

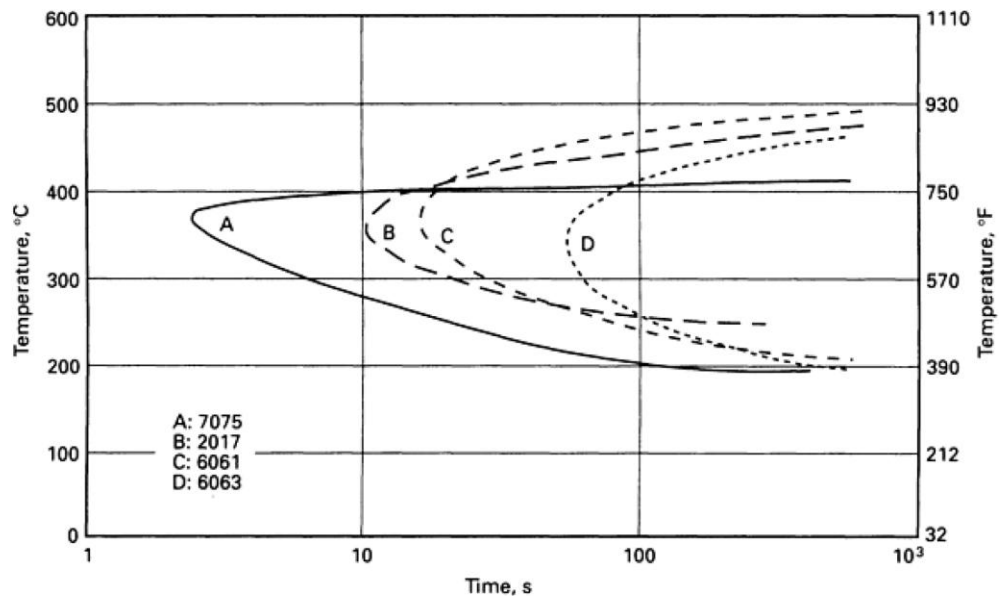


Figure 2. Time-temperature-property curves at 95% of maximum tensile stress for various alloys [8].

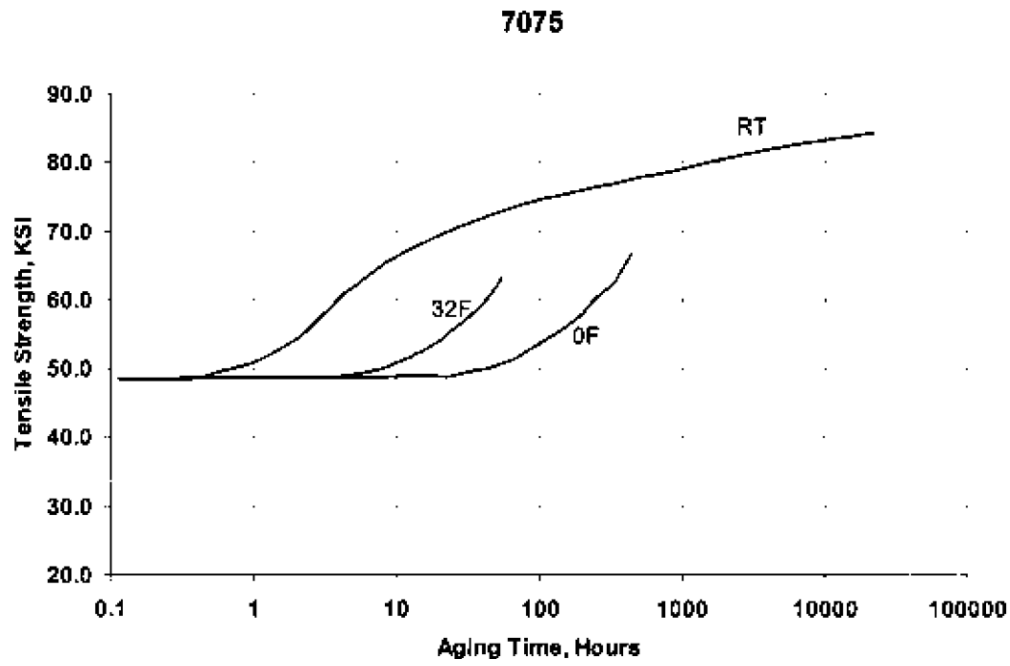


Figure 3. Effects of temperature on the natural aging [8].

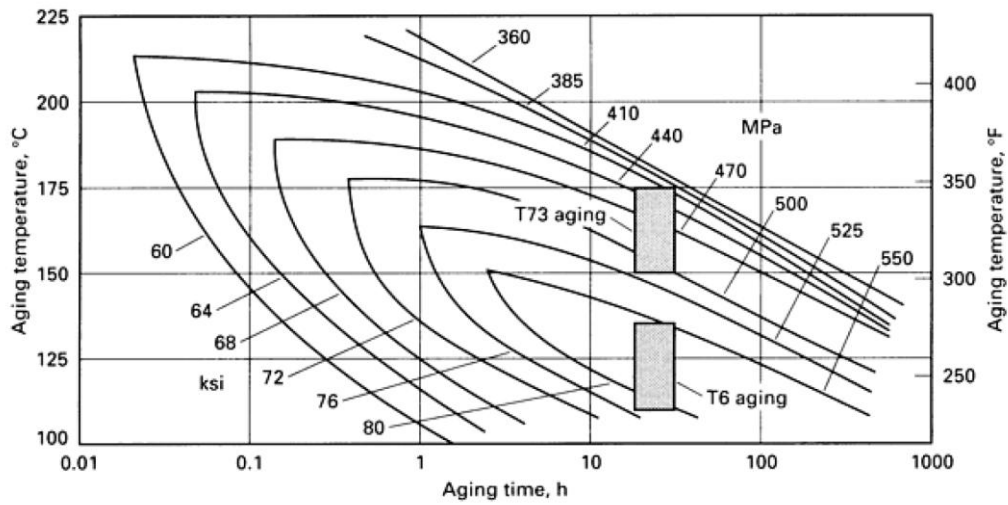


Figure 4. Yield-strength curves for alloy 7075 [8].

Table 5. Soaking Time for Solution Heat Treatment of All Wrought Products [2].

Thickness (inches)	Soaking Time (minutes)			
	Salt Bath		Air Furnace	
	Minimum	Maximum (alclad only)	Minimum	Maximum (alclad only)
0.016 and below	10	15	20	25
0.017–0.020	10	20	20	30
0.021–0.032	15	25	25	35
0.033–0.063	20	30	30	40
0.064–0.090	25	35	35	45
0.091–0.124	30	40	40	50
0.125–0.250	35	45	50	60
0.251–0.500	45	55	60	70
0.501–1.000	60	70	90	100
1.001–1.500	90	100	120	130
1.501–2.000	105	115	150	160
2.001–2.500	120	130	180	190
2.501–3.000	150	160	210	220
3.001–3.500	165	175	240	250
3.501–4.000	180	190	270	280

2.3. Thermal Analysis

Thermal analysis has broad usage in steel and foundry industries. It is used to control the quality of products that is made in those industries. Cooling curves are used in constructing early phase diagrams. On the other hand, relatively new methods, like differential thermal analysis and thermodynamic calculations, removed the undercooling effect in many phase diagrams. For example, liquidus temperatures were 20°C lower by thermal analysis than by differential scanning calorimetry (DSC) [12].

DSC identifies melting points and latent heat more accurate than cooling curve analysis for metals and alloys. DSC basically determines the heat amount that is absorbed or evolved by heating, cooling or keeping at a temperature from a material. However, DSC can only analyze very small samples which are mostly

recommended up to 10mg. That's why, it is not suitable to use in foundry shops [12, 13].

A suitable candidate is cooling curve analysis (CCA) which is simple and feasible for commercial applications. This method is a consistent method which was used in past for generating phase diagrams. Although, CCA can be done in several ways, computer aided cooling curve analysis (CA CCA) has widespread usage for metallurgical purposes. This technique enables us to obtain total latent heat and fraction solid for multi-component alloys from the cooling curve [12].

In this method, determination of zero curve (or baseline) is vital. Zero curve is the first derivative of the cooling curve with assumption of no phase transformation during solidification within the temperature range. As simple, it is the extension of the single phase region's first derivative [12].

There are two common methods for cooling curve analysis. First one is Newtonian method which creates zero curve with assumption of there is no thermal gradient and need a single thermocouple. Second one is Fourier method that creates zero curve as function of temperature and need two thermocouples [14].

Zero curve can be obtained by a curve fitting tool with a relevant software in Newtonian method. For this purpose, phase transformation zones must be excluded from the first derivative of cooling curve for drawing a polynomial line from one single-phase region to other single-phase region which starts at solidus and ends at liquidus points.

Newtonian method requires a thermocouple placed at the geometrical center of the cooling material. This method assumes there is no thermal gradient. Also, if Biot number (Bi) is less than 0.1 for a metal-mold system, this assumption is valid. D. Adrian describes the Biot number as "the Biot number is a dimensionless group that compares the relative transport resistances, external and internal."

$$Bi = \frac{ht}{k}$$

Where h is heat transfer coefficient, t is thickness and k is thermal conductivity.

“It arises when formulating and non-dimensionalizing the boundary conditions for the typical conservation of species/energy equation for heat/mass transfer problems” [15]. If the Biot number is smaller than 0.1, it means that heat conduction is faster in cooling metal than the metal-mold interface. As a consequence, temperature gradients may be neglected [14].

Fourier method requires two thermocouples that one of them on the geometrical center of the sample and the other one is near the metal-mold interface. Zero curve is generated by analyzing the data from two thermocouples and including them in Fourier equations that calculates the zero curve. Zero curve is a function of temperature in Fourier method [14].

Different zero curves can be obtained from Fourier and Newtonian methods. However, Fourier method is expected to provide more reliable result since, it uses actual temperature field. Figure 5 shows the difference between the zero curve of Newtonian method and zero curve of Fourier method for A356 Al alloy [12].

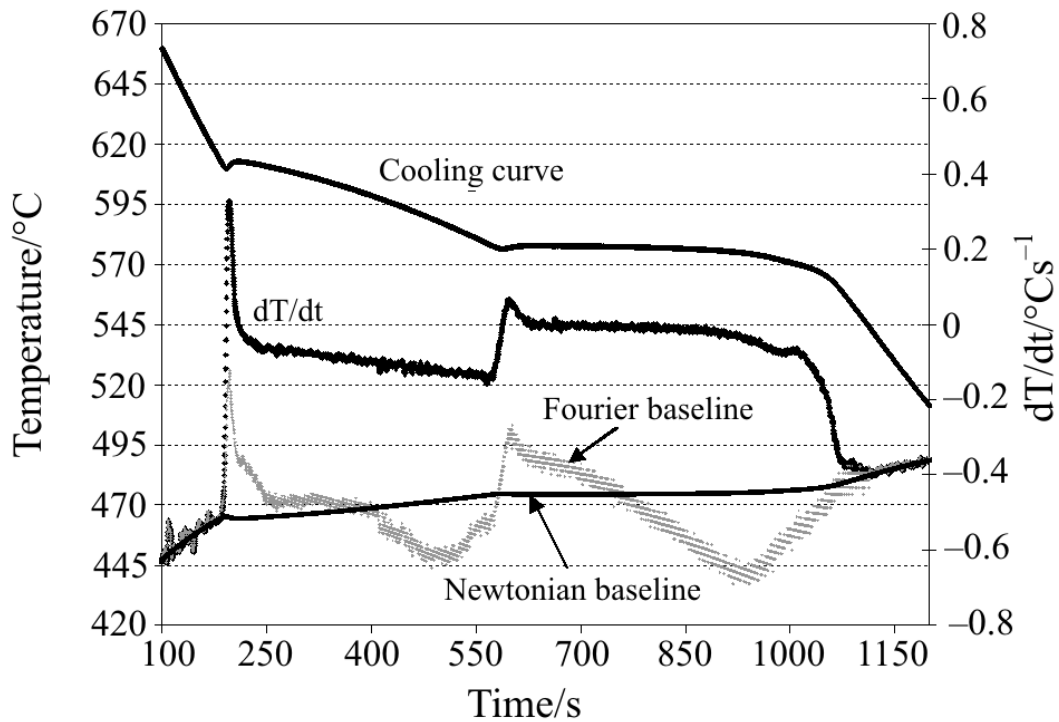


Figure 5. Zero curve (baseline) differences between Newtonian method and Fourier method of an A356 Al alloy (Al-7%Si) [16].

2.3.1. Solid Fraction Calculation

Solid fraction is an essential information for processes that operates at semi-solid temperatures like thixoforming. Solid fraction can be calculated from integration of the area which is between first derivative of cooling curve and zero curve (baseline). Newtonian method can be used to calculate the solid fraction easily, due to unnecessary of thermal properties during calculation. Comparison of Newtonian and Fourier methods on solid fraction values can be seen in Figure 6 which shows that there are some differences especially between the Al-Si eutectic temperature and liquidus temperature. Other parts of the figure have little difference which can be neglected [12].

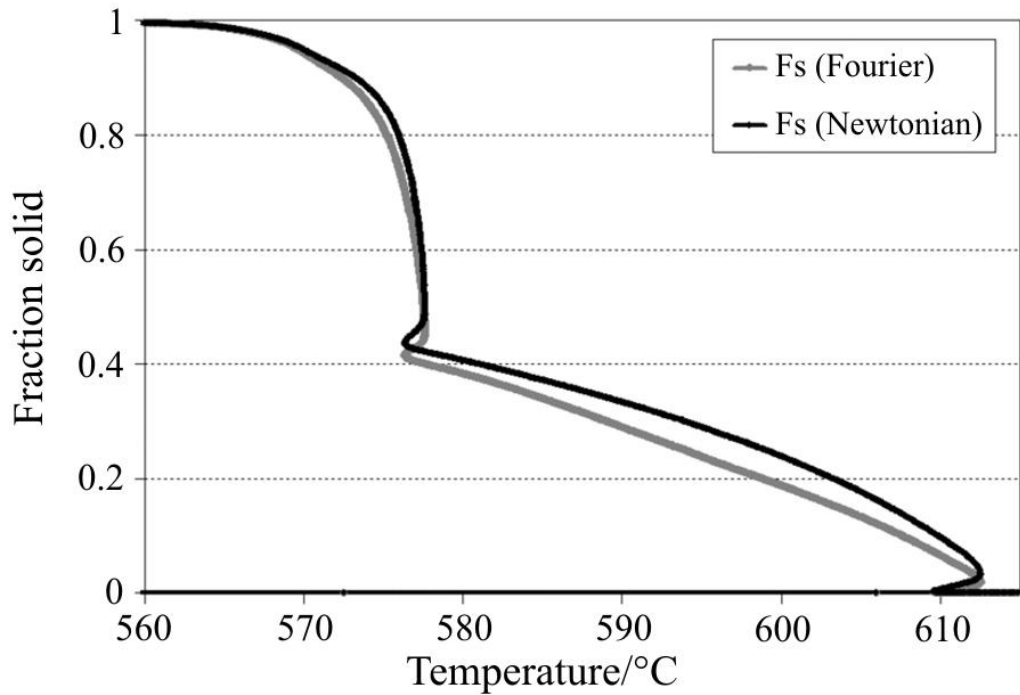


Figure 6. Comparison of Newtonian and Fourier methods on solid fraction for A356 alloy with cooling rate of 0.55 °C/s [16].

2.4. Production Methods

2.4.1. Semi-Solid Metal Casting

Massachusetts Institute of Technology is the one that first discover the semi-solid processing in 1971 [17]. After this important discovery, rheocasting and thixocasting process routes are introduced [18]. Nowadays, these processes and other processes related with semi-solid processing are known as Semi-solid metal (SSM) casting. There are three basic requirements for SSM casting which are:

- A grain structure with nondendritic or spherical,
- Solid-liquid region,
- Suitable solid fraction.

The SSM processing developed around obtaining a globular structure as alloy in semi-solid form. There are three main process routes which are:

- Thixocasting: This process consists of three stages. First one is to preparation of a solid feedstock with globular structure. Latter one is the heating the solid feedstock and then shaping [17]. This process can be seen schematically in Figure 7 and Figure 8.
- Rheocasting: Liquid metal is cooled under controlled conditions to obtain globular structure and shaping take place immediately in this process [17]. Figure 7 and Figure 8 illustrate rheoforming method schematically.
- Thixomolding: Magnesium alloy flakes are sheared and heated before injection to a mold with a plastic injection molding machine in this process [17].

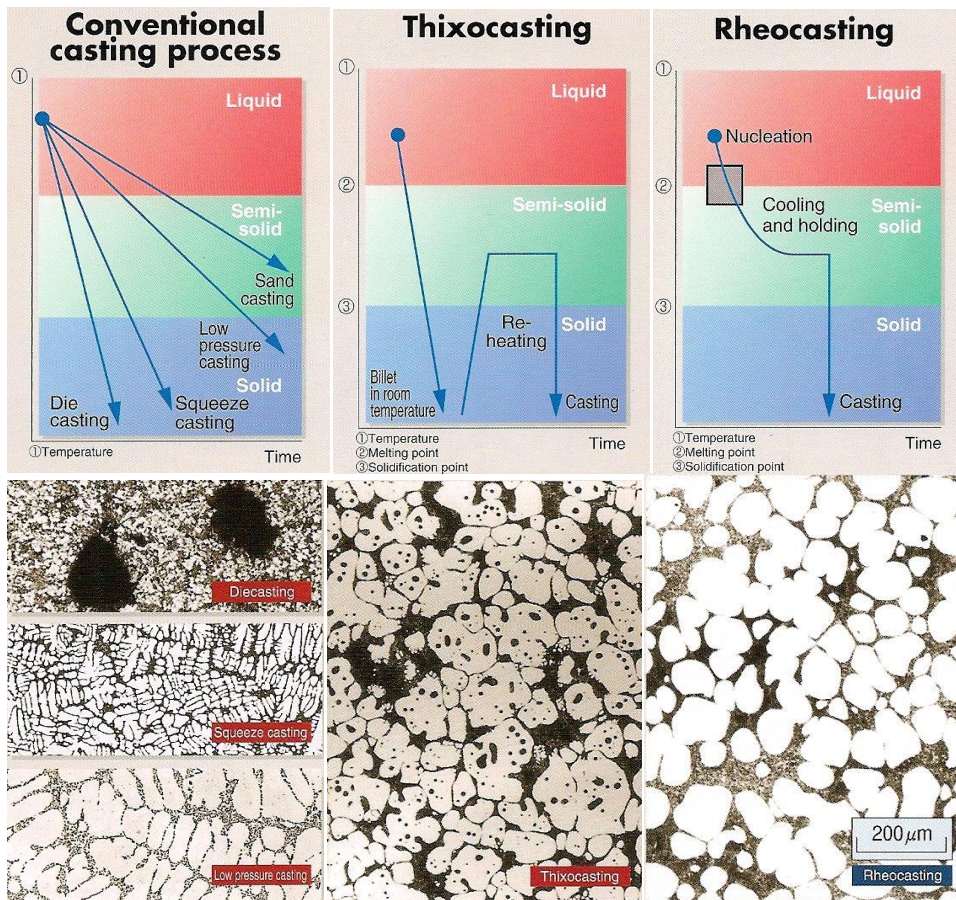


Figure 7. Cooling curves comparison of thixocasting, rheocasting and conventional casting processes. Microstructure comparison of thixocasting, rheocasting and conventional casting processes [19].

Table 6. Feasibility table of thixocasting, rheocasting and conventional casting processes [19]. (4. Excellent, 3. Good, 2. Somewhat Poor, 1. Poor)

Properties	Rheocasting	Thixocasting	Squeeze Casting	High Pressure Die Casting	Low Pressure Die Casting
Shrinkage porosity	4	4	3	2	3-2
Blow Hole	3	3	3	1	3
Segregation	3	3	2	3	3
Microstructure	Globular	Globular	Dendritic	Petal Shape	Dendritic
Mechanical Properties	3-4	3-4	3	1	2-3
Wrought Alloy Application	4	3	2	1	2
Hot Tear	4	4	2	1	3
Metal Fluidity	3	2-3	4	4	3
Casting Cycle Time	3	3	2	3	1
Die Life	4	4	2	3	3
Product Cost	3	1	2	4	4

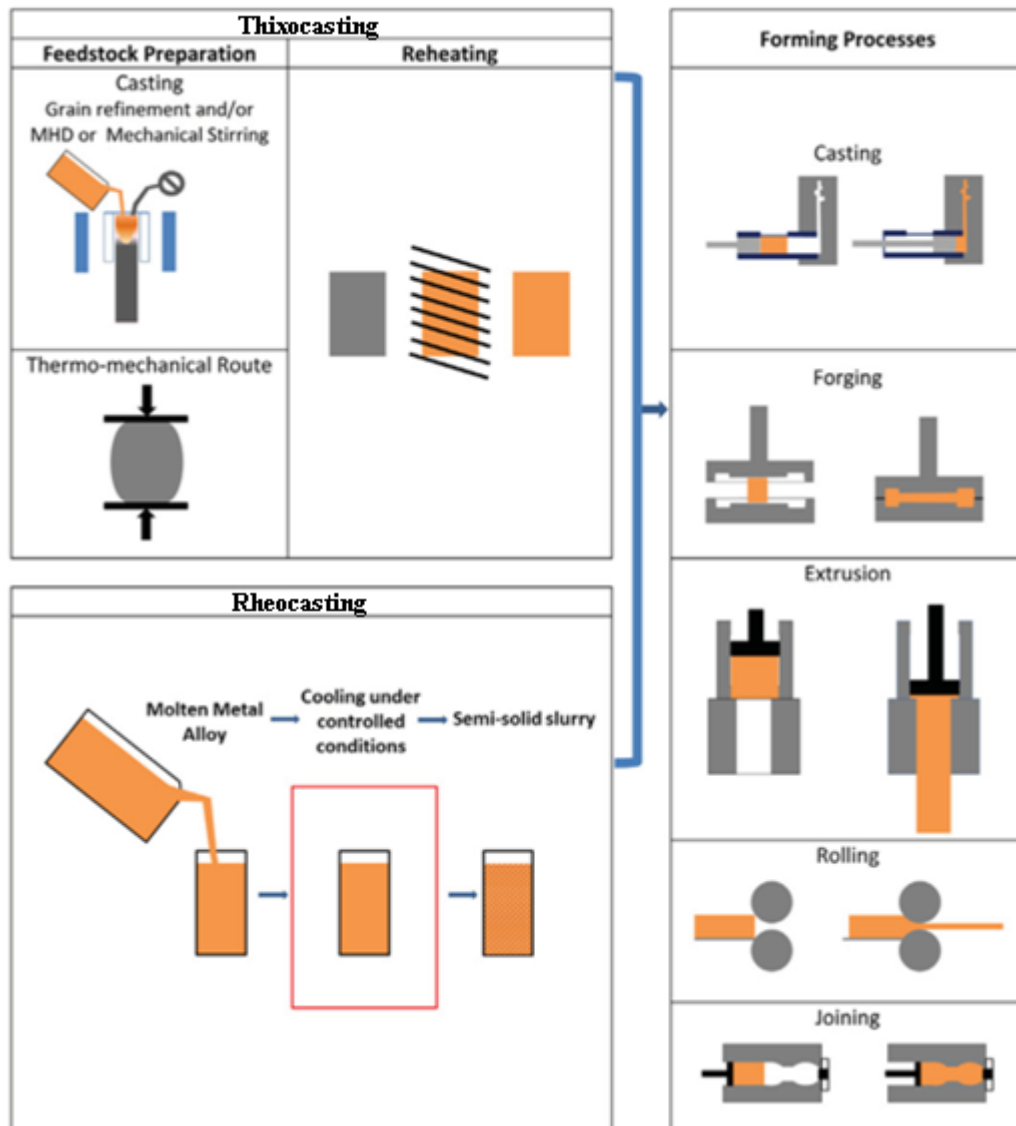


Figure 8. Schematic illustration of the thixo and rheo casting methods [20].

2.4.1.1. Thixocasting

There are three stages of thixocasting. These stages are preparation of feedstock, heating the feedstock and shaping. All of these stages have different method variations. Moreover, these stages should be done properly in order to get desired results. The benefits of the thixocasting route are that having control over the

feedstock quality, chemical composition, and gas content which provide high quality control [20].

2.4.1.1.1. Feedstock Preparation

There are many techniques to be used for feedstock preparation. However, four of them are getting attention due to their stability and feasibility. These four methods are; mechanical stirring, magnetohydrodynamic stirring, thermomechanical processing and grain refinement [20].

Mechanical stirring basically consist of stirring of molten metal as it is cooling down. Early methods were based on batch production, but later on continuous process is discovered. However, continuous process could not be commercialized due to problems like contamination and oxidation [20].

Magnetohydrodynamic stirring continuous casting process is almost same as conventional direct chill continuous casting processes. However, in this method molten metal is stirred by a rotating electromagnetic field as liquid metal solidifies. That's why dendrite formation is avoided by effecting nucleation and solidification processes. Vertical, circumferential or both stirring methods are used to produce vertical or horizontal feedstocks [20].

Thermomechanical processing is a solid state method which relies on initiating recrystallization by strain inducing. There are two main methods for this process; strain induced melt activation (SIMA) and recrystallization and partial remelting (RAP). The SIMA consists of extrusion of material above the recrystallization temperature before cold working [21]. In the RAP process, material is extruded below the recrystallization temperature to obtain the critical strain [22]. Schematic of SIMA process and RAP process are given in Figure 9.

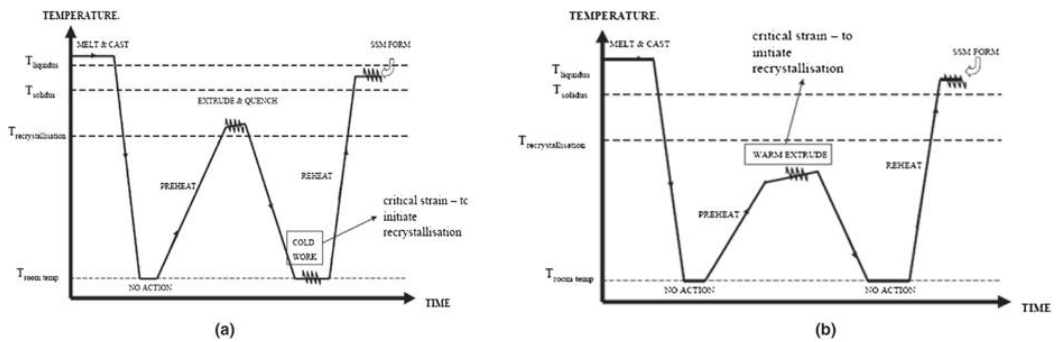


Figure 9. Schematic of SIMA (a) and RAP (b) processes [20].

Grain refinement method controls nucleation process thus, globular microstructure can be obtained. Chemical grain refiners or other techniques like cooling slope can be used for this method. These techniques limit dendritic formation by creating large amount of nuclei.

Other methods for feedstock preparation are:

- Passive stirring,
- Spray casting (Osprey process),
- Liquidus casting,
- Ultrasonic treatment,
- Powder compaction,
- Single slug production [20].

2.4.1.1.2. Feedstock Reheating

Feedstock reheating is an important step for thixoforming because, this step have direct effect on the properties of final product. However, there are many parameters to be achieved. These parameters are; heating the feedstock to the desired temperature quickly, to obtain homogenous temperature distribution, minimal grain

growth and repeatability of the process. That's why, radiation/convection heating and induction heating is evolved for this purpose [23].

Radiation/convection heating was used in industrial heating of billets for semisolid forming in the mass production of automotive components. The advantages of this technology were the low capital costs and easy process control. However, this technology was not used commonly due to the limiting parameters as slow heating cycle [23].

Induction heating is a more preferred technique than radiation/convection heating. The reason of this, induction heating provides higher heating rates in process. Unfortunately, some problems like overheating of skin and corners of the billet can be observed [23, 24]. Luckily, most of these problems can be overcome by different coil designs and heating strategies. Proper process controls can make induction heating providing high heating rates with a high degree of control over billet temperatures and properties [23, 25].

2.4.1.2. Rheocasting

Rheocasting become prominent in mid-1990s due to the high cost of the thixocasting route. Since mid-1990s many developments are achieved in this process. Main focus was on the producing globular structure SSM slurries from liquid metal directly. It was seen that achieving this purpose was through the control of nucleation and grain growth process. Adequate nucleation was needed as controlling the grain growth in order to avoid dendritic formation for obtaining globular structure [26]. Developed processes can be sum up under three categories:

- Nucleation,
- Nucleation and active contact stirring/shearing,
- Nucleation and active noncontact stirring.

2.4.1.2.1. Nucleation Based

There are many processes which are developed based on nucleation mechanism. However, two popular ones are New Rheocasting (NRC) and Cooling Slope process (CSP) [20].

New Rheocasting (NRC):

This process is composed of pouring the superheated liquid metal into a holder, which causes formation of copious amount of nuclei. Then, these nuclei grow into globular microstructure by slow cooling. After this step, a temperature adjustment is made by induction heating and shaping take place. A schematic illustration of the new rheocasting process can be seen in Figure 10 [20].

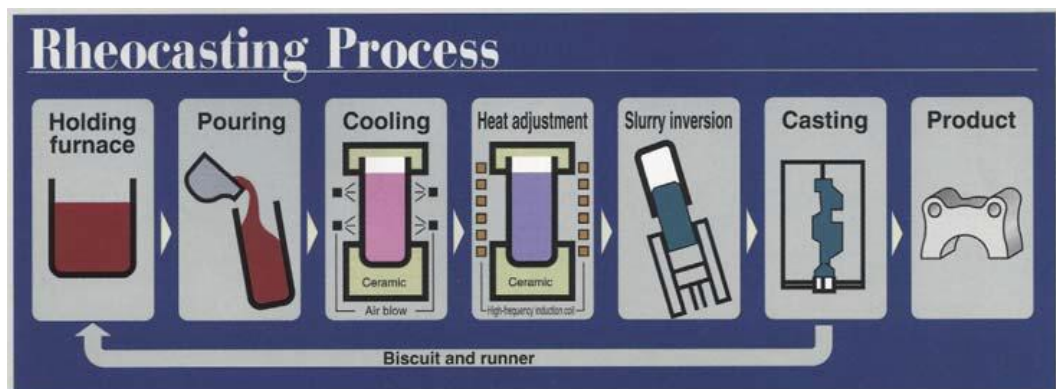


Figure 10. Schematic illustration of the NRC rheocasting process (UBE) [20].

Cooling Slope Casting (CSP):

CSP process can be explained by following steps. Firstly, slightly superheated slurry is poured onto a cooling slope with inclination. This cooling slope helps large amount of nuclei formation. Afterwards, cooling slope cause liquid metal to cool down to the semi-solid range. Then, this semi-solid metal flow into an insulated container where slow cooling occurs to desired SSM temperature [27, 28]. Prepared slurry can be used in either forming processes or solidify to use for thixoprocessing. Figure 11 illustrates cooling slope process [20].

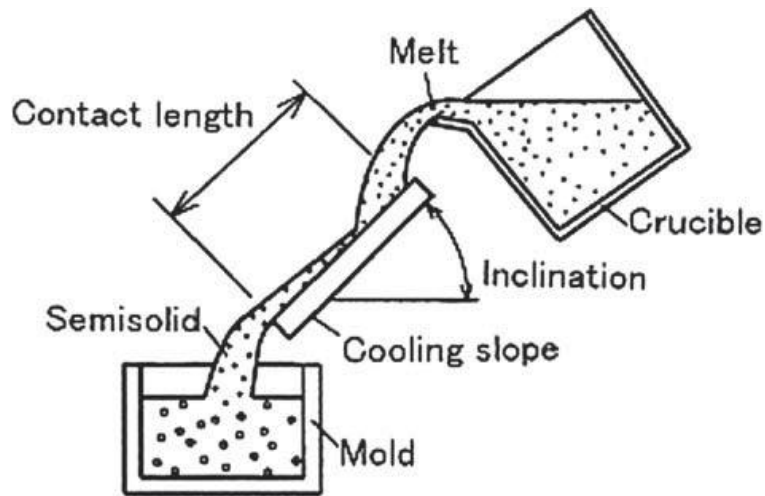


Figure 11. Schematic illustration of the cooling slope casting process [20].

Other nucleation based casting processes can be sorted as:

- Direct Thermal,
- Subliquidus Casting (SLC),
- Continuous Rheoconversion Process (CRP),
- Self-Inoculation Method (SIM),
- In-Ladle Direct Thermal Control,
- Rheocontainer Process (RCP),
- Cup-Cast Method (CCM),
- Serpentine Pouring Channel (SCP),
- Inverted Cone-Shaped Channel Process,
- Controlled Nucleation Process
- The Damper Cooling Tube Method [20].

2.4.1.2.2. Nucleation and active contact stirring/shearing

Advanced Semisolid Casting Technology, Honda:

This process contains stages as mechanical stirring of molten aluminum alloy and the transferring of the semi-solid slurry to a conventional high pressure die casting (HPDC) machine for component production [29, 30]. Figure 12 is the schematic illustration of the advanced semisolid casting technology rheocasting process developed by Honda [20].

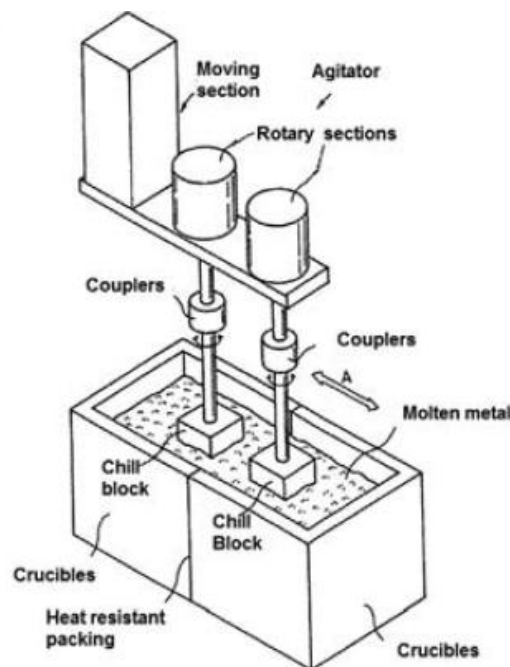


Figure 12. Schematic illustration of the advanced semisolid casting technology rheocasting process developed by Honda [20].

Semisolid Rheocasting (SSR) Process:

SSR process, also known as mechanical stirring melt conditioning, was first developed at the MIT. This process takes place as a cold rotating rod is put into a molten metal which is slightly over liquidus temperature. The cold rotating rod stays in the molten metal until molten metal cool down below the liquidus temperature. Furthermore, this allows nucleation and applies the necessary shear

forces to produce the SSM microstructure [31, 32]. After removal of the rod, the slurry is allowed to cool to the desired temperature. As the slurry reaches to the desired temperature, it is transferred into a HPDC machine and injected into the die. Figure 13 demonstrates how the SSR process happens with a schematic illustration and temperature time graph of steps [20].

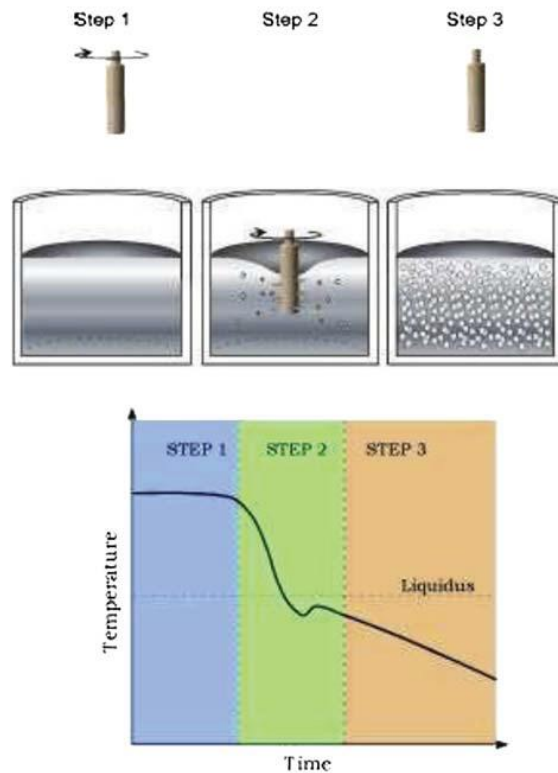


Figure 13. Schematic illustration of the semisolid rheocasting (SSR) process [20].

Other nucleation and active contact stirring/shearing based processes are given below:

- Low Superheat Pouring with a Shear Field (LSPSF) Process,
- The Swirled Enthalpy Equilibration Device,
- Rheomolding:
 - Rheodiecasting Process,

- Taper barrel,
- Rotating Barrel Rheomolding Machine Process,
- Forced convection rheomolding process.
- Rheometal Process,
- Gas-Induced Semisolid Metal Process,
- Melt Spreading and Mixing Technique (MSMT) [20].

2.4.1.2.3. Nucleation and active noncontact stirring casting

The Hitachi Process:

The process covers pouring a molten metal into a vertical injection shot sleeve then, stirring electromagnetically and cooling it as it is in the shot sleeve. After desired conditions are obtained semi-solid metal is injected to the die [33].

Other processes are given below shortly:

- Advanced Rheocasting Process a.k.a Hong-Nano Casting Method,
- In-Mold Rheocasting Process,
- Novel Hot Chamber Rheodiecasting Process,
- Multielectromagnetic Stirring Continuous Preparation Process,
- The Council for Scientific and Industrial Research Rheocasting System [20].

2.4.2. Squeeze Casting

Squeeze casting (SC) was first patented by Hollinggrak in 1819 [34]. Then, Chernov improved the idea by applying steam pressure to the molten metal in 1878 [35]. However, commercialization took place after 1960 for the production of aluminum automotive parts. Also, other alloys, steel and cast iron have been used [36]. Furthermore, the most distinguished application for SC was achieved by Toyota with production of alloy wheels in 1979. Recently, squeeze casting technique is used for metal matrix composites and magnesium alloy production [37].

SC is a combined process of permanent mold casting and die forging. In this method, specific amount of molten metal is poured into a die mold, which is preheated and lubricated, and applied pressure until solidification is completed. Fine microstructure can be obtained by increased cooling rate due to applied pressure before, during and after solidification. This applied pressure generates metal-die walls contact and increased heat flow [20].

High pressure during process also causes macro and micro shrinkage porosity prevention or elimination. Moreover, porosities, which are formed due to dissolved gases, are limited by applied pressure [20].

SC products are resulted with fine grained, weldable, heat treatable and denser. These properties tend to excellent mechanical properties and surface quality. SC can produce more complex part with reduced labor and material cost than forging [20]. However, mechanical properties of SC are lower than forging because, plastic deformation does not create hardening unlike forging. Also, applied pressure is between 50MPa and 300MPa which is lower than forging [38, 39].

Relatively low ram velocity, which is about 0.5 m/s, enables low turbulence during transferring liquid metal into the mold. Because of this low turbulence, air entrapment and porosity formation possibilities are avoided. Furthermore, growing dendrites are broke down and shrinkages are covered by ram pressure during solidification [40].

SC dies have thick gates in order to avoid premature solidification. Also, thick gates help to maintain low flow speed. Accuracy of dimension for SC is: 0.25mm in 100mm to 0.6mm in 500mm [41].

SC applications cover aluminum casting for automotive parts, brass and bronze for bushing and gears, steel for missile parts and pinion gears and ductile iron for mortar shells [39, 42].

2.4.2.1. Squeeze Casting Methods and Parameters

There are two SC methods which are direct squeeze casting and indirect squeeze casting. The differences and principles of these SC methods are given in the following paragraphs [20].

Direct squeeze casting method which is called as liquid metal forging as well has similarity with forging process. In this method, specific amount of molten metal is poured into the lower half die mold, which is preheated and lubricated, and upper half die mold closes on the lower half die mold [43, 44]. Closed upper half die mold drives molten metal into the cavity with applying pressure during solidification which forms casting shape [20].

There is no need for runners, gating systems and risers for this system which is a great advantage. That's why, almost no scrap metal is produced and output is very high [36, 41, 43]. On the other hand, scrap rate can be high, if the specific volume of the molten metal is surpassed. Furthermore, direct SC can produce porosity free casting but, oxides and inclusions can be seen due to the lack of runners [41, 43]. To sum up, direct SC have many advantages and disadvantages however, it is mainly used for production of relatively simple geometries [20].

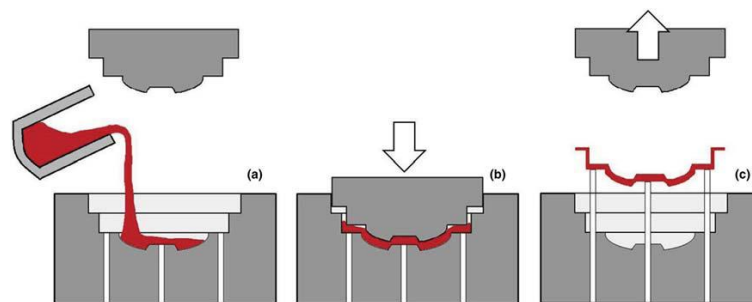


Figure 14. Schematic illustration of direct squeeze die casting [20].

Indirect squeeze casting method is generally a vertical indirect squeeze casting process. This method is a mixture of high pressure die-casting (HPDC) and low-pressure die-casting (LPDC) methods. Molten metal is poured in the shot sleeve which is slightly tilted. Then, shot sleeve moves to a vertical position to push the molten metal in the die cavity [45]. Die cavity is above the shot sleeve which makes this process a counter-gravity process. Shot sleeve keep applying pressure until solidification is completed. Applied pressure is kept constant before, during and after solidification. As comparison is made with a direct SC machine, in direct SC machine is a more complex and expensive machine [20].

The flow speed is kept low to evade turbulence which keeps the flow front flat and help ventilation of air entrapped. In some cases, metallic mesh filters can be used in gate for inclusion reduction in the product [41].

The cost of the product is higher than direct SC due to the scrap rate. On the other hand, specific volume of molten metal is not used in indirect SC unlike direct SC. To conclude, indirect SC method has higher commercial use than direct SC, although it is more complex and expensive [20].

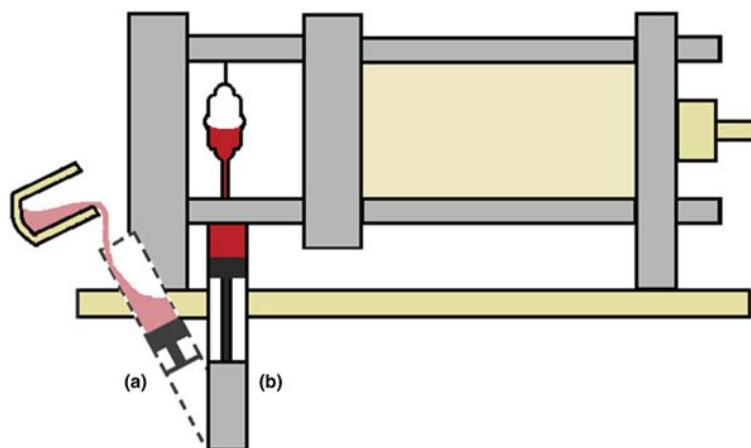


Figure 15. Schematic illustration of indirect squeeze casting [20].

Numerous process parameters are effective on both direct squeeze casting and indirect squeeze casting. These parameters can be ordered as follows: [36, 37, 39].

- First parameter is the quality of alloy and alloys itself. Melting temperature and thermal conductivity of alloy is very important in terms of die life and selection of die temperature. Hence, Al and Mg alloys which have low melting temperature should be preferred in squeeze casting operations. Furthermore, metal cleanliness affect inclusion rate in the product.
- Since amount of the molten metal is vital in direct SC, systems that prevent excess amount of molten metal transfer into the mold should be used. Overflows and compensating hydraulic pistons can be used
- Die temperature and punch temperatures should be observed, in order to have control over heat transfer rate and solidification. Range between 200°C and 300°C is recommended for Al and Mg alloys. Higher temperatures can cause surface defects and metallization while low temperatures can cause premature solidification and cold laps. Also, graphite based lubricants can be applied to the mold.
- The time between pouring the molten metal in the die and start of applied pressure onto the molten metal is called as time delay. Time delay is an important parameter for reducing shrinkage porosities. However, there are many opinions on this subject. Mostly, 6s is used as time delay but it is up to 1 min for large components [46]. As some researches [47, 48] claim that optimum time is the midway between solidus and liquidus, some researchers [37, 49] claim that alloy should be mainly liquid as pressure starts to be applied.
- Die coating and lubrication agents vary with respect to die material and casting alloy. For instance, water based colloidal graphite can be used for non-ferrous castings. Furthermore, coatings can be used for SC die molds. However, thickness of coatings and lubricants should not exceed 50 mm in order to prevent coating stripping and damaging the casting.

- Other two important parameters are duration and magnitude of applied pressure. Because, solidification temperature thus, microstructure of product is greatly related with pressure. An explanation can be made by using Clausius–Clapeyron equation.

$$\frac{\Delta T}{\Delta P} = \frac{T_m \cdot \Delta V}{\Delta H_f}$$

In this equation, T_m is equilibrium melting temperature, ΔV is specific volume differences of liquid and solid, ΔH_f is the latent heat of fusion, ΔT is temperature difference and ΔP is pressure difference. T_m and ΔH_f are negative due to shrinkage and released heat by the molten metal during solidification. Consequently, $\Delta T/\Delta P$ is positive. This also means increasing applied pressure is resulted with higher solidification temperature [20].

2.4.2.2. Process Advantages, Disadvantages, and Defects

Applied pressure and slow filling provide a shrinkage and gas porosity free product for squeeze casting. As a consequence, SC products are heat-treatable and weldable. Furthermore, near net shape castings with high surface finish can be obtained by SC method. High pressure application provides decreased grain size and dendrite arms which improve mechanical properties of the product. The reason for this is increased molten metal-die heat transfer rate [20].

Ferrous and non-ferrous castings can be done without any cast composition or wrought composition differentiation is made by SC. Moreover, from 10 g to 5 kg casting can be produced easily. Automated operations are suitable since, scraps can be recycled in SC [20].

On the other hand, there are also some disadvantages of SC. Macrosegregation can be observed with high temperature gradients. Macrosegregation causes non-uniform microstructure and mechanical properties. Furthermore, eutectic can be pushed to the surface which cause surface defect, if some high segregation elements exist in the alloy [20].

Frankly, foundry defect can be observed like porosity, inclusions, cold shuts etc. when process parameters are not taken into account [20].

2.4.3. Gravity Die Casting

Gravity die casting which is also called as permanent mold casting, is casting method. Two or more metals molds are used repeatedly to produce same shape. After metal molds are assembled or placed in order to perform a casting, molten metal is poured into the molds with the help of gravity. This process can be called as semi-permanent mold casting when sand or plaster cores are used [50].

Gravity die casting is more preferable for high volume productions. Moreover, it should be considered that product should have uniform thickness and need uncomplicated coring. On the other hand, complex casting can be achieved with high production amount that will compensate mold costs [50].

More uniform casting with lower dimensional tolerances are performed by gravity die casting as it is compared with sand casting. Furthermore, good surface finish and higher mechanical properties are obtained [50].

Unfortunately, there are some limitations for gravity die casting. These limitations are [50]:

- Gravity die casting limits the number of alloys that can be casted.
- Low amount production is not feasible due to high tooling cost.
- Certain shapes are not suitable for this technique due to some problems like parting line, undercuts and removal of dies.
- Coatings are necessary in order to increase die life.

2.4.4. Vacuum Assisted Gravity Die Casting

This method is a combination of gravity die casting and vacuum. Although there is not much information on this method in literature, it is known that vacuum is used for reducing gas porosities and blisters [20]. Also, it can be said that vacuum helps the molten metal filling the mold, since vacuum apparatus is at the end of the vertical die.

2.4.5. Sand Casting

Sand casting is a very ancient casting process. A destructible sand mold is made for a specific product and molten metal is poured into this mold for sand casting process. However, sand casting is still used due to the design possibilities that are shape and size [50].

Silica and zircon are the most used sands in aluminum casting although, zirconia, olivine and chromite are used in sand casting processes. Silica sands that are used in foundries mostly consist of quartz (SiO_2). On the other hand, some ferrous impurities can be found in this sand like Fe_3O_4 or FeO-TiO_2 . The reason of silica sand usage in foundries is its low cost and availability. Unfortunately, volume changes in silica during heating can cause some defects in the casting. For example, at 573°C there is α to β transformation which causes 1.6% volume expansion and

above 867°C, β to tridymite transformation occurs which shrink volume by 0.3% [50].

Quality of the mold is related with the size, shape and distribution of sand grains. Shape of grains affects the sand surface area. Permeability of the sand is related with the size distribution. Size, shape and distribution directly affect the binder amount that must be used in the mold. Since, binder amount must increase as sand surface increase in order to have required mechanical properties. Round grains need less binder amount due to their low surface to volume ratio and they are favorable in core making. However, angular grains need more aggregates due to their surface to volume ratio [50].

2.4.5.1. Green Sand Molding

The sand molds that can be transformed to clay-bonded sand by water addition is called as green sand. Bentonites and fireclays are the most common clays that is used for aluminum casting [50].

Bentonites are a kind of a montmorillonite that is expanding with water addition and shrink with drying. There are two kinds of bentonites that one of them replaces its Na atoms with aluminum atoms and the other one replaces its Ca atoms with aluminum atoms. Bentonites provide plasticity to the sand. This plasticity helps compensating the volume change effects in silica. Fireclays are compromise of kaolinite. Fireclays are refractory and have low plasticity [50].

Sand mold gases form as the molten metal is poured into the sand mold. These gases are result of binder decomposition. At this point of casting, permeability of the sand mold becomes important. If the permeability is not sufficient these gases can cause casting defects by disrupting metal flow or damaging mold walls. On the other hand, these gases avoid metal penetration to the sand mold. That's why, a balance must be obtained in the sand mold. Furthermore, as molten metal is poured

into the cavity, sand grains are subjected to heat of molten metal. This leads expansion on neighbor sand grains. In order to maintain cavity shape, these neighbor sand grains should not be dense [50].

2.4.6. Grain Refinement in Aluminum Alloys

Grain refinement is a method for having fine (smaller) grains in alloys. Proper usage of grain refinement methods provide a fine grained structure in all aluminum alloys. Most common methods for grain refinement are master alloys of titanium or master alloys of titanium boron addition in aluminum alloys. Al-Ti based additives usually have 3-10% Ti while Al-Ti-B based additives have 0.2-1% B. Grain refiners should be added in operative quantities to give optimum results. There are forms of grain refiners for specific usage. Rod form wrought refiners are used for continuous casting systems. Also, it can be found in short lengths for foundry use. Same grain refinement composition can be found as waffle form. Salts that are usually in compacted form can be found to form $TiAl_3$ or TiB_2 [50].

2.4.6.1. Grain Refinement Mechanisms

Actually there are no commonly accepted mechanism theory exist. There are some theories but, none of them persuade all researchers. $TiAl_3$ affects nucleation of aluminum crystals. This is because crystallographic lattice spacing similarities between $TiAl_3$ and aluminum. Nucleation might take place on $TiAl_3$ substrates. These substrates can be either undissolved or precipitate at higher Ti concentrations by peritectic reaction. On the other hand, at lower Ti concentrations than 0.15% which is the Al-Ti peritectic point, grain refinement can be attained. That's why, theories like co-nucleation of the aluminide by TiB_2 or carbides and inherent effects on the peritectic reactions are assumed to be effective. Also, it is claimed that complex borides of Al-Ti-B affects grain nucleation. Normally, Ti addition to casting results with finer grain size. Furthermore, TiB_2 existence in the alloy provides extended grain refinement effectiveness. Also, it is seen in the tests that

just additive of aluminum boride and titanium boride without excess Ti addition provide significant grain refinement. However, it is accepted that optimum results are achieved with usage of excess Ti balanced with TiB_2 . Effect of boride on grain refinement is observed both casting and wrought alloys. However, boride usage in large amounts cause agglomeration and affect casting quality badly as inclusions. Furthermore, it is recommended that after boride usage, furnaces should be cleaned due to inclusion possibility [50].

The aim of the grain refinement is to provide fine, uniform and equiaxed grain structure to the casting. This is the reason why selection of grain refiner is important. Proper grain refiner selection is mostly related with the experience of the foundry. Most of the foundries select grain refiners in order to fulfill the requirements of the product. Even though this is a case work, 5Ti-1B and 5Ti-0.6B types of grain refiners are recommended for optimum results in most cases. Also these grain refiners with 0.01-0.03%Ti additive are characterized by their cleanliness and uniform distribution of aluminide and boride phases [50].

There are various test methods for grain refinement effectiveness. However, most of them are based on comparison of samples. Foundries usually sand cast an alloy with and without a grain refiner into the similar molds. Then, grain size comparison is made by metallographic methods like etching and polishing. Moreover, NDT techniques like thermoanalytical and electrical conductivity methods are developing for grain structure prediction [50].

CHAPTER 3

EXPERIMENTAL PROCEDURE

3.1. Squeeze Casting

A vertical squeeze casting machine, which can be seen in Figure 16, was used in this experiment. Molten 7075 and 7085 aluminum alloys were poured into the pre-heated die mold separately. Molten aluminum alloys were solidified under 175MPa pressure in the mold. 3 samples were prepared by this method for 7075 alloy. Figure 17 shows the samples of this experiment. Dimensions of those samples are; 90 mm diameter, 12 mm, 17mm and 23mm height, respectively. Four samples were prepared for 7085 alloy which can be seen in Figure 18. Later on, hardness test was conducted on these as cast samples. Finally, these samples were subjected to T6 heat treatment. Solution treatment was done at 540 °C for 6 hours in a muffle furnace (Figure 19) then samples were quenched in water. Artificial aging treatment was conducted at 160°C for 6 hours in muffle furnace for 7075 alloy according to Table 5. However, 7085 alloy sample was solution treated at 485 °C for 90 minutes and quenched to avoid blisters based on Table 5. Artificial aging was performed at 120°C for 24 hours.



Figure 16. Vertical squeeze casting machine used in experiments.



Figure 17. Squeeze cast 7075 alloy discs. First, second and third from left to right.

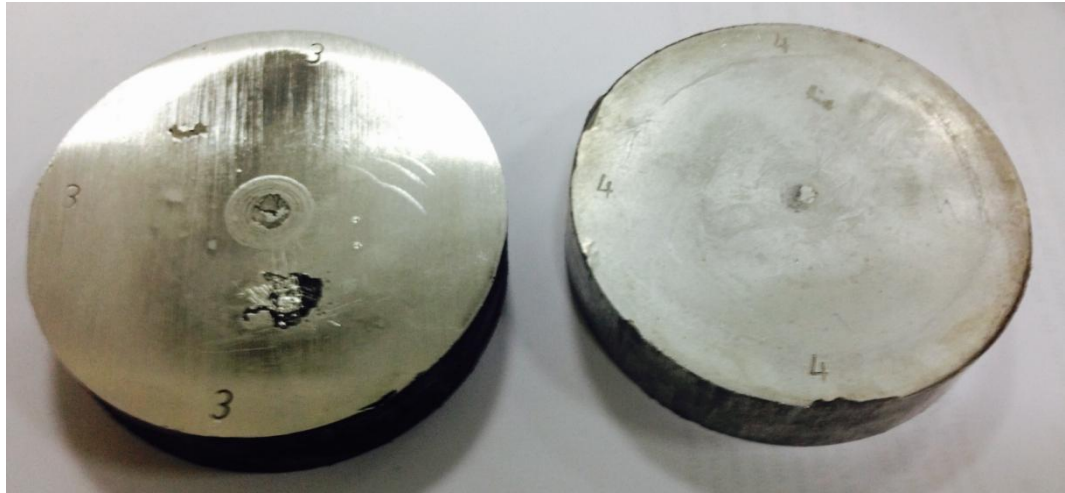


Figure 18. Squeeze cast 7085 alloy discs.



Figure 19. Muffle furnace used for heat treatment in experiments.

3.2. Vacuum Assisted Gravity Die Casting

A controlled vacuum was applied during melt delivery to increase filling speed and cooling rate. The reason of using vacuum application is to fill the die mold as quickly as possible before molten 7075 alloy solidification. The setup for this experiment consist of a copper die mold, an apparatus to connect die mold with

vacuum hose, vacuum pump and a sprue made out of green sand. Setup can be seen in Figure 20.

After assembly of the setup, 7075 aluminum alloy was melted in an induction furnace. After melting of aluminum alloy, copper die mold was heated up to 250°C by a torch. Vacuum pump was activated before casting. Since, high vacuum would cause defects in casting, low vacuum was applied. A vacuum machine that has three vacuum levels was used on the lowest level. After these steps, molten 7075 aluminum alloy was poured into sprue at about 700°C and was filled the horizontal copper die mold under controlled vacuum condition.

As cast specimen was cut in 7 mm x 60 mm x 70 mm dimensions for heat treatment as shown in Figure 21. ASTM heat treatment standard was based in order to determine heat treatment temperatures and durations. T6 heat treatment was performed for this sample. Since, sample thickness is 7 mm, solution treatment was done at 480°C for 70 minutes in muffle furnace following a water quench was done. Artificial aging treatment was done at 120°C for 24 hours in convection furnace.

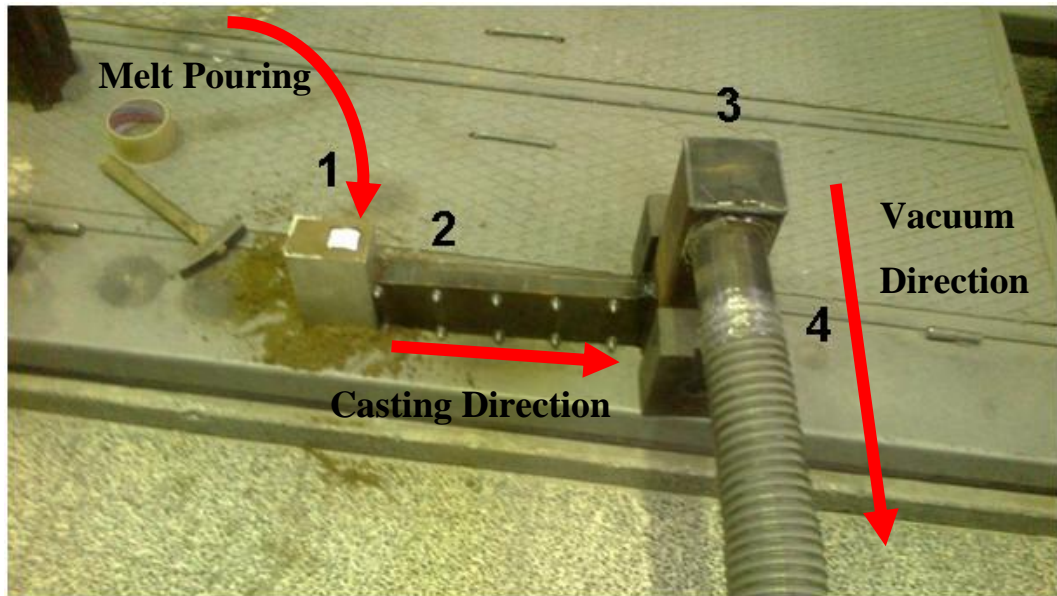


Figure 20. Vacuum assisted gravity die casting experiment setup. 1. Sprue, 2. Horizontal copper die mold, 3. Vacuum hose-die mold connector part, 4. Vacuum hose.

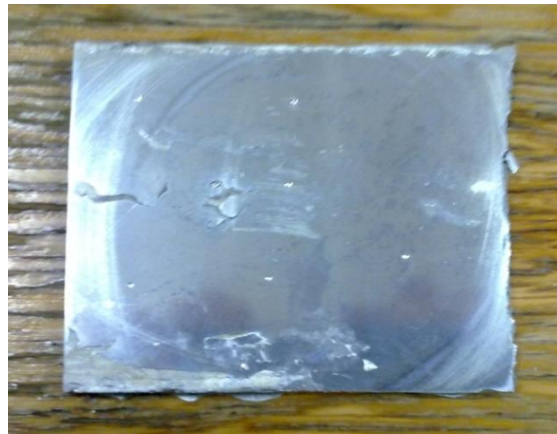


Figure 21. Polished and heat treated vacuum assisted gravity die cast sample.

3.3. Gravity Die Casting

A vertical permanent copper die mold was used to produce 7075 alloy slab. 7075 aluminum alloy was melted by induction furnace. Vertical copper die mold was preheated up to 250°C by a torch. Molten 7075 alloy was poured into the preheated vertical copper die mold at 850°C. Casting was done through gravitational force. A part of cast sample was cut for testing. This sample had dimensions as 7 mm x 60 mm x 20 mm as shown in Figure 22.

ASTM heat treatment standard was based in order to determine heat treatment temperatures and durations similar to vacuum assisted gravity die casting experiment. T6 heat treatment was conducted on sample. Since, sample thickness is 7 mm, solution treatment was done at 480°C for 70 minutes in muffle furnace following a water quench was done. Artificial aging treatment was done at 120°C for 24 hours in convection furnace.



Figure 22. Sample that was used for testing in gravity die casting experiment.

3.4. Sand Casting

Rifle receiver dimensions were measured and used for this experiment. Since, our aim is to produce a near net shape preform. Resin coated sand and green sand mold were prepared in accordance with the measured dimensions of rifle receiver. Resin coated sand core was prepared by heating at 200°C for 1 hour in convection

furnace. This core corresponds to the hollow part of rifle receiver. Green sand mold was prepared to cover other parts of rifle receiver. For this purpose a wood pattern of rifle receiver was prepared. After preparation of sand mold, 7075 aluminum alloy was melted in an induction furnace. Then, molten 7075 alloy was poured into mold at 750°C which gives adequate time to molten alloy to fill the cavity completely. Sand cast samples can be seen in Figure 23.

Casting was exposed to heat treatment after removal of runner. T6 heat treatment was performed on the casting. Solution treatment was completed at 480°C for 2 hours in muffle furnace. This duration is out of ASTM standardization but, this duration was considered appropriate for solutionizing. 120°C was used for artificial aging treatment with duration of 24 hours in convection furnace.



Figure 23. 7075 aluminum alloy casting after shake out of sand.

Al5TiB was used as grain refiner to decrease grain size of sand casting. Before melting in induction furnace, 7075 aluminum alloy that was melted was weighted. It

had 1612 gr weight and 3 gr of Al5TiB was added to charge which corresponds to 0.18%. After alloy preparation, molten alloy was poured into a mold at 750°C which was the same pouring temperature of sand casting.

3.5. Vertical Semi Solid Metal Casting

The aim of this experiment is to observe formability of 7075 at different temperatures and at different solid fractions. In this experiment, a vertical press with a die mold that have 90 mm diameter was used as in Figure 24. 3 parts are cut from extruded 7075-T6 billet (40 cm x 7.5 cm x 2 cm). 40 cm is length, 2 cm is thickness and 7.5 cm is width of the billet. Prepared specimens have dimensions as 7.5 cm x 5 cm x 2 cm (Figure 25). Then, specimens were put in the muffle furnace for heating up to desired temperatures. Three different temperatures were used for this experiment; 580°C, 595°C and 605°C. Before pressing, die mold of the vertical press was preheated with a torch to 250°C. Preheated specimens were placed in the pre-heated die cavity with the 90 mm diameter for subsequent pressing. Specimens were pressed at 150 MPa pressure in the die cavity. Three semi-solid formed disks were produced during experiments.

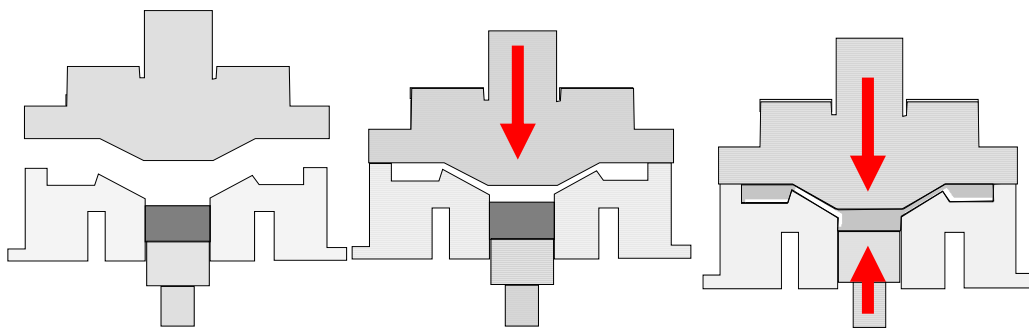


Figure 24. Die mold and working principle of vertical squeeze casting press that is used during semi solid experiments in the Foundry laboratory at METU.

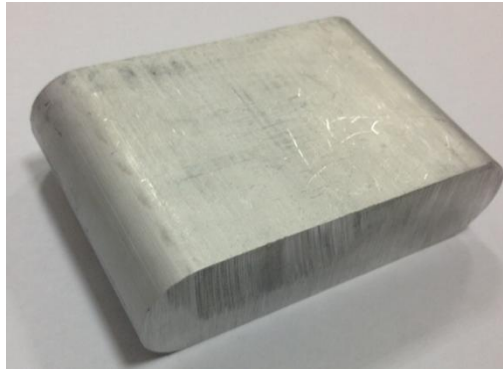


Figure 25. A prepared sample of extruded 7075 alloy.

Heat treatment was applied to the disks. T6 was applied to reach high strengths. First, parts were solutionized by heating up to solutionizing temperature 480°C and parts are kept at that temperature for 70 minutes. Then, parts were quenched in water. Secondly, solutionized parts were artificially aged at 120°C and kept at that temperature for 24 hours. Processed disks after T6 heat treatment can be seen in Figure 26. Moreover, second phase fraction calculations are made by using Dewinter Materials Plus image analysis program.



Figure 26. Produced disks after T6 heat treatment.

3.6. Vertical Squeeze Casting

In this experiment, aim was to observe mold filling properties of the 7075 alloy in a hollow shaped mold. The same vertical squeeze casting press with a die was used for this experiment. However, a special die was used in this experiment. This mold produces rectangular shaped parts having cavity that have dimension as 31cm x 5cm x 3.5cm and a hollow part as in Figure 27. Extruded 7075-T6 billet was melted in an induction furnace. Then, molten 7075 aluminum alloy, at 650°C temperature was poured into the preheated rectangular die that has temperature less than 250°C. 100 tones force was applied to the molten alloy in the die. By using this method two rectangular prism shape preforms were produced which are in Figure 28. After producing these preforms, T6 heat treatment was applied to these samples similar to casting samples.

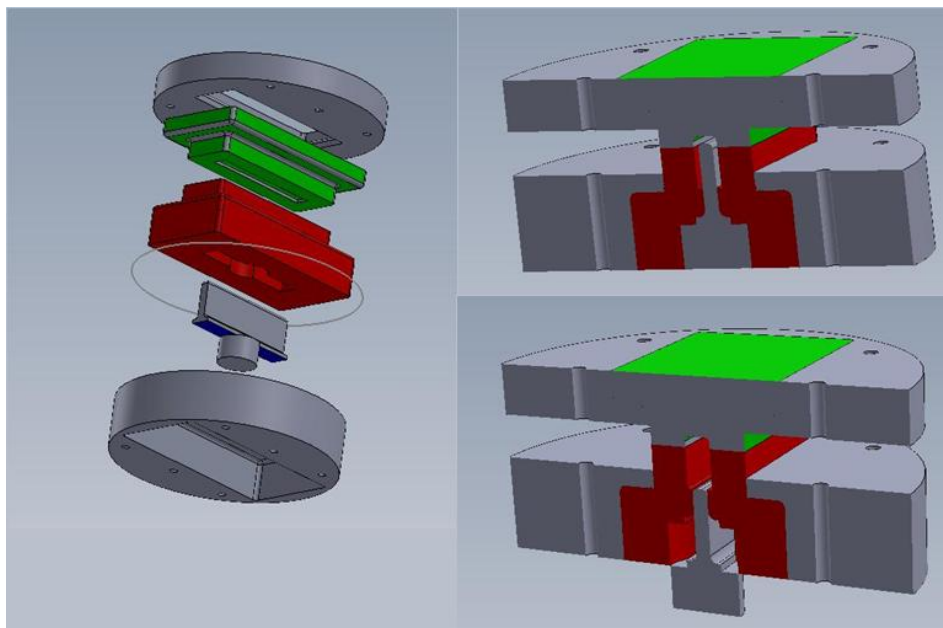


Figure 27. Burst drawing of the mold that produces hollow shaped parts.



Figure 28. Produced hollow shaped parts after T6 heat treatment.

3.7. Semi-Solid Metal Casting

The aim of this experiment is to observe effects of a particular solid fraction during high pressure die casting of 7075 alloy at an injection molding process. A HPDC machine was used for this experiment (Figure 29). A special die that can produce tensile test specimen and bending test specimen was used (Figure 30). 7075 alloy was processed with HPDC. By the time, die was heated up to 200°C. Before pouring the molten alloy, alloy in the crucible was stirred with a rod containing a thermocouple to read the temperature of the alloy to reach desired temperature. As alloy temperature decreases below the liquidus temperature, alloy was poured into shot sleeve and pressed. A sample was pressed at 630°C which is lower than the liquidus temperature of 7075. Liquidus temperature for 7075 is determined as 635°C by ASM. However, this temperature depends on chemical composition of the alloy. Even the smallest variation in the composition can change liquidus temperature. Same procedure was repeated with a modified 7075 alloy. The chemical composition can be seen from Table 7. For the modified 7075 alloy, five different temperatures were used as processing temperature. These temperatures were; 602°C, 613°C, 616°C, 620°C and 624°C.

The porosities were calculated by weighting the specimens. Porosity calculation of 3rd specimen is done by Dewinter Material Plus image analysis program. Porosity of other specimens assumed related to their weight with respect to 3rd specimen.



Figure 29. The high pressure die casting (HPDC) machine used in semi-solid metal casting.

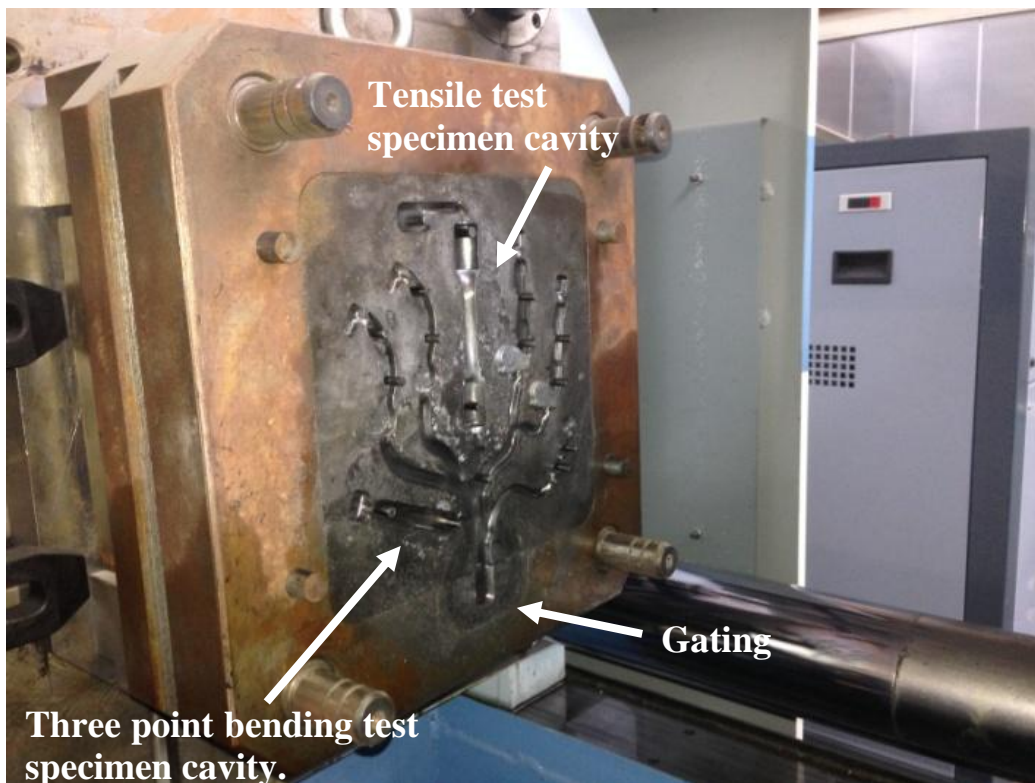


Figure 30. The die that can produce tensile and bending test specimens.

Table 7. The chemical compositions of extruded and modified 7075 alloys produced.

	Zn (wt. %)	Mg (wt. %)	Cu (wt. %)	Mn (wt. %)	Ti (wt. %)	Al (wt. %)
Extruded 7075-T6	6.04	2.06	1.20	0.10	0.04	Bal.
Modified 7075	6.96	4.68	2.63	0.05	0.04	Bal.

3.8. Strain Induced Melt Activation (SIMA) Process for Thixocasting

This experiment was aimed to observe effects of ultrasonic stirring and mechanical stirring on mechanical properties and grain size. Ultrasonic stirring method and mechanical stirring methods were used in this experiment.

First, 7075 aluminum alloy was prepared in an induction furnace for casting. In mechanical stirring method, an air cooled copper mold was used and molten 7075 alloy was poured into this mold at 700 °C. Molten alloy was stirred by graphite rod until solidification was completed. Then, solidified 7075 alloy which had cylindrical shape was removed from the copper mold at about 200 °C in order to perform forging. This cylindrical shaped 7075 alloy was placed vertically under the punch. 20 tons of force was applied to the alloy for about 1 minute, which caused 33 % increment in cross section area. After forging process, disc shaped sample was cut from forging sample for further processes. For recrystallization, this disc shaped sample was kept in muffle furnace at 200 °C for 100 minutes. Then, this recrystallized sample was heated up to 590 °C for semi-solid pressing. T6 heat treatment was applied to the specimen after semi-solid pressing operation.

In ultrasonic stirring method, an air cooled copper mold which was placed into ultrasonication bath was used and molten 7075 alloy was poured into this mold at

700 °C. Stirring was provided by ultrasound from ultrasonication bath. The same procedure was followed for next steps. However, semi-solid casting temperature of this sample was 610 °C. Cylindrical shaped alloy billets can be seen in Figure 31. Moreover, experimental parameters of ultrasonic stirring and mechanical stirring were tabulated at Table 8.



Figure 31. Cylindrical shaped alloy billets produced (left: ultrasonic stirring, right: mechanical stirring).

Table 8. Experimental parameters of ultrasonic and mechanical stirring.

	Ultrasonic Stirring	Mechanical Stirring
Casting Temperature (°C)	700	700
Forging Temperature (°C)	~ 200	~ 200
Cross Section Area Increase (%)	33	33
Recrystallization Temperature (°C)	200	200
Pressing Temperature (°C)	610	590
Heat Treatment	T6	T6

3.9. Thermal Analysis and Solid Fraction Calculations

Different cooling rates were used to obtain solid fraction curves. Calculation of solid fraction can be done by many methods. However, it was determined that using Newtonian thermal analysis method is suitable for this. In Newtonian thermal analysis, a cooling curve should be obtained from a solidifying alloy as illustrated in Figure 32. Then, first derivative of the cooling curve is obtained which should give phase transformation temperatures of the solidifying aluminum alloy by using a special computer program as shown in Figure 33. A zero curve or baseline should be drawn onto the first derivative of the cooling curve. This zero curve can be drawn by using polynomial curve fitting. However, the part of the first derivative which phase transformation occurs must be excluded during curve fitting. Since, zero curve is assumed that there is no phase transformation through phase transformation temperatures. After that point, the best fitting polynomial degree should be chosen as zero curve as seen in Figure 34. In this case and for most cases 3rd degree polynomial fit would be appropriate. In the next stage, the area between the zero curve and the first derivative should be integrated from liquidus

temperature to solidus temperature to obtain the solid fraction data. Figure 35 shows the area between the first derivative and zero curve which should be integrated. Moreover, Figure 36 shows the graph of solid fraction change with respect to temperature which is obtained after integration of the area in Figure 35 [12-16]. In order to explain this calculation following equation can be used. t_i and t_f are instantaneous and final times respectively where Fs_i is instantaneous solid fraction. $\left(\frac{dT}{dt}\right)_{cc}$ represents first derivative of cooling curve and $\left(\frac{dT}{dt}\right)_{zc}$ represents zero curve.

$$Fs_i = \frac{\int_0^{t_i} \left[\left(\frac{dT}{dt}\right)_{cc} - \left(\frac{dT}{dt}\right)_{zc} \right] dt}{\int_0^{t_f} \left[\left(\frac{dT}{dt}\right)_{cc} - \left(\frac{dT}{dt}\right)_{zc} \right] dt}$$

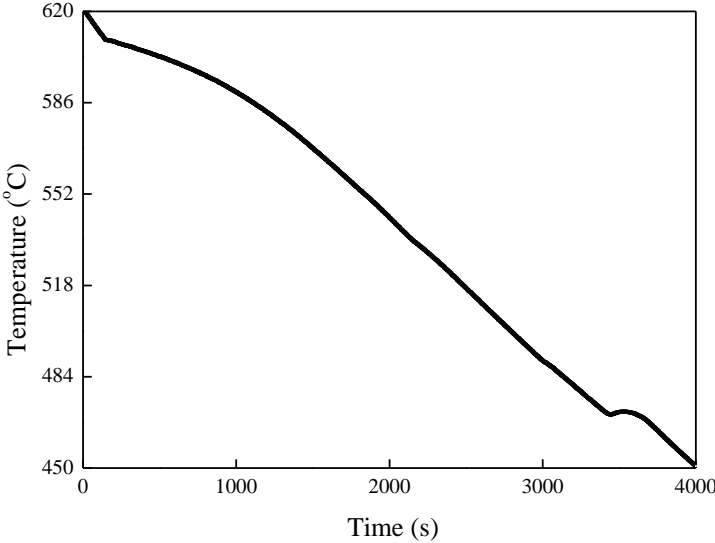


Figure 32. Cooling curve of 7075 alloy with 0.04°C/s cooling rate with respect to time.

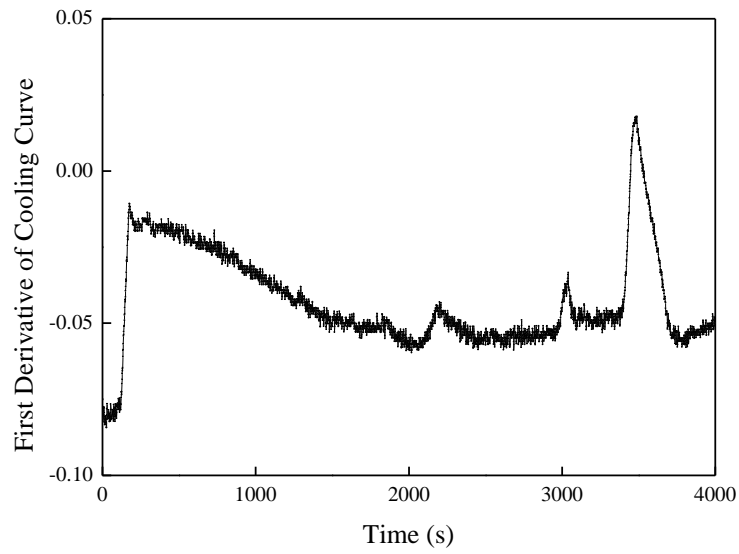


Figure 33. First derivative of 7075 alloy cooling curve with 0.04°C/s cooling rate with respect to time.

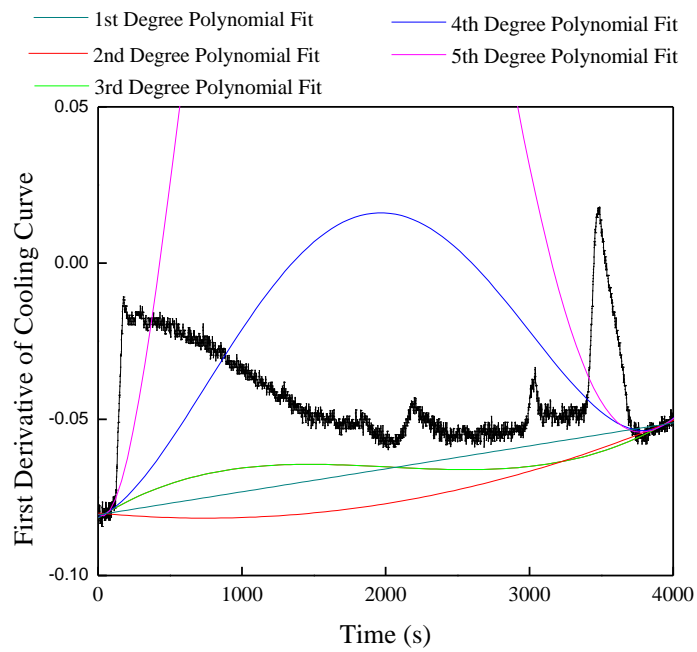


Figure 34. Polynomial fits in several degrees for zero curve drawing.

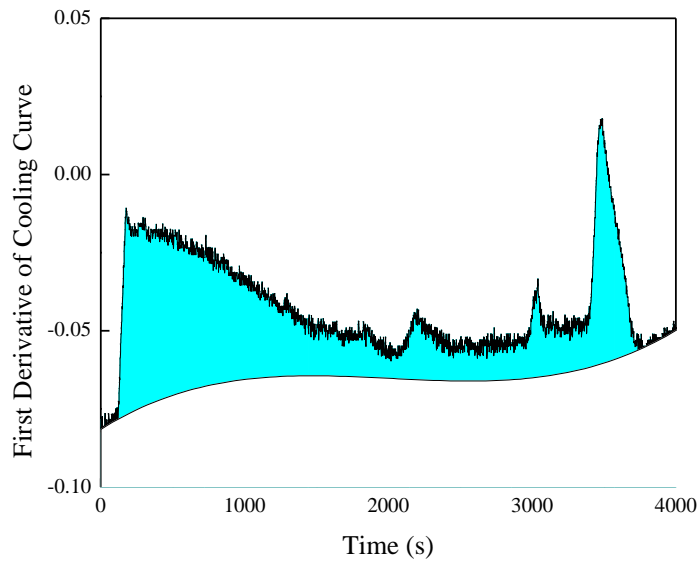


Figure 35. The area between the first derivative and the zero curve is represented as colored.

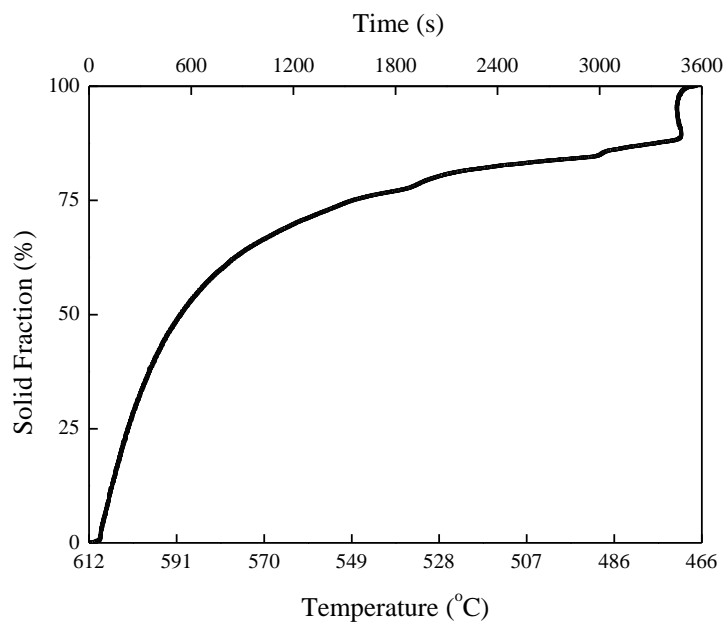


Figure 36. After integration of the area between the first derivative and the zero curve, solid fraction with respect to temperature graph can be obtained.

For thermal analysis experiment, a K-type thermocouple and data acquisition setup were used. This system can be seen in Figure 37. For faster cooling rate, molten alloy was placed in a graphite pot which was covered with thermal blankets from sides to avoid heat loss from sides. For slower cooling rate, graphite crucible with solid alloy in it, was placed inside the muffle furnace. Then, muffle furnace was heated above the melting temperature of alloy to melt the alloy. After melting, K-type thermocouple was placed in the graphite crucible and furnace was turned off to let alloy cool slowly.

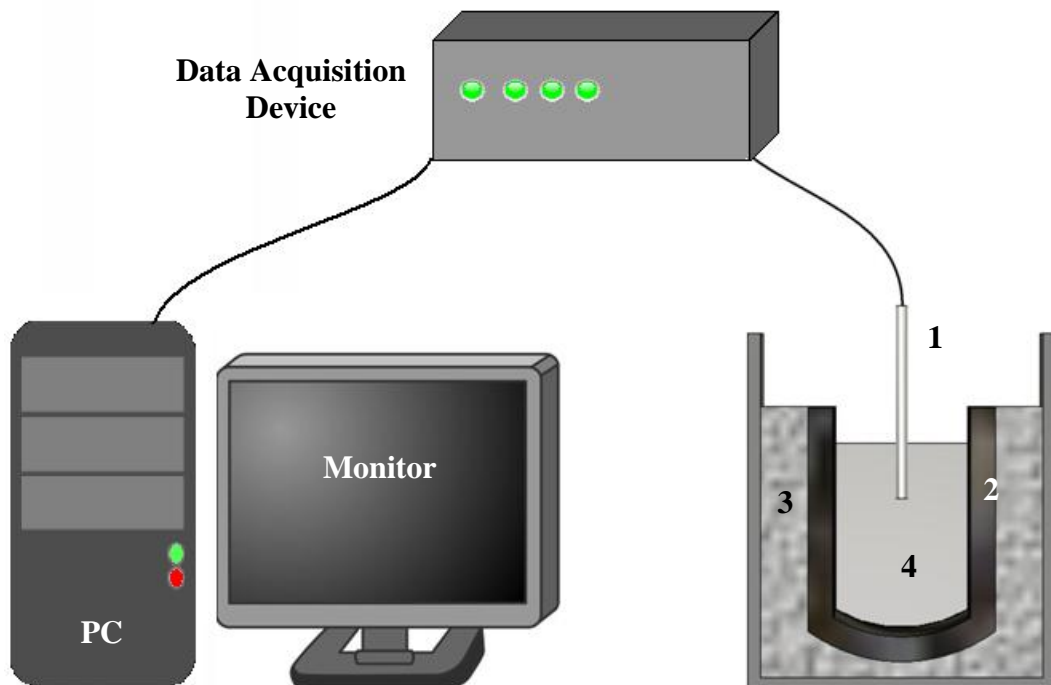


Figure 37. Data acquisition setup of the thermal analysis and solid fraction calculations experiment and the graphite crucible that was used in experiments (1. Thermocouple, 2. Graphite Crucible, 3. Thermal Blanket, 4. Molten alloy).

During cooling of the molten alloy, data was collected via K-type thermocouple. This collected temperature vs. time data, was processed by MATLAB program to obtain first derivative vs. time graph and zero curve. Finally, solid fraction vs. temperature graph was obtained.

3.10. Characterization

3.10.1. Mechanical Testing

3.10.1.1. Tensile Test

Tensile tests were done at two different tensile test machines. Mares tensile test machine used for large specimens is capable of completing tests up to 50 tons of hydraulic forces. Figure 38 represents Mares tensile test machine setup.



Figure 38. Mares tensile test machine setup [51].

The second tensile test machine that was used in experiments was 100 KN Instron 5582 tensile test machine for relatively smaller specimens. Instron 5582 tensile test machine is given in Figure 39.

1mm/min elongation rate was used in both machines for all test samples. Moreover, all the tensile test specimens were prepared according to the ASTM B 557M – 10 which is “Standard test methods for tension testing wrought and cast aluminum and magnesium alloy products” [52].

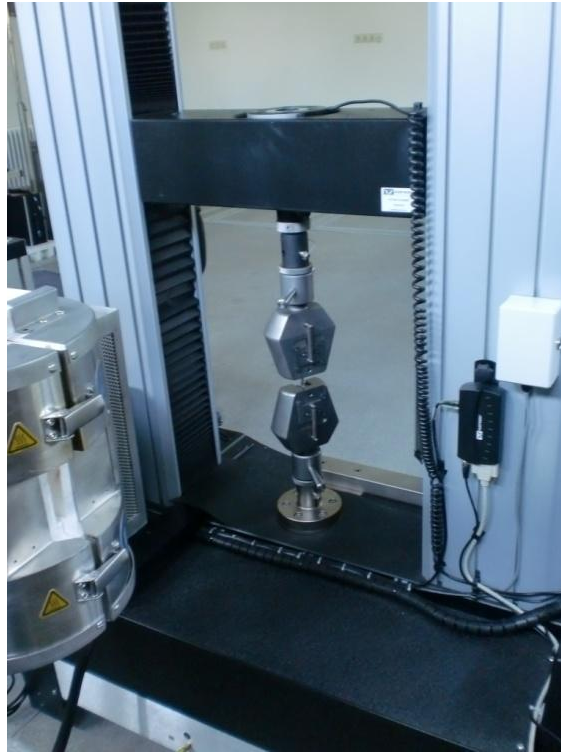


Figure 39. Instron 5582 Tensile test machine [53].

3.10.1.2. Hardness Test

Universal Emco M4U-025 hardness testing machine was used in all hardness tests. The hardness tests were done in accordance with ASTM E10 – 01 which is “Standard Test Method for Brinell Hardness of Metallic Materials” [54]. During hardness tests, a tungsten carbide ball that has 2.5 mm diameter was indented on the surface with 187.5 kg load.

3.10.2. Metallography

SEM and optical microscopy were used in this study. The samples were cut to proper sizes for the microscopy. Metacut-M 250 Cut-Off Machine was used for cutting operations as shown in Figure 40.



Figure 40. Metacut-M 250 Cut-Off Machine [51].

After cutting, grinding was applied to specimens. Several abrasive grinding paper numbers were used according to the surface roughness with increasing order for grinding. Polishing was applied after grinding. 3 μm diamond solution was used for first step polishing. Latter step, 1 μm Al_2O_3 solution was the choice for polishing.

Samples were etched after proper polishing. Keller's reagent was used as etchant for revealing grains of samples. Keller's reagent consists of 2 mL HF (48%), 5 mL HNO_3 , 3 mL HCl, and 190 mL H_2O . Samples were etched in Keller's reagent until proper contrast and microstructural details were obtained.

3.10.3. Optical Microscopy

SOIF XJP - 6A Optical Microscope was used for all 100x optical microscopy images with the help of DeWinter Material Plus 4.1 Image Analysis Software. SOIF XJP - 6A Optical Microscope is an inverted microscope which helps obtaining

images from misshapen bottomed specimens. SOIF XJP - 6A Optical Microscope is given in Figure 41.

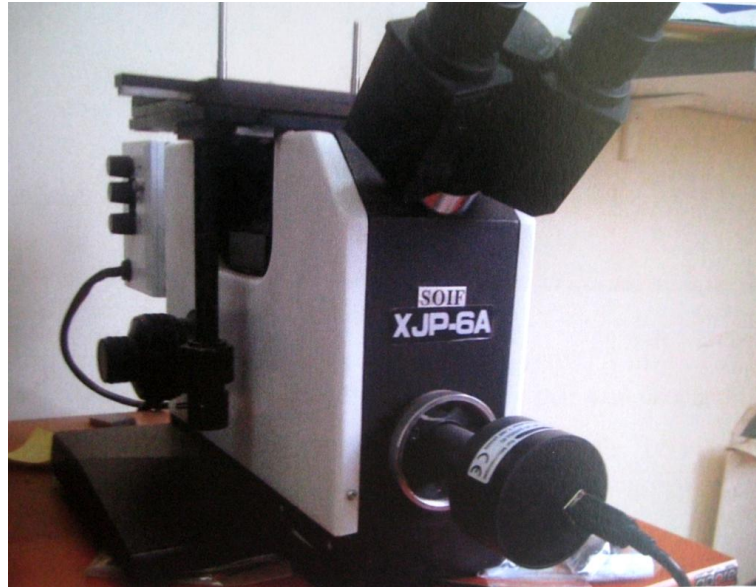


Figure 41. SOIF XJP - 6A Optical Microscope [51].

DeWinter Material Plus 4.1 Image Analysis Software was used for obtaining images and grain size analysis.

3.10.4. Scanning Electron Microscopy (SEM)

JEOL JSM-6400 Electron Microscope and NOVA NANO SEM 430 were used for SEM images. JEOL JSM-6400 Electron Microscope is equipped with secondary and backscattered electron detectors. Moreover, NOVA NANO SEM 430 is also capable of EDX analysis.

3.10.5. X-Ray Diffraction (XRD)

Rigaku D/Max 2200/PC X-Ray diffractometer was used for XRD analysis. Cu-K α radiation was used for diffraction at 40kV. Samples were scanned from 10^o to 100^o 2 θ angles with a of 2^o/min scanning speed.

3.10.6. Optical Emission Spectrometer Analysis

Foundry Master UV Vacuum CCD optical emission spectrometer was used for chemical analysis. Foundry Master UV Vacuum CCD optical emission spectrometer is given in Figure 42.



Figure 42. Foundry Master UV Vacuum CCD optical emission spectrometer.

CHAPTER 4

RESULTS AND DISCUSSION

The results of several casting techniques used to replace 7075-T6 extrusions with as cast and T6 heat treated alternative performs having similar grain size and tensile strength is presented in this chapter. In literature, hardness value of extruded 7075-T6 aluminum alloy was reported as 150 HB hardness and it was confirmed by hardness test. Since, there is a relation between hardness and tensile strength of the alloy. 150 HB hardness value was accepted to be a reference value for experiments. Furthermore, metallographic investigation of extruded 7075-T6 alloy showed that it has about 124 microns of average grain diameter.

4.1. Squeeze Casting Experiment

As a near net shape casting technique squeeze casting was performed. Surface oxidation was observed on the samples after T6 heat treatment of samples. Moreover, blister problem was observed on the samples of squeeze cast 7075 alloy. This can be explained by gas entrapment in solidified metal. As the heat was introduced to samples, gases were expanded in accordance with ideal gas law. Surface oxidation takes place due to the relatively high temperatures in heat treatment.

Hardness values were found to be 71 ± 1 HB for 7075 alloy and 72 ± 1 HB for 7085 alloy, before heat treatment. After heat treatment, hardness test was conducted on samples after removal of oxides from the surface. According to test results, hardness of samples were found as 137 ± 7 HB, 151 ± 1 HB and 116 ± 7 HB

respectively for 7075 alloy. Hardness values of 2nd sample are given in Table 9. On contrary, 167 ± 4 HB hardness was found for 7085 alloy. Target value for hardness 150 HB was reached at 2nd sample of 7075 and sample of 7085. As it was written in experimental procedure part, hardness values of all 7075 alloy samples were almost the same as 71 HB. However, there are scattering of hardness values of samples after heat treatment. Variation of the hardness values in 1st and 3rd samples of 7075 were due to temperature contours within the furnace. Hardness values of 1st sample of 7075 fluctuate between 128 HB and 147 HB. Moreover, hardness values of 3rd sample of 7075 fluctuate between 103 HB and 123 HB.

Grain size measurement was performed and by optical microscope examination 38 microns average grain diameter was found during metallographic investigation of 2nd sample of 7075. Optical microscope image of squeeze cast specimen can be seen in Figure 43. Also, SEM image of this sample can be seen in Figure 44. It can be seen that this average grain diameter is lower than extruded 7075-T6 alloy. Moreover, tensile tests were resulted as 441 MPa tensile strength and 410 MPa yield strength values with 1.5% EL.

Kim et. al. claims that 470 MPa tensile strength can be obtained in squeeze casting of 7075 alloy with pressures as 25 MPa, 50 MPa and 75 MPa. Also, 152 HB hardness values are claimed to be found in their research [55]. If a comparison is made, it can be seen that 2nd sample has 151 HB hardness values and 441 MPa tensile strength which are almost close to the related research.

Table 9. Hardness values of 2nd squeeze cast sample.

Test No	1	2	3	4	Average and STD
Hardness Brinell(HB)	151	151	150	151	151 ± 1

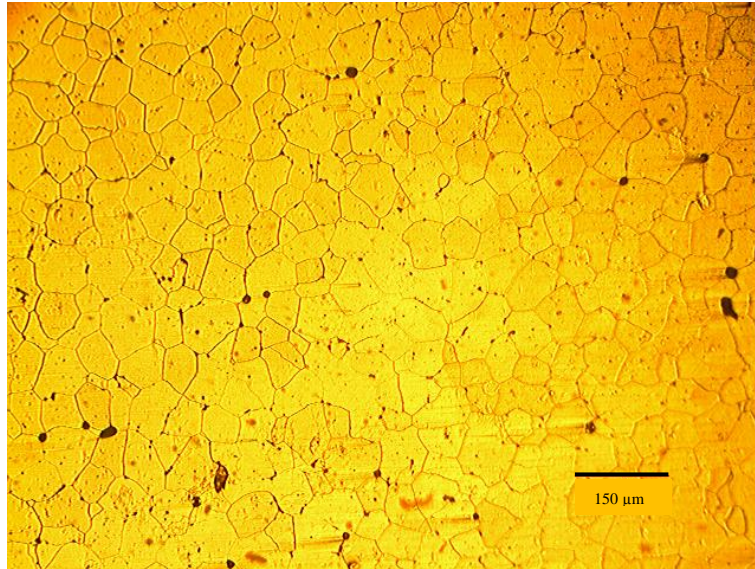


Figure 43. Microstructure of squeeze casting experiment specimen having 37 micron average grain size (100x).

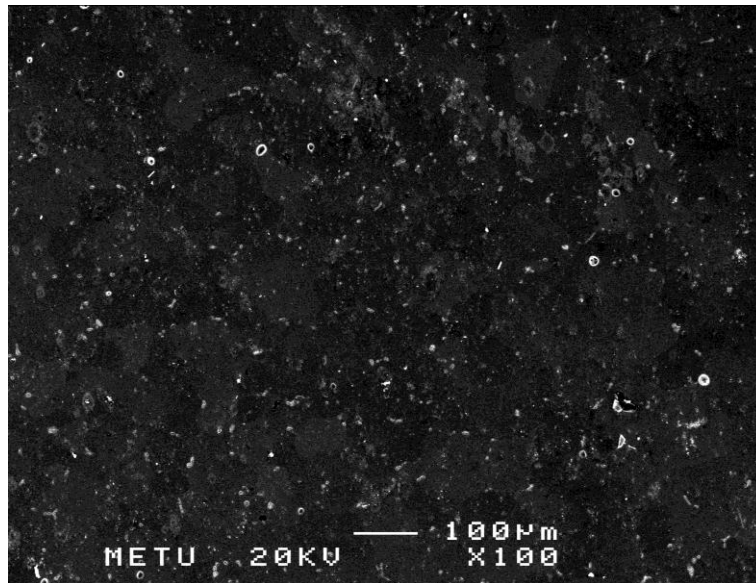


Figure 44. SEM image of squeeze casting experiment specimen (100x).

4.2. Gravity Die Casting Experiment

Hardness test was conducted after T6 heat treatment on gravity die cast specimens. It was found to be 131 ± 3 HB as average hardness value. Table 10 shows average hardness values. This hardness value is lower than our target hardness 150 HB. Moreover, metallographic investigation was conducted to measure grain size of the specimens as shown in Figure 45. SEM image for further comparison is given in Figure 46. Average grain size was measured as 41 microns. Furthermore, tensile strength was obtained as 191 MPa with 3.8% EL which can be seen in Figure A. 8.

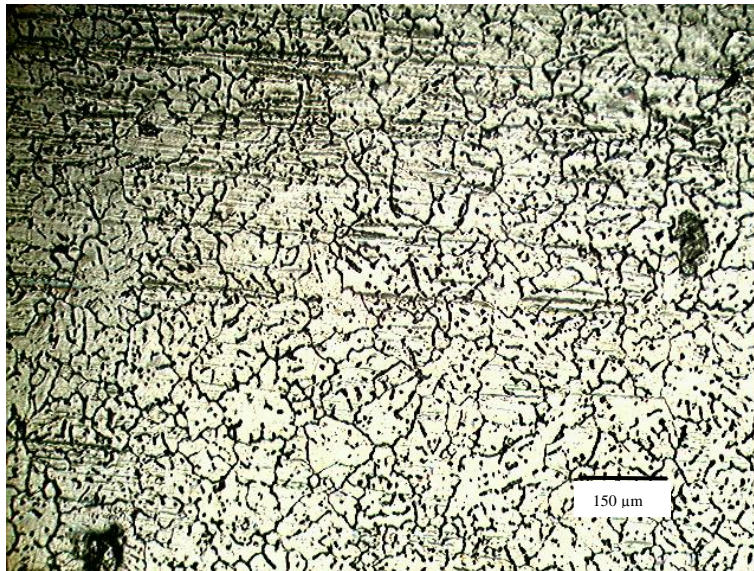


Figure 45. Microstructure of gravity die casting experiment specimen with 41 micron average grain size (100x).

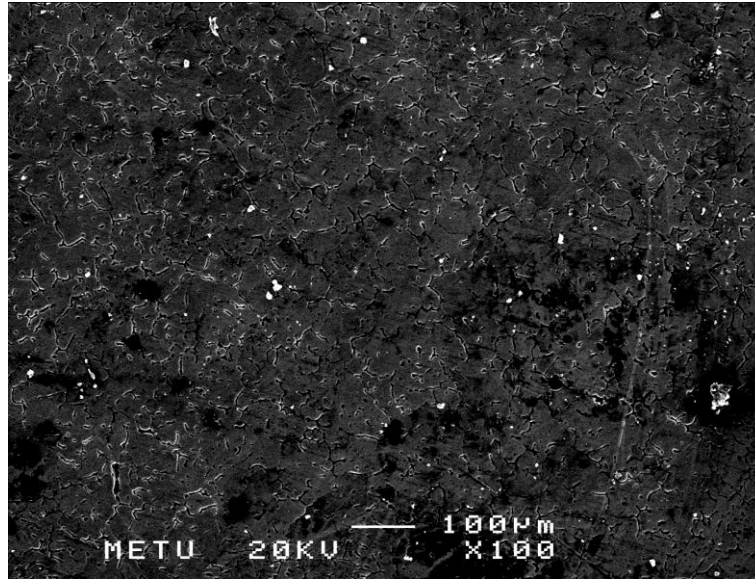


Figure 46. SEM image of gravity die casting experiment specimen (100x).

Table 10. Hardness values of gravity die cast samples.

Test No	1	2	3	4	5	6	Average and STD
Hardness Brinell(HB)	128	131	134	126	131	135	131 ± 3

4.3. Vacuum Assisted Gravity Die Casting Experiment

Heat treated specimen was found to be average 160 ± 8 HB hardness, can be seen in Table 11 with its standard deviation value. They are higher than hardness of extruded 7075-T6 specimens. Furthermore, metallographic investigation revealed that specimen has 38 microns average grain diameter. Optical microstructure shows microstructure of vacuum assisted gravity die cast specimen can be seen in Figure 47. SEM image of this microstructure can be seen in Figure 48.

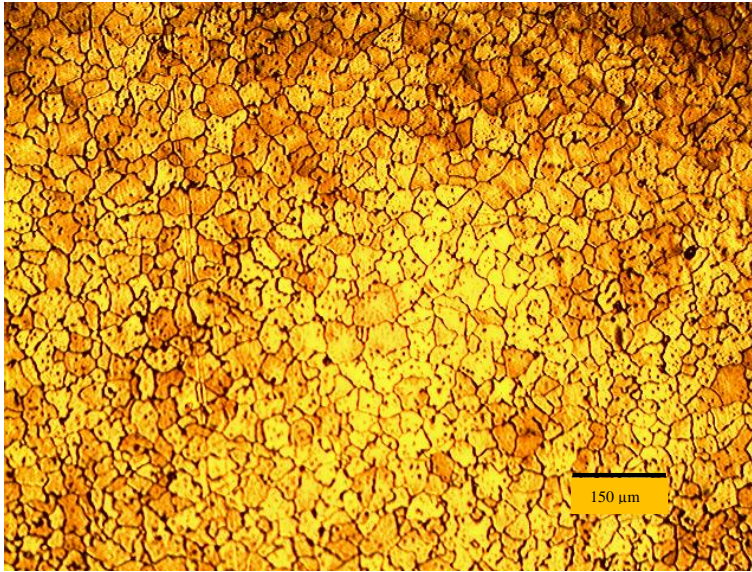


Figure 47. Microstructure of vacuum assisted gravity die casting experiment specimen having 38 micron average grain size (100x).

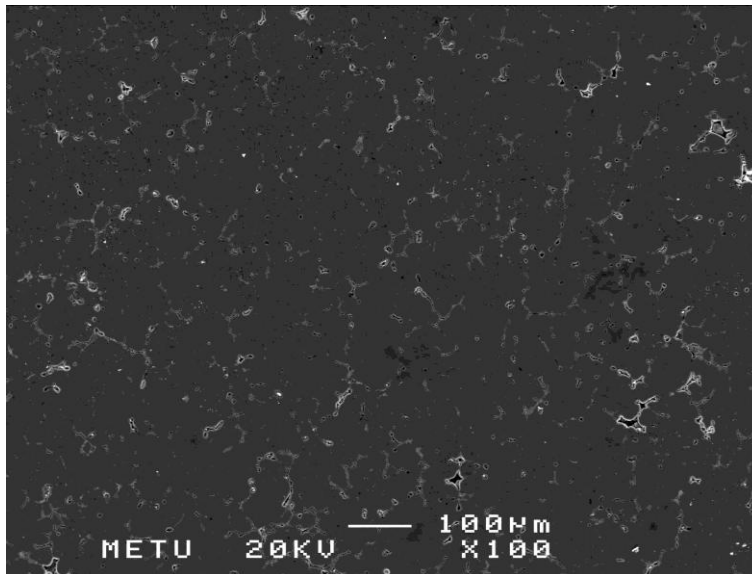


Figure 48. SEM image of vacuum assisted gravity die casting experiment specimen (100x).

Blister and surface oxidation after T6 heat treatment were not observed in this sample. It is thought that blister problem is overcome by vacuum application. Surface oxidation problem is vanished after using lower heat treatment temperatures. On the other hand, cold shuts were observed due to higher solidification rate. Thus, die mold was not filled properly. Therefore, tensile specimens could not be prepared for this casting trial.

Table 11. Hardness values of vacuum assisted gravity die casting experiment.

Test No	1	2	3	4	5	6	Average and STD
Hardness Brinell(HB)	159	146	168	159	157	171	160 ± 8

4.4. Sand Casting Experiment with/without Al5TiB Additive

Sand casting experiment was performed to produce 7075 preform castings without additive of grain refiner. It was obtained that it has 100 ± 9 HB hardness after T6 heat treatment. Even though, it had relatively low hardness values, no casting defect was observed on surface except for some surface pores by macro-investigation. Later, metallographic investigation was conducted on this sample. Examination revealed 98 microns average grain diameter. Figure 49 shows microstructure of sand casting specimen obtained by optical microscopy. Figure 50 shows SEM image of this sample.

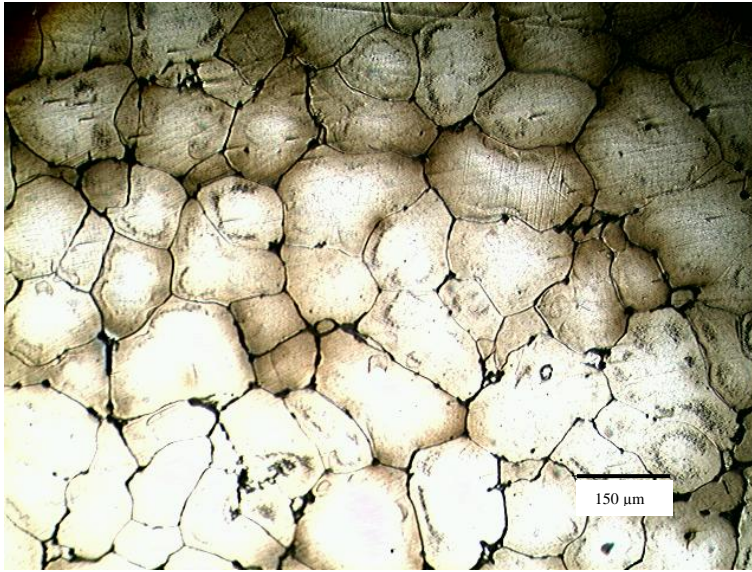


Figure 49. Microstructure of sand cast specimen having 98 micron average grain size (100x).

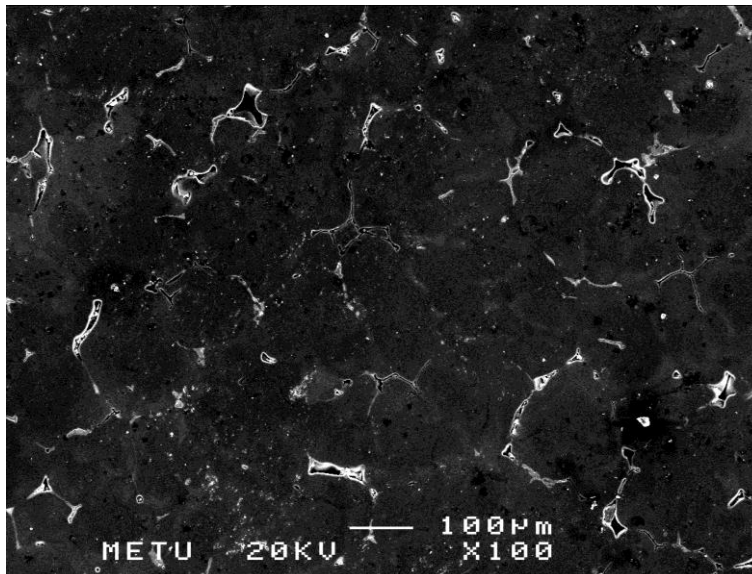


Figure 50. SEM image of sand cast specimen (100x).

Table 12. Hardness values of sand casting without Al5TiB additive experiment.

Test No	1	2	3	4	5	6	7	Average and STD
Hardness Brinell(HB)	101	116	97	97	112	86	97	100 ± 9

Sand casting was carried with Al5TiB master alloy as grain refiner (TiB_2) to molten alloy. Grain refiner additive was about 0.18% by weight. T6 heat treatment was applied on these specimens. After heat treatment, hardness test was conducted on the specimen. 106 ± 19 HB hardness was the result of the hardness test. Although this hardness is lower than the target value, it is slightly higher than the hardness of normal sand casting (without grain refiner additive). No casting defect was observed except for some surface pores. Metallographic investigation revealed that specimen of sand casting with grain refiner has 74 microns average grain diameter as shown in Figure 51. SEM image of the specimen can be seen in Figure 52. If a comparison can be done between sand casting with grain refiner and normal sand casting, it can be seen that Al5TiB increased hardness by 6% and forms finer grains as 24.5%.

Tensile test were performed on these specimens and following results were obtained. Tensile strength of sand cast alloy with Al5TiB addition was 131 MPa and tensile strength of sand cast specimen was 88 MPa. Yield strength values of specimens could not be obtained due to premature failure.

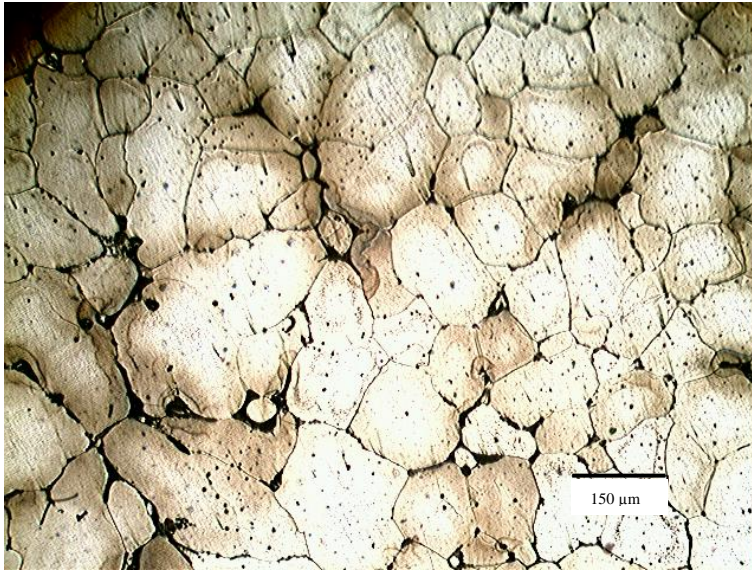


Figure 51. Microstructure of sand cast alloy with Al5TiB addition, specimen having 74 micron average grain size (100x).

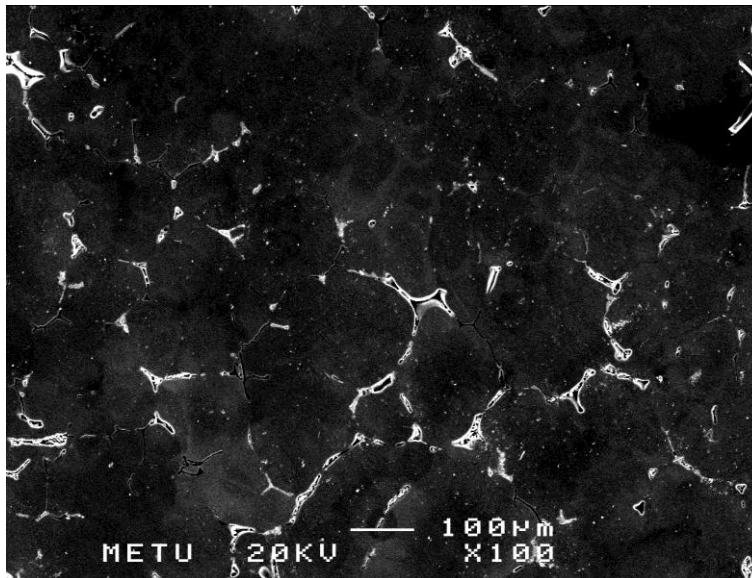


Figure 52. Microstructure of sand cast with Al5TiB addition, specimen SEM analysis (100x).

Table 13. Hardness values of sand casting with Al5TiB addition.

Test No	1	2	3	4	5	6	7	8	Average and STD
Hardness Brinell(HB)	85	90	110	138	126	115	80	106	106 ± 19

Furthermore, a comparison can be made between the hardness and average grain size results of these casting experiments in Table 14. It can be concluded that target hardness value was reached by squeeze casting and vacuum assisted gravity die casting methods. Furthermore, squeeze casting and vacuum assisted gravity die casting methods were resulted with fine grains. That's why, it can be said that squeeze casting and vacuum assisted gravity die casting methods are better than other method. However, squeeze casting can be chosen as the best technique due to tensile test results.

Table 14. Hardness and average grain size comparison of all casting experiments performed in this study.

No	Experiment	Average Hardness (HB)	Average Grain Size (microns)
1	Extruded 7075-T6	150	124
2	Squeeze Casting	150 ± 1	37
3	Vacuum assisted gravity die casting	160 ± 8	38
4	Gravity die casting	131 ± 3	41
5	Sand casting	100 ± 9	98
6	Sand casting with Al5TiB additive	106 ± 19	74

4.5. X-Ray Diffraction (XRD) Results of Casting Experiments

XRD results were obtained to reveal the intermetallics inside the castings after T6 heat treatment. In Figure 53, it can be seen that there are 5 peaks in each casting results. These peaks are at 38° , 45° , 64° , 78° and 82° which correspond to 2θ values. These peaks were defined as overlap peaks after a brief investigation. That's why, they have larger intensities than expected. Aluminum peaks were indexed according to ICDD card number of 4-0787. Planes of aluminum were found to be (111) at 38° , (200) at 44° , (220) at 65° , (311) at 78° and (222) at 82° as in Figure 53. Figure 54 shows $\text{Al}_{0.403}\text{Zn}_{0.597}$ peaks which has 52-0856 ICDD card number. In this figure, planes were found to be (001) at 38° , (110) at 45° , (121) at 65° , (012) at 78° and (200) at 83° . After T6 heat treatment, intermetallics like MgZn_2 , Al_2CuMg and $\text{Mg}_{32}(\text{Al}, \text{Zn})_{49}$ were specially searched in the diffraction chart. These intermetallics are known to be contributing increase in strengthening mechanism in 7075 alloy. MgZn_2 results can be seen in Figure 55. Its planes are (103) at 38° , (202) at 45° , (302) at 65° , (206) at 78° and (107) at 82° . ICDD card number of MgZn_2 is 34-0457. Al_2CuMg results are given in Figure 56. Its ICDD card number is 28-0014 and its planes are (131) at 38° , (132) at 44° , (062) at 65° , (154) at 78° and (064) at 82° . Another expected intermetallic is $\text{Mg}_{32}(\text{Al}, \text{Zn})_{49}$. Planes of this intermetallic were determined as (661) at 39° , (550) at 45° , (770) at 65° and (1060) at 78° as shown in Figure 57. ICDD card number of $\text{Mg}_{32}(\text{Al}, \text{Zn})_{49}$ is 19-0029.

However, there are also some undesired intermetallics for 7075 alloy that reduce strength of the alloy. Iron containing intermetallics are amongst them. After brief investigation, Fe_3Si and FeV intermetallics were found through XRD examination. Fe_3Si results can be seen in Figure 58. (110) at 45° , (200) at 65° and (211) at 83° planes are found as shown in Figure 58. ICDD card number of Fe_3Si which is known as Suessite is 35-0519. Other iron based intermetallic was FeV . Its planes were shown as (110) at 45° , (200) at 65° and (211) at 81° in Figure 59. ICDD card number of FeV is 18-0664.

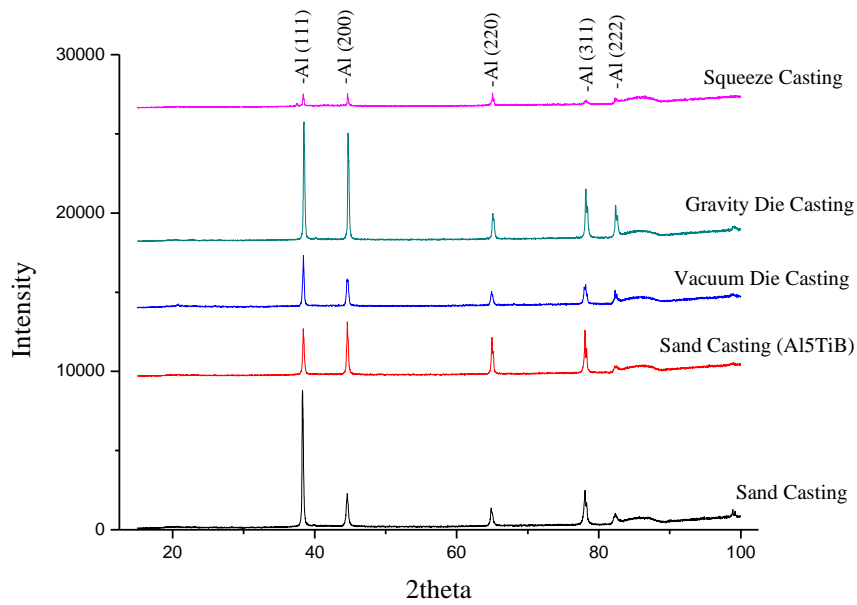


Figure 53. XRD results of casting for Al with indicated planes.

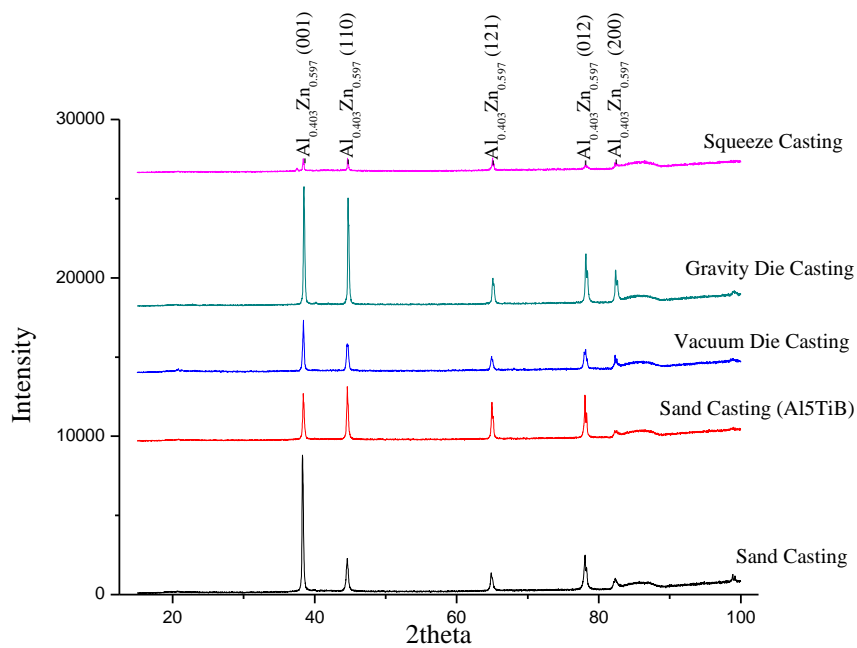


Figure 54. XRD results of casting for Al_{0.403}Zn_{0.597} with indicated planes.

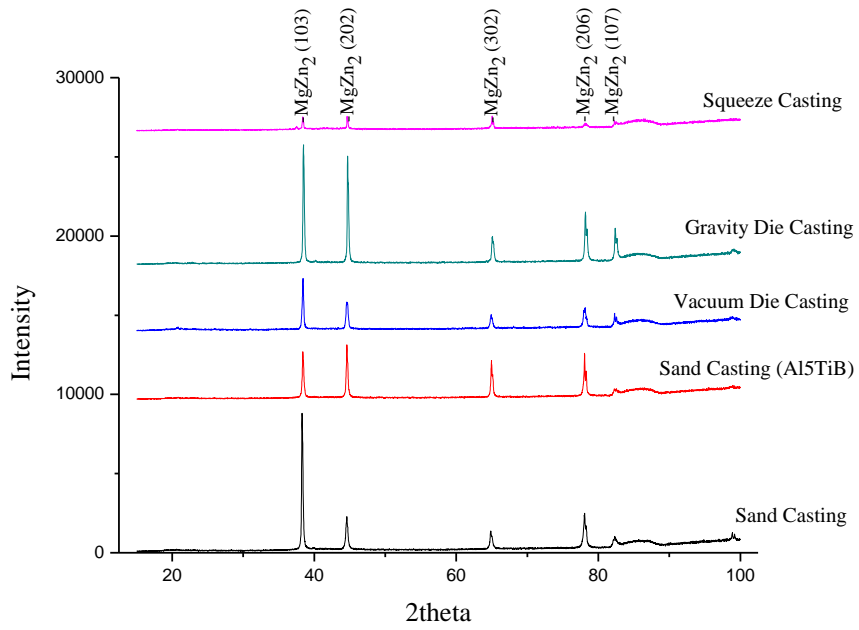


Figure 55. XRD results of casting for MgZn₂ with indicated planes.

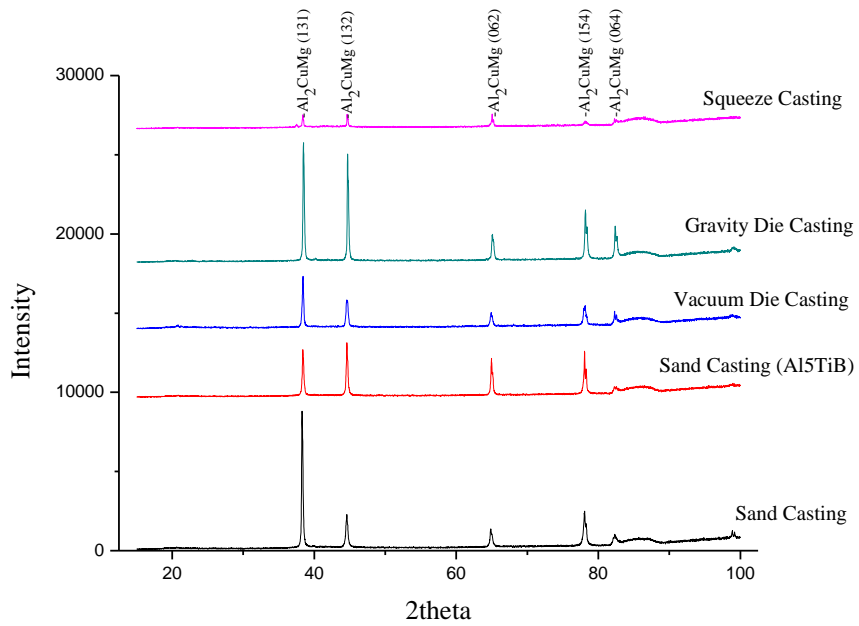


Figure 56. XRD results of casting for Al₂CuMg with indicated planes.

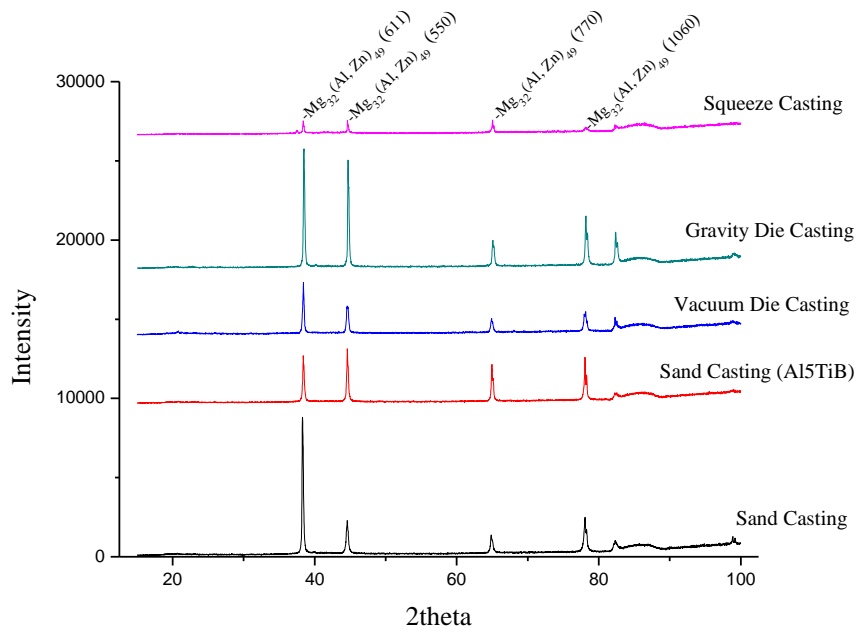


Figure 57. XRD results of casting for $Mg_{32}(Al, Zn)_{49}$ with indicated planes.

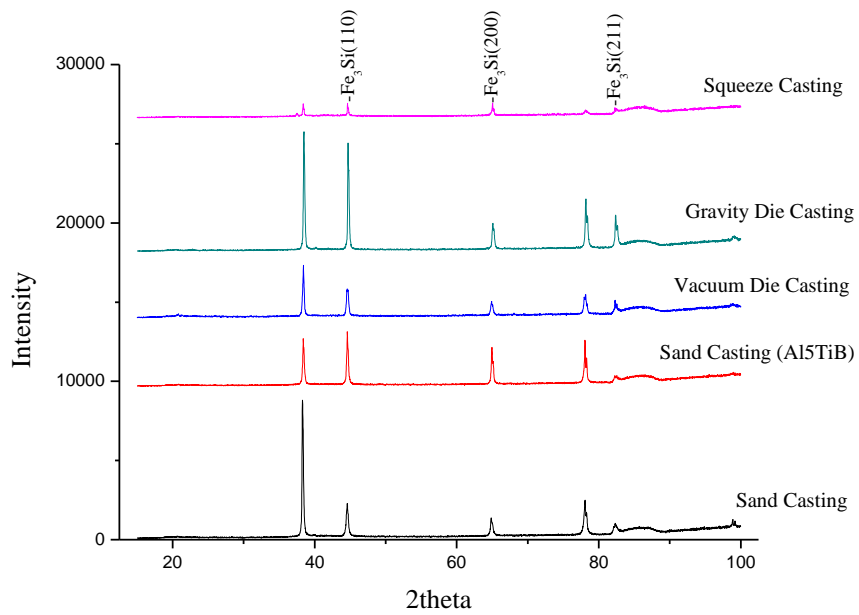


Figure 58. XRD results of casting for Fe_3Si with indicated planes.

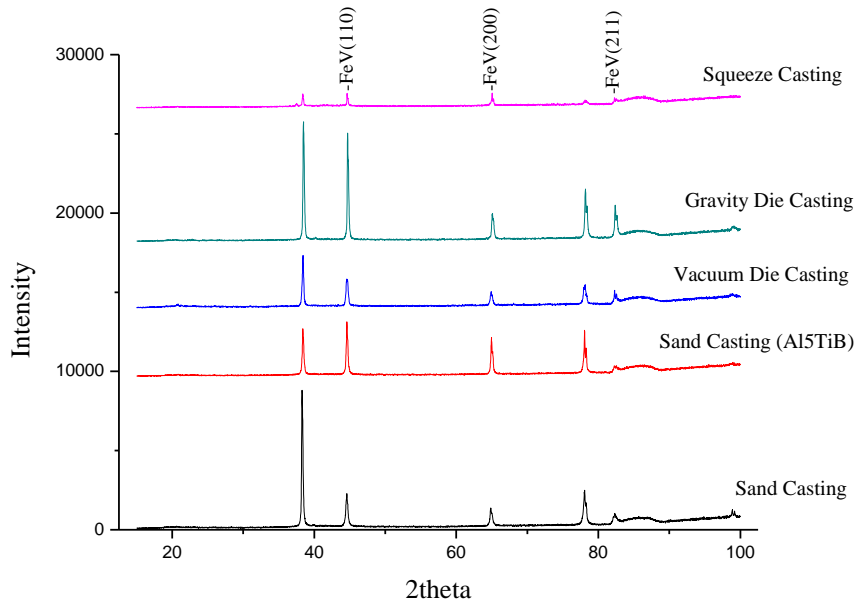


Figure 59. XRD results of casting for FeV with indicated planes.

4.6. Thermal Analysis and Solid Fraction Calculations

Thermal analysis and solid fraction calculation experiment is applied to remelted extruded billet of 7075 aluminum alloy at $0.25^{\circ}\text{C}/\text{s}$ cooling rate and modified 7075 aluminum alloys at different cooling rates; $0.04^{\circ}\text{C}/\text{s}$, $0.25^{\circ}\text{C}/\text{s}$ and $0.38^{\circ}\text{C}/\text{s}$. These cooling rates are obtained during experiments. According to the experimental data following graphs were obtained. The reason for experimenting modified 7075 alloy is to modify semi solid castability properties of 7075 alloy. Modifications in the chemical composition of the alloy were performed based on the study of Atkinson [56].

4.6.1. Extrusion Billet of 7075 Aluminum Alloy at 0.25°C/s Cooling Rate

Variation of temperature against time for 7075 aluminum alloy at 0.25°C/s cooling rate can be seen in Figure 60. Figure 61 and Figure 62 demonstrate first derivative and solid fraction of solidifying 7075 aluminum alloy at 0.25°C/s cooling rate with respect to time.

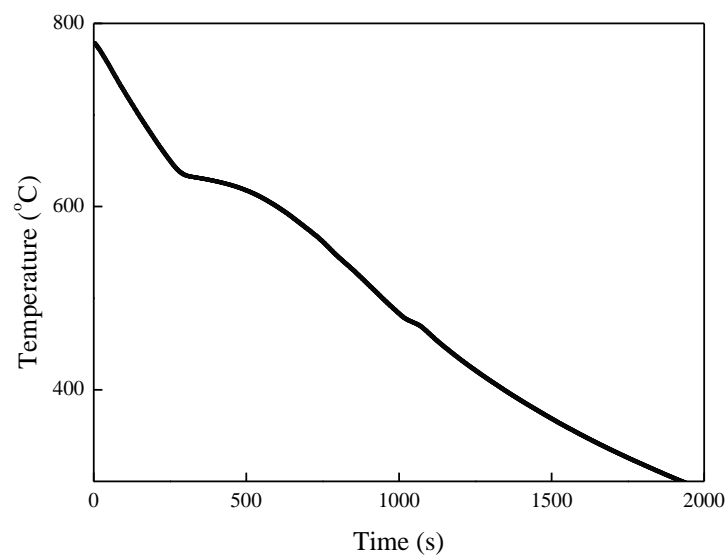


Figure 60. Temperature vs. time graph of Extrusion billet of 7075 aluminum alloy at 0.25°C/s cooling rate.

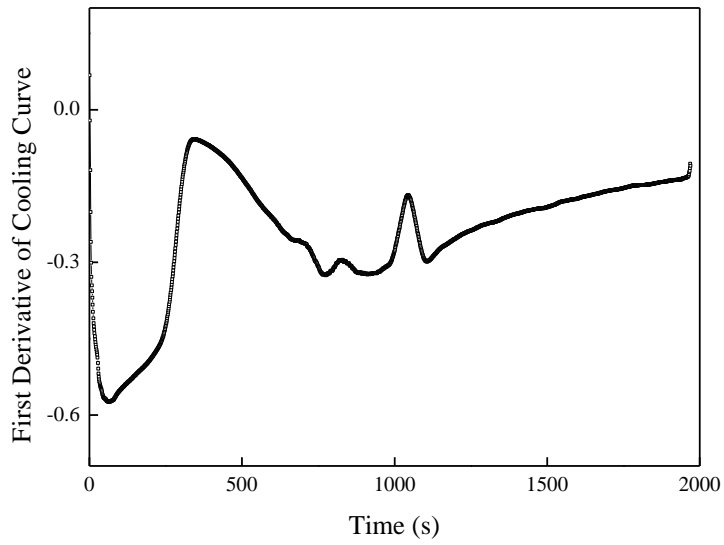


Figure 61. First derivative $\left(\frac{dT}{dt}\right)_{cc}$ vs. time graph of Extrusion billet of 7075 aluminum alloy at 0.25°C/s cooling rate.

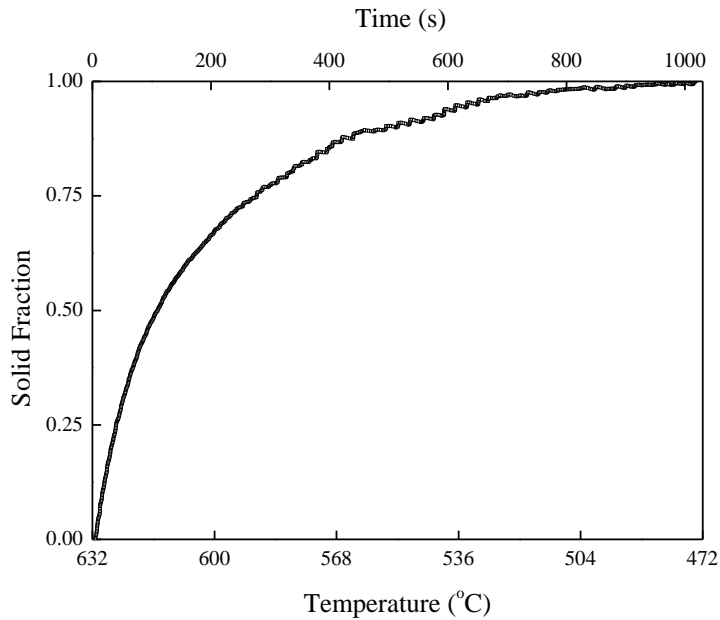


Figure 62. Solid fraction vs. temperature and time graph of Extrusion billet of 7075 aluminum alloy at 0.25°C/s cooling rate.

4.6.2. Modified 7075-1 Aluminum Alloy at 0.04°C/s Cooling Rate

Cooling curve for modified 7075-1 aluminum alloy at 0.04°C/s cooling rate can be seen in Figure 63. Figure 64 and Figure 65 demonstrate first derivative and solid fraction of solidifying modified 7075-1 aluminum alloy at 0.04°C/s cooling rate with respect to time.

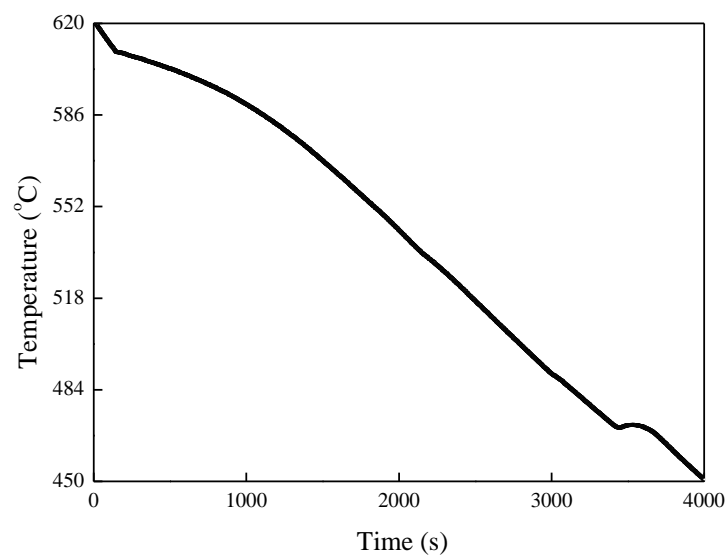


Figure 63. Temperature vs. time graph of modified 7075-1 aluminum alloy with 0.04°C/s cooling rate.

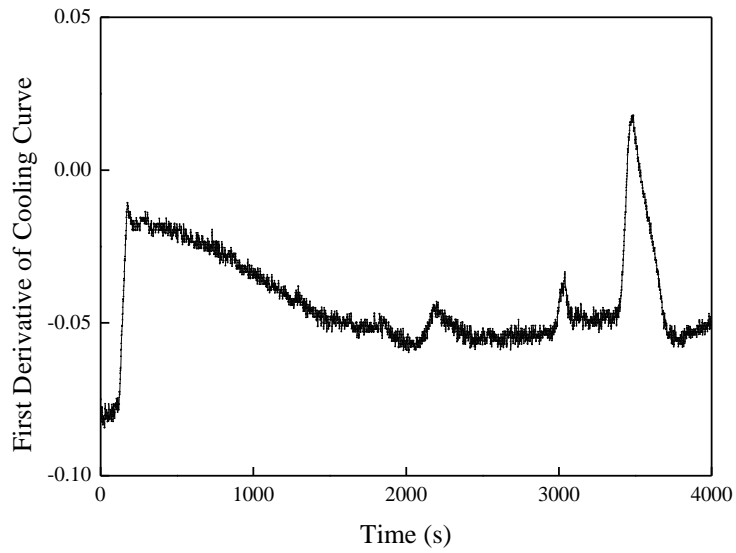


Figure 64. First derivative $\left(\frac{dT}{dt}\right)_{cc}$ vs. time graph of modified 7075-1 aluminum alloy with 0.04°C/s cooling rate

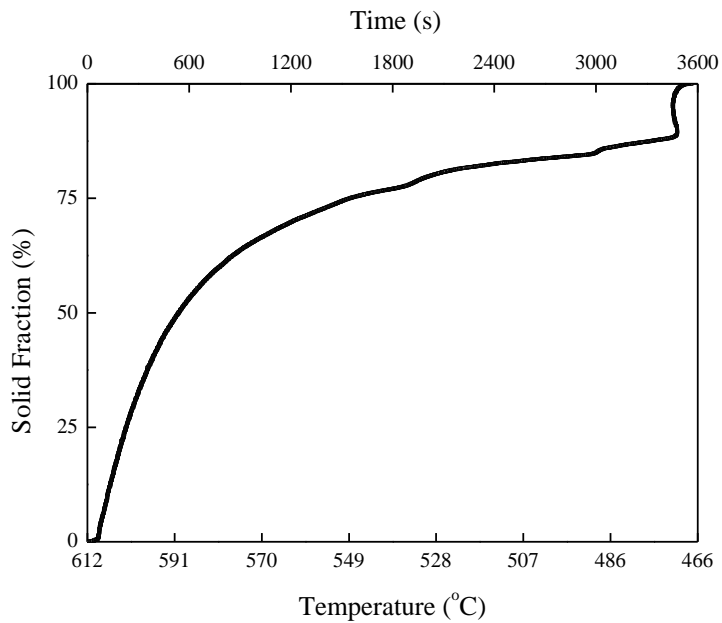


Figure 65. Solid fraction (%) vs. temperature graph of modified 7075-1 aluminum alloy with 0.04°C/s cooling rate.

4.6.3. Modified 7075-1 Aluminum Alloy 0.25°C/s Cooling Rate

Temperature with respect to time graph for modified 7075-1 aluminum alloy at 0.25°C/s cooling rate can be seen in Figure 66. Figure 67 and Figure 68 show first derivative and solid fraction of solidifying modified 7075-1 aluminum alloy at 0.25°C/s cooling rate with respect to time.

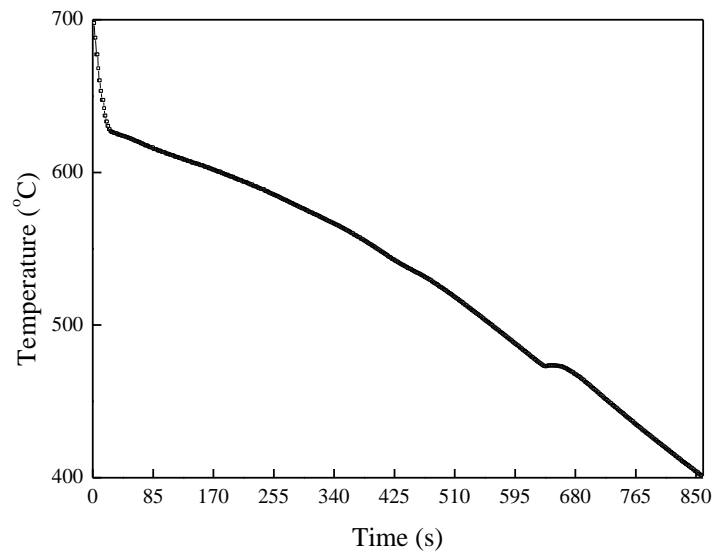


Figure 66. Temperature vs. time graph of modified 7075-1 aluminum alloy with 0.25°C/s cooling rate.

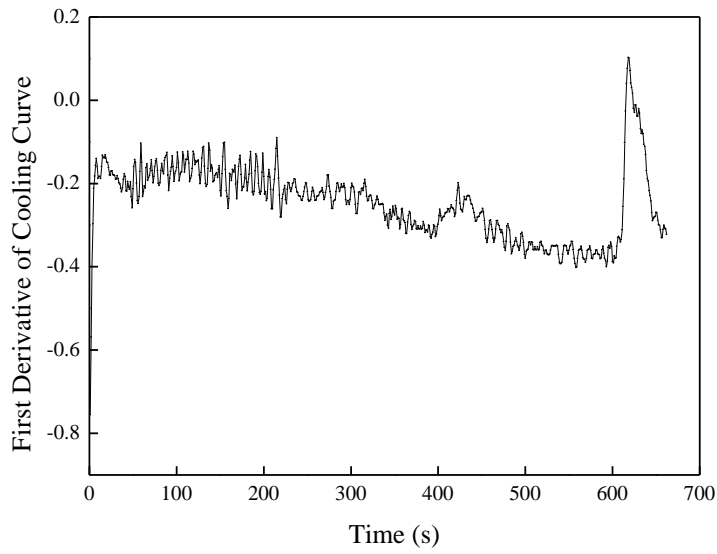


Figure 67. First derivative $\left(\frac{dT}{dt}\right)_{cc}$ vs. time graph of modified 7075-1 aluminum alloy with 0.25°C/s cooling rate.

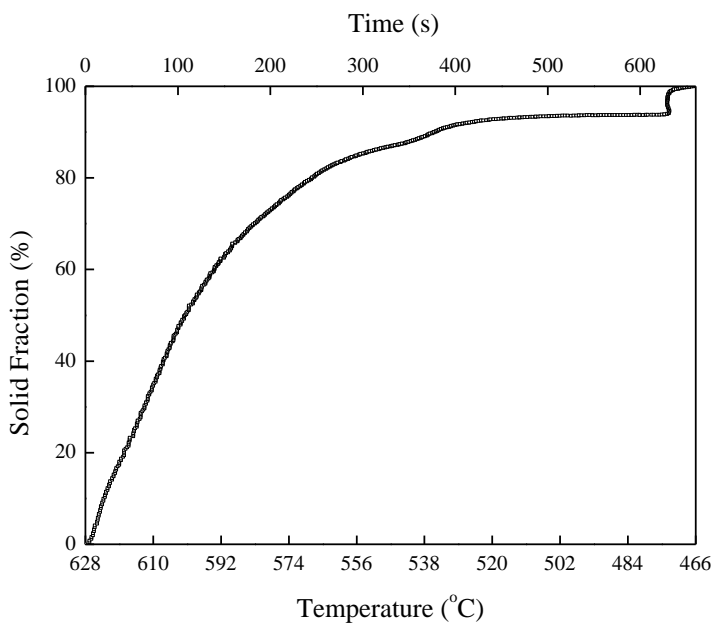


Figure 68. Solid fraction (%) vs. temperature graph of modified 7075-1 aluminum alloy with 0.25°C/s cooling rate

4.6.4. Modified 7075-2 Aluminum Alloy 0.38°C/s Cooling Rate

Cooling curve for modified 7075-2 aluminum alloy at 0.38°C/s cooling rate can be seen in Figure 69. Figure 70 and Figure 71 illustrate first derivative and solid fraction of solidifying modified 7075-2 aluminum alloy at 0.38°C/s cooling rate with respect to time.

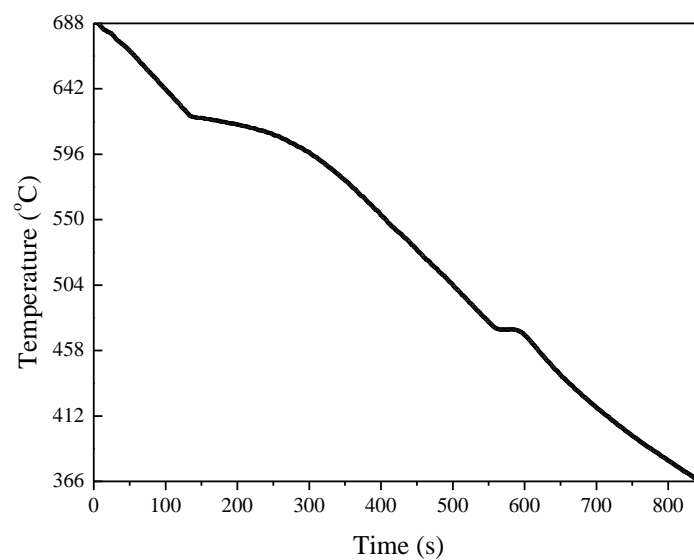


Figure 69. Temperature vs. time graph of modified 7075-2 aluminum alloy with 0.38°C/s cooling rate.

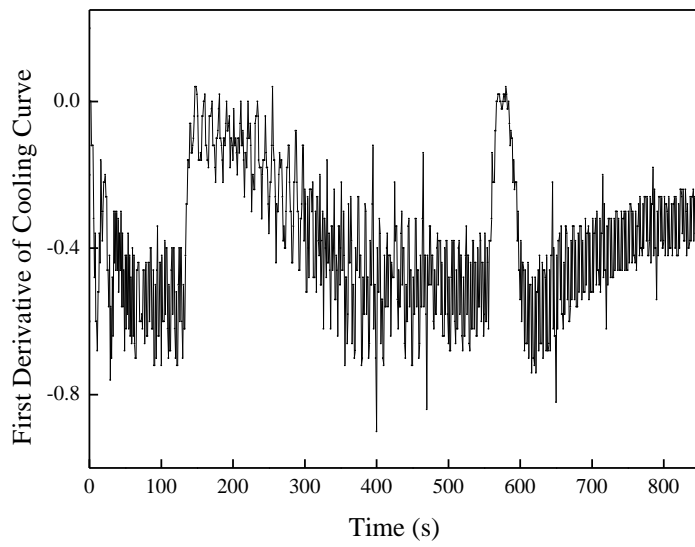


Figure 70. First derivative $\left(\frac{dT}{dt}\right)_{cc}$ vs. time graph of modified 7075-2 aluminum alloy with 0.38°C/s cooling rate.

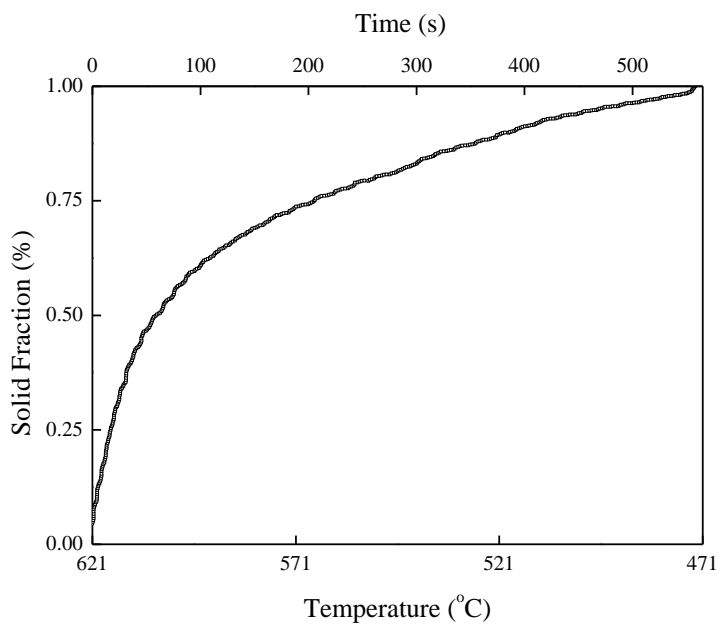


Figure 71. Solid fraction vs. temperature graph of modified 7075-2 aluminum alloy with 0.38°C/s cooling rate.

Table 15 shows chemical composition differences between literature and this work. Table 16 also shows critical temperatures of these works. As comparing same cooling rates of different alloy, it can be concluded that liquidus temperature decreases with increasing amount of Mg addition. It can be clearly seen that Zn and Cu addition to the alloy can only have a decrease in liquidus temperature when modified 7075-1 and modified 7075-2 alloys are compared. When these values are compared with the literature data, they show some differences due to variation in chemical compositions. Even though Ahmad shows that solidus and eutectic temperatures are increasing with increasing cooling rate [56], in this experiment this trend cannot be observed. This may be due to variation of surrounding temperature. Since, variation of temperature during the environment can also affect cooling rates and solid fraction [58].

Table 15. Literature comparison of chemical compositions of the alloys used at thermal analysis experiments.

Source	Zn (wt. %)	Mg (wt. %)	Cu (wt. %)	Mn (wt. %)	Fe (wt. %)	Si (wt. %)	Ti (wt. %)	Al (wt. %)
Modified 7075-1	5.97	4.85	1.55	0.06	0.43	0.34	0.04	86.4
Modified 7075-2	6.96	4.68	2.63	0.05	0.23	0.21	0.04	84.9
Bäckerud[59]	-	2.49	1.36	-	0.28	0.11	-	Bal.
Ahmad[57]	6.04	2.38	2.02	0.12	0.24	0.14	0.09	88.5
ASM[5]	5.1- 6.1	2.1- 2.9	1.2- 2.0	<0.3	<0.5	<0.4	<0.2	87.1- 91.4

Table 16. Literature comparison of thermal data obtained during thermal analysis experiments.

Source	Cooling Rate(°C/s)	Liquidus Temperature(°C)	Eutectic Temperature(°C)	Solidus Temperature(°C)
7075	0.25	631.2	478.1	473.8
Modified 7075-1	0.04	623.1	476.2	471.1
Modified 7075-1	0.25	628.2	473.2	466.5
Modified 7075-2	0.38	621.5	485.3	472.8
Ahmad[57]	0.03	639.9	470.2	467.6
Ahmad[57]	0.21	638.0	474.7	470.2
Ahmad[57]	0.41	638.2	477.2	472.8
Bäckerud[59]	0.30	630.0	469.0	469.0
Bäckerud[59]	0.70	630.0	470.0	470.0
ASM[5]		635.0		477.0

When 7075 and modified 7075-1 are compared with the same cooling rate, it can be seen that liquidus temperature is almost the same. However, solidus and eutectic temperatures are different.

4.7. Semi-Solid Casting with Vertical Pressure Die Casting

Processing of 7075 alloy was performed by semi-solid forming with vertical squeeze casting press, there are three samples that are produced and T6 heat treatment. First sample was processed at 580°C. This temperature corresponds to 0.8 solid fraction according to Figure 62. The thickness of the first sample is reduced from 20 mm to 13.9 mm. The first sample also has hardness value as 180 ± 5 HB. Second sample is pressed at 595°C which corresponds to 0.67 solid fraction. Thickness of the second sample was reduced from 20mm to 11.1 mm. This sample has hardness value which is 173 ± 5 HB. Third sample was pressed at 605°C that matches with 0.62 solid fraction value. Third sample has 158 ± 9 HB hardness value and also 10.8 mm thickness.

Table 17. The process data of semi-solid casting with vertical squeeze casting.

Part No.	Experimental Temperature (°C)	Solid Fraction	Thickness (mm)	Hardness (HB)	UTS (MPa)	Yield Strength (MPa)	Elongation (%)
1	580	0.80	13.9	180 ± 5	246.6	212.5	2.6
2	595	0.67	11.1	173 ± 5	583.0	526.0	4.6
3	605	0.62	10.8	158 ± 9	302.0	292.0	0.9

It is seen from Table 17 that as solid fraction increases, formability (thickness reduction) decreases. However, formability does not change after a certain point of solid fraction. It can be observed that hardness values are decreasing with decrease in solid fraction. This can be explained by second phase densities of specimens. Furthermore, UTS and elongation values can be seen as 2nd part has the highest UTS and elongation values. However, 1st and 3rd parts' tensile tests are resulted in a premature break due to cracks on the holding part of tensile specimens. On the other hand, when 0.67 solid fraction has reached the target value of 505 MPa yield strength and 150 HB hardness value were obtained. Table 18 illustrates a comparison between values of reduction rates and hardness values and second phase fractions. Figure 72, Figure 73, Figure 74 and Figure 75 are the SEM photographs of parts. Precipitate size and distribution can be seen in these figures.

Table 18. Comparison between values of reduction rates, hardness values and second phase densities.

Part No.	Reduction Rate (%)	Hardness (HB)	Second Phase Fraction (%)
1	30.5	180 ± 5	2.096
2	44.5	173 ± 5	1.534
3	46	158 ± 9	1.058

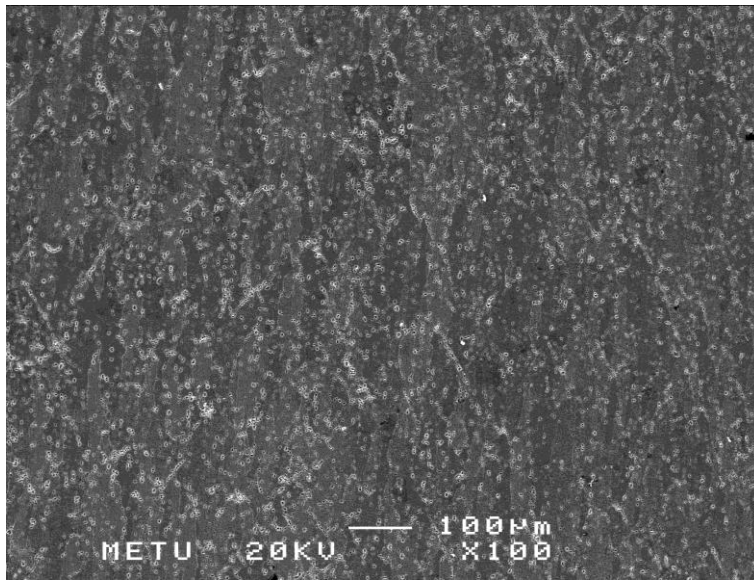


Figure 72. SEM picture of semi-solid casting specimen 1 at 580°C.

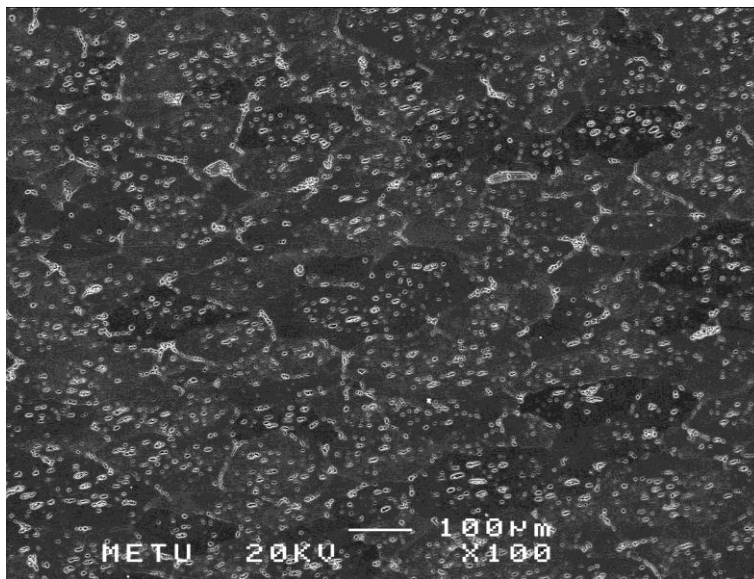


Figure 73. SEM picture of semi-solid casting specimen 2 at 595°C.

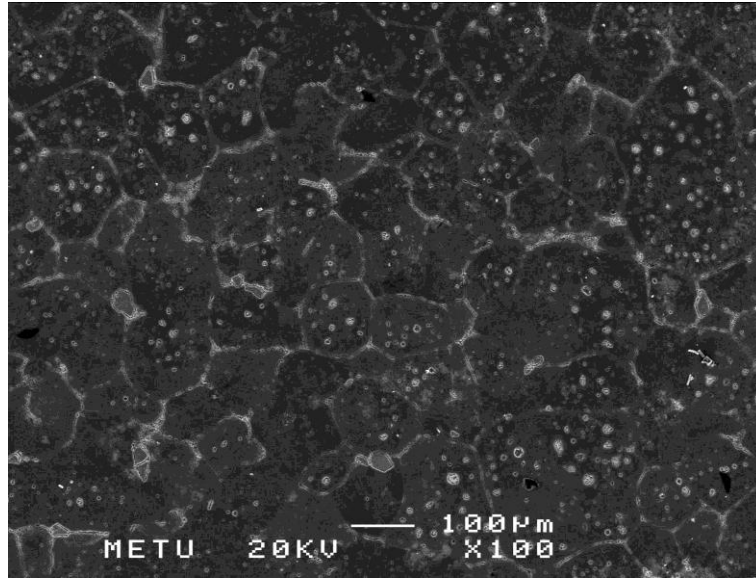


Figure 74. SEM picture of semi-solid casting specimen 3 at 605°C with 100x magnification.

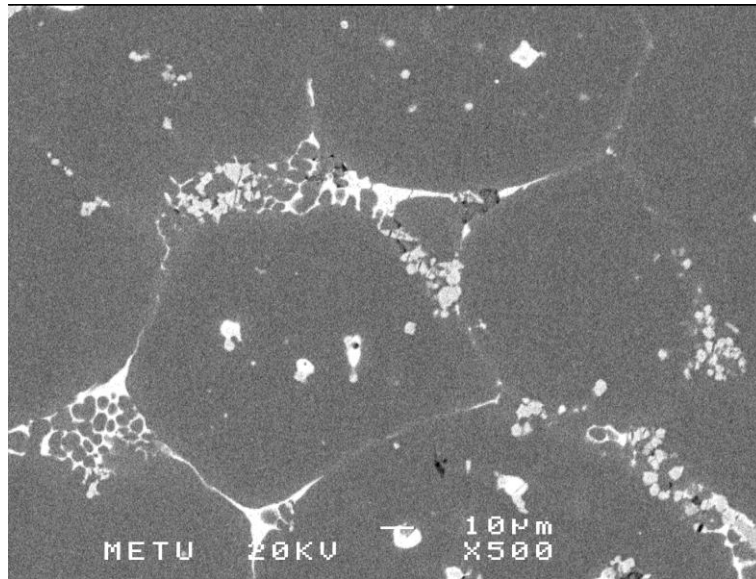


Figure 75. SEM picture of semi-solid casting specimen 3 at 605°C with 500x magnification.

4.8. Pressure Die Casting

Pressure die casting experiment was done at just above liquidus temperature of 7075 which is about 630°C and then molten alloy was poured into the relatively cold die which was below 250°C. It takes about 10-15 seconds to close the die and squeeze the alloy. It is experienced that, 10 to 15 seconds cooling make great differences to alloys temperature. If it is considered as cooling in an isolated graphite pot, it would make its temperature just below liquidus. However, since there are more surface area to cool the molten alloy, cooling rate will be higher. From experience of modified 7075-2 with a cooling rate of 0.38°C/s, it can be predicted that 1 or 2°C cooling occurs during processing which gives 4-8% solid phase. This small amount of solid causes some problems like hot tear [60] or liquid segregation [61] since it is assumed as thixoforming. 2 specimens are made by this method. One of them is made from 7075 extrusion billet and the other one is made from scrap 7075. Chemical composition differences between the two specimens are given at Table 19. During macroscopic inspection of the specimens, it is seen that problems like surface cracks, shrinkage and bad surface quality are observed. However, blister was not observed after T6 heat treatment to the specimens. Since, it not possible to make a tensile specimen due to the cracks, hardness values of specimens were investigated.

Table 19. Comparison of chemical compositions of alloys produced during pressure die casting experiments.

Specimen	Zn (wt. %)	Mg (wt. %)	Cu (wt. %)	Fe (wt. %)	Si (wt. %)	Al (wt. %)
Extr. 7075	6.04	2.06	1.20	0.15	0.09	90.1
Scrap 7075	5.27	2.56	1.84	0.18	0.24	89.4

Table 20. Hardness values of pressure die cast samples.

Specimen	Hardness (HB)
Extr. 7075	156 ± 11
Scrap 7075	175 ± 5

As can be seen from Table 20 hardness values are between 156 and 175 HB. This hardness difference is believed due to the chemical composition differences and heat distribution in the furnace during heat treatment. Because hardness values of extruded 7075 show hardness value distribution from 144 HB to 173 HB. Furthermore, T6 heat treatment may cause more precipitation, yielding MgZn₂ intermetallic phase precipitate yielding higher hardness values [62].

4.9. Semi-Solid Metal Casting

In semi-solid metal casting experiment, 6 specimens from modified 7075-2 alloy and two specimens of 7075 alloy were produced. Specimens were pressed at 620°C, 616 °C, 602 °C, 624 °C, 613 °C and at fully liquid state as modified 7075-2 alloy. Also, two specimens of 7075 alloy are pressed at 630°C. These temperatures correspond to 0.01, 0.265, 0.535, 0 and 0.351 solid fractions for modified 7075-2 and 0.04 to 0.075 solid fraction range for extruded 7075 alloy respectively. Then, T6 heat treatment was applied to these at 480°C for 17 hours to solutionize and 121°C for 34 hours for artificial aging for modified 7075-2 alloy [162]. The same T6 procedure (times and temperatures) were used for extruded 7075. After heat treatment, it was observed that large amount of oxidation occurred on the specimens (diameters of tensile specimens are enlarged from 19mm to approximately 20mm). Even though there are large oxidation on the surface, tensile test could be made. Ultimate tensile strength, elongation at break, pouring temperature and solid fraction values are given in Table 21.

Table 21. Ultimate tensile strength, elongation at break, pouring temperature and solid fraction values.

Specimen	Pouring Temperature (°C)	Solid Fraction	UTS (MPa)	Elongation at Break (%)
1 st of mod. 7075-2	620	0.010	145	6.56
2 nd of mod. 7075-2	616	0.265	115	7.69
3 rd of mod. 7075-2	602	0.535	196	11.45
4 th of mod. 7075-2	624	0	162	8.87
5 th of mod. 7075-2	613	0.351	165	6.42
6 th of mod. 7075-2	Above liquidus	0	207	5.91
1 st of extr. 7075	630	0.040-0.075	268	4.16
2 nd of extr. 7075	630	0.040-0.075	185	4.71

After tensile test, it was observed that porosities exist in the specimens that cause premature breaks. Moreover, 4th specimen of modified 7075-2 alloy has a cavity in the middle of structure. Furthermore, atomization during high pressure die casting lets air entrapment porosities and cause blister problem after T6 heat treatment.

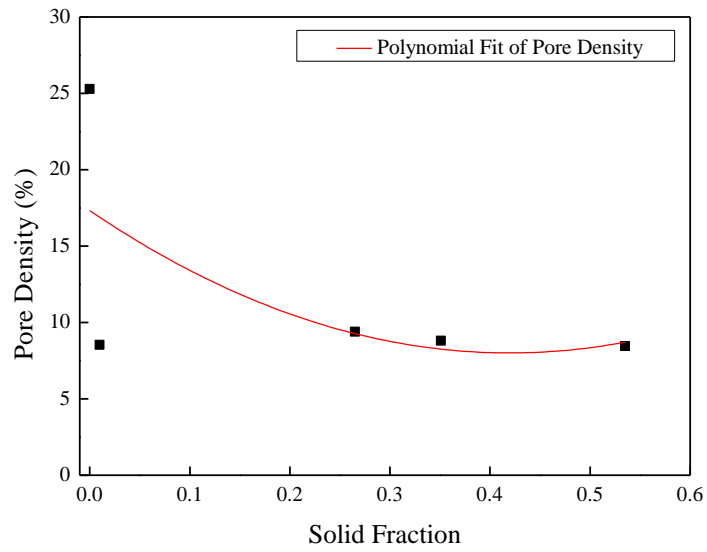


Figure 76. Pore density vs. solid fraction graph of modified 7075-2 alloy produced by semi solid metal casting.

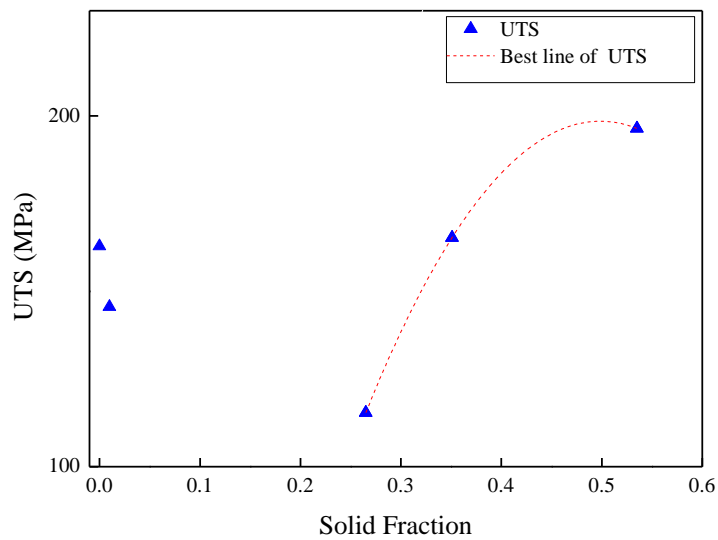


Figure 77. UTS vs. solid fraction graph of modified 7075-2 alloy produced by semi solid metal casting.

It can be clearly seen from Figure 76 that, pore density of specimens decrease with increasing solid fraction. This can be explained by micro liquid shrinkages decreases as liquid amount decrease. Furthermore, Figure 77 shows that if low solid fraction values are not included, higher solid fraction gives higher UTS values. Since, solid fraction increase causes less porous microstructure.

4.10. Strain Induced Melt Activation (SIMA)

Ultrasonic stirring and mechanical stirring methods were used in this experiment. Appearance of the pressed sample of mechanically stirred alloy was relatively smoother than ultrasonic stirred specimen. However, there were little cracks on the surface which can be seen by naked eyes. Hardness results of mechanical stirred sample were found as 156 ± 6 HB. This hardness result shows that T6 heat treatment was successfully applied. There were 2 tensile specimens machined from disc shaped sample of mechanical stirring method. These samples were tested and results are given in Table 22. According to tensile test results, it can be interpreted that even though target tensile strength could not be reached, mechanical stirring method provided satisfactory results. However, it can be seen that elongation result is fairly lower than target elongation value.

It was observed that ultrasonic stirring caused molten alloy to cool faster due to vibration in the mold which gave more homogenized temperature distribution through the air cooled copper mold and led a higher cooling rate [63, 64]. Appearance of ultrasonic stirred specimen was poor with respect to mechanical stirred specimen. There were deep crack on the surface. It is believed that higher liquid fraction caused this cracks during pressing. However, 2 tensile test specimens were removed from ultrasonic stirred disc shaped sample. One of the test specimens had a large crack that cannot be tested. Other tensile test specimen was tested but, it failed prematurely due to a small crack which could not be noticed.

However, tensile test results can be seen in Table 22. Hardness test was conducted on specimens and it resulted as 151 ± 12 HB. This hardness test result is coherent with target hardness value. Moreover, high standard derivation value is a result of cracked structure of disc shaped specimen.

Table 22. Tensile test results of SIMA experiment.

	Ultrasonic Stirring	Mechanical Stirring
UTS (MPa)	211	397 ± 32
YS (MPa)	-	343 ± 31
EL%	1.6	3 ± 0.3

Grain size analysis performed on specimens of both methods. Ultrasonic stirred specimen yielded $70 \mu\text{m}$ average grain size. On the other side, mechanical stirred specimen had average grain size as $78 \mu\text{m}$. It can be concluded that ultrasonic stirring provide 10% finer grains than mechanically stirring. Figure 78 and Figure 79 shows microstructure images which were obtained by optical microscopy with 100x magnification. Furthermore, SEM images of samples can be seen in Figure 80, Figure 81 and Figure 82.

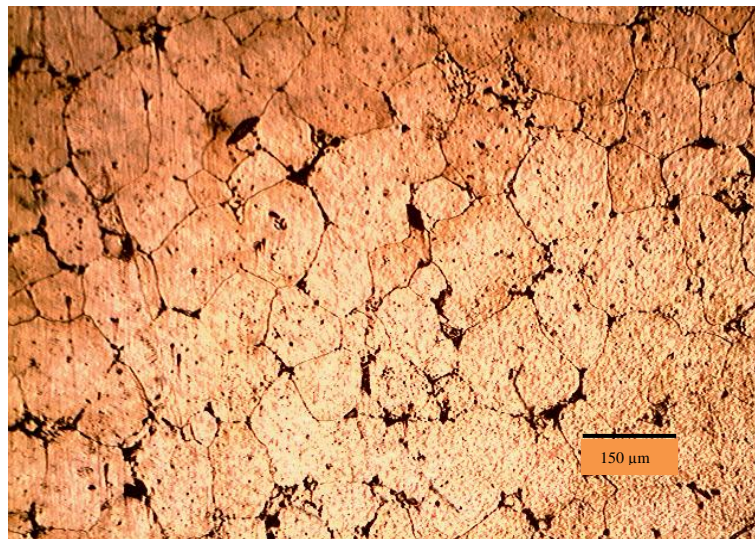


Figure 78. Microstructure image of ultrasonic stirred specimen (100x)

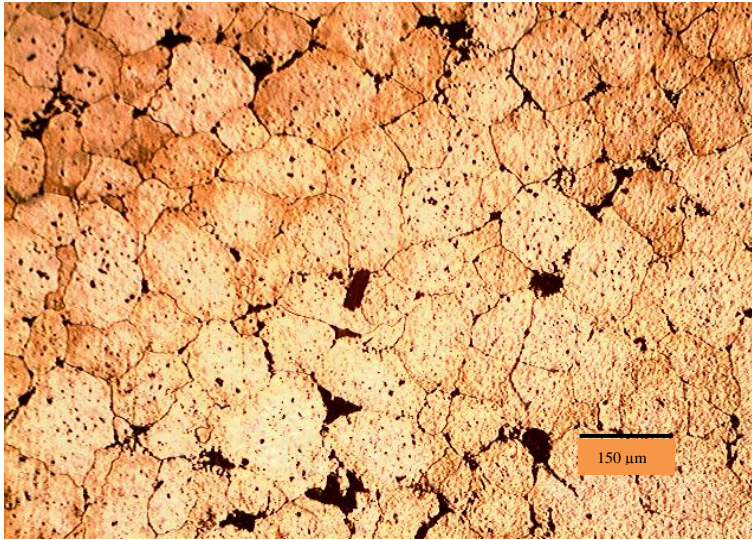


Figure 79. Microstructure image of mechanical stirred specimen (100x).

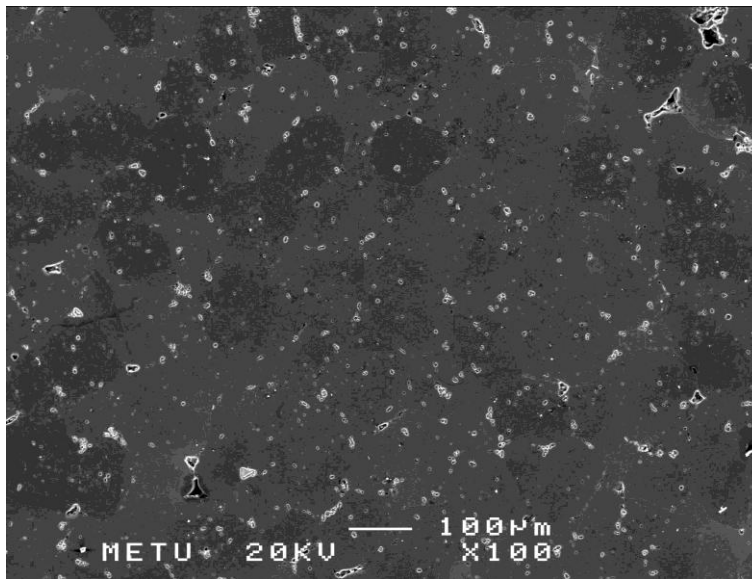


Figure 80. SEM image of mechanical stirred specimen (100x).

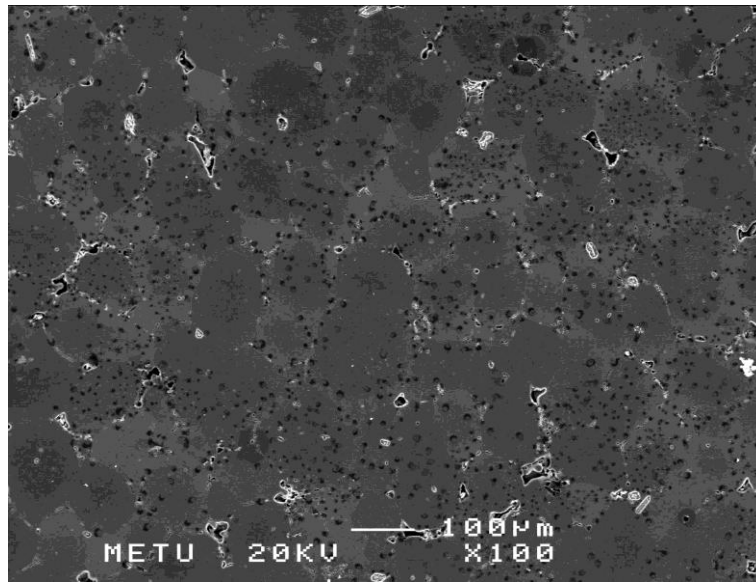


Figure 81. SEM image of mechanical stirred specimen (100x).

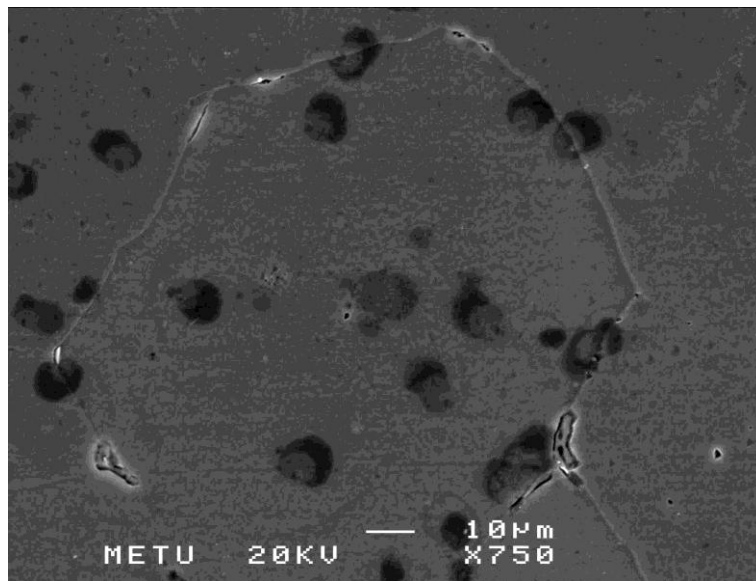


Figure 82. SEM image of mechanical stirred specimen (750x).

CHAPTER 5

CONCLUSIONS

To replace extruded, T6 heat treated and machined 7075 rifle receiver body with as cast and T6 heat treated perform that requires less machining before to be used as rifle mechanism body receiver, several casting methods and heat treatments were experimentally practiced to achieve a near net shape product without blistering problem after T6 heat treatment in this work. Main focus is on to achieve high hardness and tensile properties of cast and heat treated alloy. Pore densities and average grain size of specimens were obtained to assess their direct effect on tensile properties. Solid fractions were calculated via Newtonian thermal analysis method for semi-solid casting. Moreover, the effect of grain refinement and vacuum application were observed during experiments. After these experiments, following statements were concluded:

1. Vacuum assisted permanent die casting improves hardness values of the specimen while slightly decreasing average grain size to 38 μm . Vacuum helps decreasing pore density which cause increase in hardness. Vacuum also helps the molten alloy to solidify faster by decreasing average grain size. Moreover, no blister was observed after T6 heat treatment.
2. Al5TiB usage as grain refiner results with finer grain and slightly higher hardness. It was observed that 0.18% additive of Al5TiB to molten alloy resulted 24.5% finer grains in sand casting. Furthermore, hardness increased by 6%.
3. Mg addition to the alloy decreases the liquidus temperature by 8-10 $^{\circ}\text{C}$. As comparison is made between same cooling rate and different chemical composition, it can be seen that good correlations could be obtained with

work of Ahmad. Hence, Zn amounts of modified 7075-1 and Ahmad are identical, it can be seen that Mg is the only distinctive element.

4. Blistering was observed after heat treatment of high pressure die casting and squeeze casting samples which can decrease tensile properties of samples even though squeeze casting provides lower grain size.
5. Optimum solid fraction was found to be 0.67 in semi-solid casting for 7075 aluminum alloy. Processing temperature 595°C corresponds to 0.67 solid fraction according to the Newtonian thermal analysis results. 583 MPa UTS, 526 MPa yield strength, 4.6% elongation and 173.4 HB were obtained at this solid fraction which is close to extruded 7075-T6 alloy.
6. Increasing solid fraction, UTS values are also increasing and pore density were found to be decreasing. Semi-solid casting samples showed that UTS values are improved with increase in solid fraction causing decrease in pore density.

CHAPTER 6

SUGGESTED FUTURE WORKS

This work is considered as pre-experiments of a commercializing production process. Semi-solid casting technique was chosen as the best method with the guide of this work. Following works can be suggested as future works:

- A special horizontal high pressure casting machine with high shot speed can be designed to obtain desired shape and mechanical properties with vertical die as in Figure 83.
- Semi-solid casting experiment can be performed with different parameters for better optimization.
- Semi-solid casting experiments can be performed on different alloys like 7085.
- Various heat treatments can be applied on produced 7075 to improve elongation results.

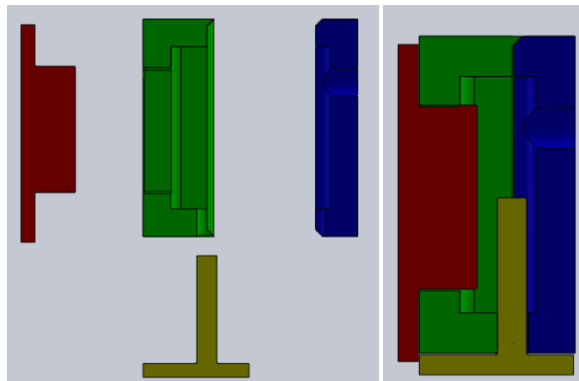


Figure 83. Designed suggested vertical die.

REFERENCES

1. Davis, J. R. and Associates, *Aluminum and Aluminum Alloys Handbook*. Prepared under the direction of the ASM International Handbook Committee, 1993, Materials Park, OH.: ASM International.
2. Totten, G., & MacKenzie, D. (2003). *Handbook of Aluminum: Physical Metallurgy and Processes*. (Vol. 1). Marcel Dekker.
3. M.F. Ashby, *Materials Selection in Mechanical Design*, 3rd Edition, 2005, Elsevier Butterworth-Heinemann.
4. Walker, R. (2013). *Cartridges and Firearm Identifications*. 1st ed. Boca Raton: CRC Press.
5. *ASM Handbook, Volume 02 - Properties and Selection: Nonferrous Alloys and Special-Purpose Materials*. (1990). S.I.: ASM International.
6. Aluminum Association. (2006). International alloy designations and chemical composition limits for wrought aluminum and wrought aluminum alloys. *The Aluminum Association, Arlington, Virginia*. Revised 2009.
7. Mueller L., Suffredini L., Bush D. (2006) Alcoa Green Letter Volume I: Alcoa 7085 Die Forgings. Cleveland, OHIO.
8. Handbook, A. S. M. (1991). Heat treating, vol. 4. *ASM International, Materials Park, OH*, 860.
9. Verhoeven, J. (1975). *Fundamentals of physical metallurgy*. New York: Wiley.
10. Totten, G. E., Xie, L., & Funatani, K. (2003). *Handbook of mechanical alloy design* (Vol. 164). CRC Press.
11. ASTM B918/B918M-09, "Standard Practice for Heat Treatment of Wrought Aluminum Alloys", ASTM International, West Conshohocken, PA, www.astm.org.
12. Emadi, D., Whiting, L. V., Nafisi, S., & Ghomashchi, R. (2005). Applications of thermal analysis in quality control of solidification processes. *Journal of thermal analysis and calorimetry*, 81(1), 235-242.

13. Phase Transitions and Differential Scanning Calorimetry. (n.d.). Retrieved December 13, 2014, from <http://www.dartmouth.edu/~pchem/75/pdfs/DSC.pdf>. Last accessed on May 01, 2015.
14. Çetin, A. (2008) *Assessment and modelling of particle clustering in cast aluminum matrix composites*, Middle East Technical University, Ankara, Turkey.
15. David Adrian, course materials for 10.37 Chemical and Biological Reaction Engineering, Spring 2007. MIT OpenCourseWare (<http://ocw.mit.edu>), Massachusetts Institute of Technology. Downloaded on [14 December 2014].
16. Emadi, D., & Whiting, L. V. (2002). Determination of solidification characteristics of Al-Si alloys by thermal analysis. *Transactions of the American Foundry Society, Vol. 110: Part 1*, 285-296.
17. Fan, Z. Semisolid Metal Processing. *Int. Mater. Rev.* 2002, 47 (2), 49–85.
18. Flemings, M. C. Semi-solid Forming: The Process and the Path Forward. *Metall. Sci. Technol.* 2000, 18 (2), 3–4.
19. Ube Industries Ltd, Thixoforming Technical Information Bulletin: Japan.
20. Hashmi, S. (2014). *Comprehensive Materials Processing*. Vol 5. Newnes. <http://dx.doi.org/10.1016/B978-0-08-096532-1.00516-1>. Last accessed on May 01, 2015.
21. Zhou, Y., Lu, J., Saluja, N. S., Riviere, V. A. (2000). Process for Producing Fine Grained Metal Compositions Using Continuous Extrusion for Semi-solid Forming of Shaped Articles. US Patent 6,120,625.
22. Kirkwood, D. H., Sellars, C. M., Boyd, L. G. E. (1992). Thixotropic Materials, US Patent 5,133,811.
23. Hirt, G., Kopp, R. (2009). *Thixoforming: Semi-solid Metal Processing*; Wiley-VCH Verlag GmbH & Co. KGaA: Weinheim.
24. Rassili, A., Geuzaine, C., Legros, W., Bobadilla, M., Cucatto, A., Robelet, M., Abdelfattah, S., Dohmann, J., Haornrad, C. H. (2000). Simulation of Adequate Inductive Heating Parameters and Magneto-thermal Coupling Involved in the SSM Processing of Steels. In *Proceedings of the 6th International Conference on Semi-solid Processing of Alloys and Composites*, Turin, Italy, pp 559–564.
25. ASM Handbook (2008). ASM International: Ohio, USA, Vol. 15, pp 761–782.

26. Flemings, M. C., Martinez, R. A. (2006). Principles of Microstructure Formation in Semi-solid Metal Processing. In Proceedings of the 9th International Conference on Semi-solid Processing of Alloys and Composites, Busan, Korea; pp 1–8.
27. Haga, T., Suzuki, S. (2001). Casting of Aluminium Alloy Ingots for Thixoforming Using a Cooling Slope. *J. Mater. Process. Technol.* 118, 169–172.
28. Haga, T. (2001). Semi-solid Roll Casting of Aluminium Alloy Strip by Melt Drag Twin Roll Caster. *J. Mater. Process. Technol.* 111, 64–68.
29. Sakamoto, K., Hamazoe, N., Ohwada, K., Suzuki, A. (2004). Method and Apparatus for Manufacturing Semi-solidified Metal. European Patent EP 1050353, issued November 24, 2004.
30. Kuroki, K., Suenaga, T., Tanikawa, H., Masaki, T., Suzuki, A., Umemoto, T., Yamazaki, M. (2004). Establishment of a Manufacturing Technology for the High Strength Aluminum Cylinder Block in Diesel Engines Applying a Rheocasting Process. In Proceedings of the 8th International Conference on Semi Solid Processing of Alloys and Composites, Limassol, Cyprus.
31. Yurko, J. A., Martinez, R. A., Flemings, M. C. (2002). Development of the Semi-solid Rheocasting (SSR) Process. In Proceedings of the 7th International Conference on Semi-solid Processing of Alloys and Composites, Tsukuba, Japan. pp 659–664.
32. Martinez, R. A., Flemings, M. C. (2005). Evolution of Particle Morphology in Semi-solid Processing. *Metall. Mater. Trans. A*, 36 (8), 2205–2210.
33. Kaneuchi, T., Shibata, R., Ozawa, M. (2002). Development of New Semi-solid Metal Casting Process for Automotive Suspension Parts. In Proceedings of the 7th International Conference on Semi-solid Processing of Alloys and Composites, Tsukuba, Japan; September; pp 145–150.
34. Hollingrath, J. Casting Metals. UK Patent n. 4371, 1819.
35. Chernov, D. K. Reports of the Imperial Russian Metallurgical Society, 1878.
36. Ghomashchi, M. R., Vikhrov, A. (2000). Squeeze Casting: An Overview. *J. Mater. Process. Technol.* 101, 1–9.

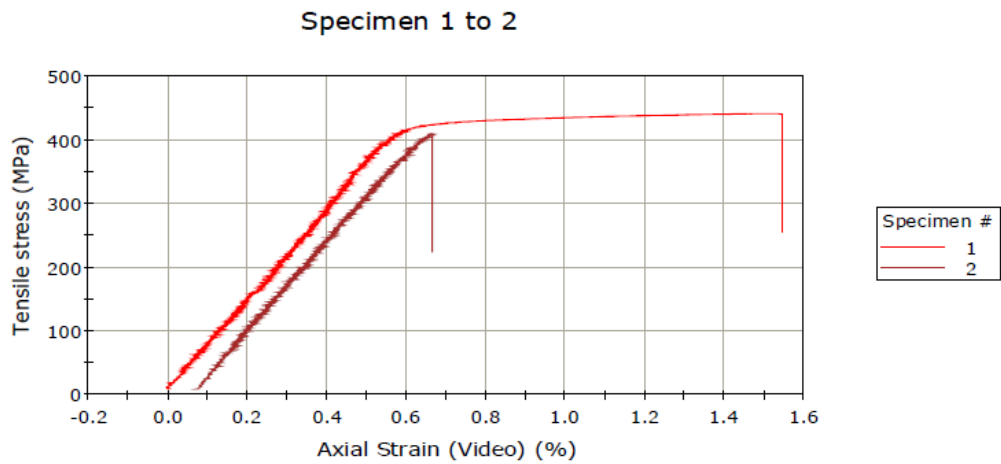
37. Hu, H. (1998). Squeeze Casting of Magnesium Alloys and Their Composites. *J. Mater. Sci.*, 33 (6), 1579–1589.
38. Czerwinski, F. (2008). Magnesium Injection Molding; Springer, November 4, pp 56–57.
39. Stefanescu, D. M. (1998). Casting.; 9th ed. In: *ASM Handbook* , Vol. 15; ASM International, 323–326.
40. Clyne, T. W., Withers, P. J. (1995). *An Introduction to Metal Matrix Composites*; Cambridge University Press, pp 321–325.
41. Kaufmann, H., Uggowitz, P. J. (2007). *Metallurgy and Processing of High Integrity Light Metal Pressure Castings*; Fachverlag Schiele & Schoen GmbH, pp 49–62.
42. Kaufman, J.G., Rooy, E.L., (2004) *Aluminum Alloy Castings: Properties, Processes, and Applications*, 29.
43. Friedrich, H. E., Mordike, B. L. (2006). *Magnesium Technology: Metallurgy, Design Data, Applications*; Springer, 259–261.
44. Kainer, K. U. (2003). *Magnesium Alloys and Technologies*; Wiley-VCH, pp 58–66.
45. Campbell, J. (2011). *Complete Casting Handbook: Metal Casting Processes, Techniques and Design*; Butterworth-Heinemann, pp 991–995.
46. Chakrabarti, A. K. (2005). *Casting Technology and Cast Alloys*; Prentice-Hall of India Pvt. Ltd, pp 124–126.
47. Rajagopal, S. (1981). Squeeze Casting: A Review and Update. *J. Appl. Metalwork*, ASM, 1 (4), 3–14.
48. Franklin, J. R., Das, A. A. (1984). Squeeze Casting – A Review of the Status. *Br. Foundrymen*, 77, 150–160.
49. Fujii, N., Okada, S., Morimoto, S., Fujii, M. (1984). Mass Effect of Al-8%Si Alloy in Squeeze Casting. *J. Jpn. Inst. Light Met.* 34, 446–453.
50. Handbook, A. S. M. (2008). Volume 15 Casting. *Materials Park: ASM International*.

51. Alat, E (2012) *Analysis Of Magnesium Addition, Hydrogen Porosity And T6 Heat Treatment Effects On Mechanical And Microstructural Properties Of Pressure Die Cast 7075 Aluminum Alloy*, Middle East Technical University, Ankara, Turkey.
52. ASTM B557M - 10 Standard Test Methods for Tension Testing Wrought and Cast Aluminum- and Magnesium-Alloy Products.
53. OKCU, I. Y. (2011) *Effect Of Process Parameters On Mechanical Properties Of High Pressure Die Cast Magnesium Az91 Components*, Middle East Technical University, Ankara, Turkey.
54. ASTM E 10 - 01 Standard Test Method for Brinell Hardness of Metallic Materials.
55. Kim, S. W., Kim, D. Y., Kim, W. G., & Woo, K. D. (2001). The study on characteristics of heat treatment of the direct squeeze cast 7075 wrought Al alloy. *Materials Science and Engineering: A*, 304, 721-726.
56. H. Atkinson, (2003). "Alloy Development for Thixoforming" Final Report for GR/M89096/01: 2003.
57. A.H.Ahmad, S.Naher, and D.Brabazon. (2013). "Thermal Profiles and Fraction Solid of Aluminium 7075 at Different Cooling Rate Conditions." *Key Engineering Materials* 554: 582-595.
58. J. W. Gibbs and P.F. Mendez, (2008). "Solid Fraction Measurement Using Equation Based Cooling Curve Analysis", *Scripta Materialia* 58 (2008) 699–702.
59. L. Backerud, G. Chai, J. Tamminen, (1991). *Solidification Characteristics of Aluminum Alloys. Volume 2: Foundry Alloys*. University of Stockholm.
60. D. Liu, H.V. Atkinson, P. Kapranos, W. Jirattiticharoean, H. Jones, (2003). *Mater. Sci. Eng. A*361, 213.
61. S. Chayong, H.V. Atkinson, P. Kapranos, (2005). "Thixoforming 7075 aluminium alloys" *Materials Science and Engineering A* 390, 3–12.
62. A.D. Isadare, B. Aremo, M. O. Adeoye, O. J. Olawale, M. D. Shittu., (2013). "Effect of Heat Treatment on Some Mechanical Properties of 7075 Aluminium Alloy", *Materials Research*; 16(1): 190-194.
63. Abu-Dheir N., Khraisheh M., Saito K., Male A. (2005), *Mater. Sci. Engg. A*, vol A393w, pp 109-117.

64. Abu-Dheir N (2004), Solidification of aluminum alloys, TMS, pp 361-368

APPENDIX A

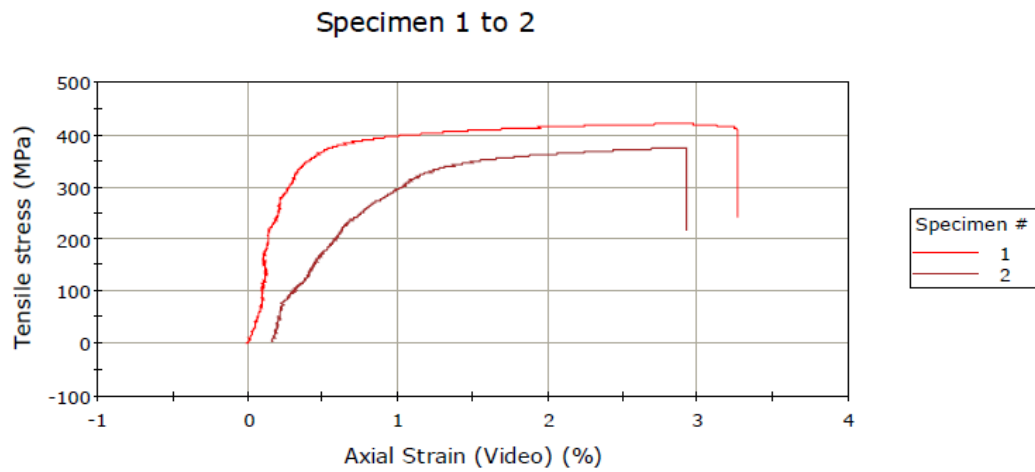
TENSILE TEST ANALYSIS



	Axial Strain (Video) at Break (Standard) (%)	Modulus (Automatic Young's) (MPa)	Tensile stress at Tensile Strength (MPa)
1	1.54375	77630.94595	441.35013
2	0.58716	73401.43672	409.84915

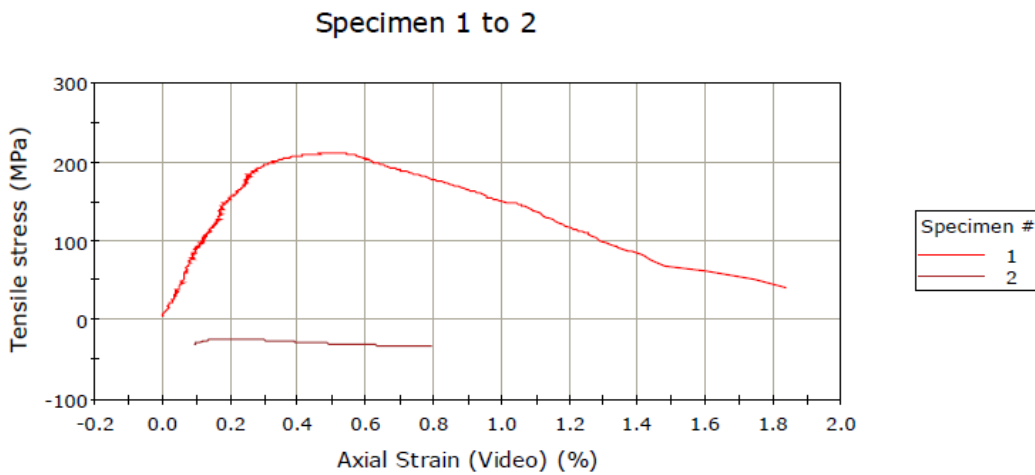
	Tensile stress at Yield (Offset 0.2 %) (MPa)
1	429.75139
2	300.80337

Figure 841. Tensile test results of squeeze casting experiment.



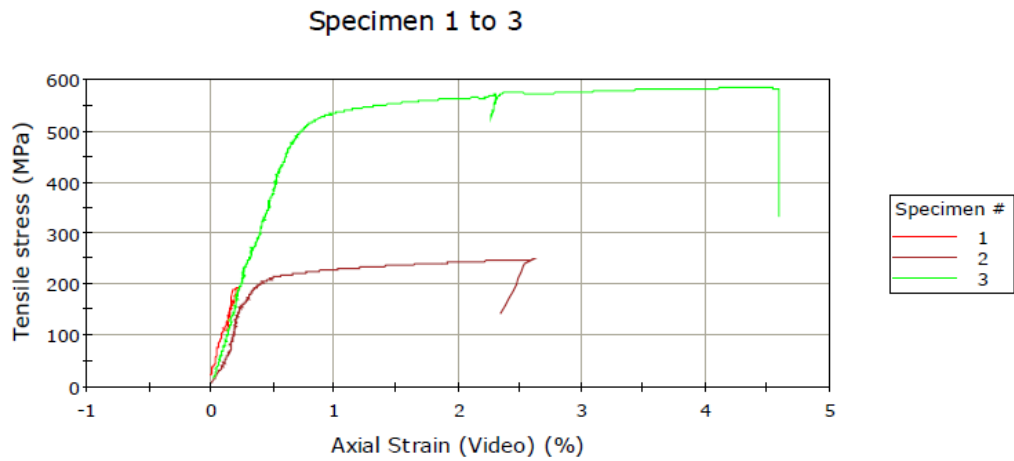
	Axial Strain (Video) at Break (Standard) (%)	Maximum Tensile stress (MPa)	Modulus (E-modulus) (MPa)	Tensile stress at Yield (Offset 0.2 %) (MPa)
1	3.26610	420.48700	118953.45459	365.47345
2	2.76167	374.42737	34862.96387	321.03377

Figure 85. Tensile test results of mechanical stirred SIMA sample.



	Axial Strain (Video) at Break (Standard) (%)	Maximum Tensile stress (MPa)	Modulus (E-modulus) (MPa)	Tensile stress at Yield (Offset 0.2 %) (MPa)
1	1.60623	211.67030	70103.44238	211.08792
2	0.70315	-24.59815	-----	-----

Figure 863. Tensile test results of ultrasonic stirred SIMA sample.



	Axial Strain (Video) at Break (Standard) (%)	Maximum Tensile stress (MPa)	Modulus (E-modulus) (MPa)	Tensile stress at Yield (Offset 0.2 %) (MPa)
1	0.18138	192.57904	-----	-----
2	2.60476	246.65300	77041.28418	212.54733
3	4.57701	583.12378	72247.79053	526.62436
4	0.93253	302.30682	47409.41162	292.99196

	Load at Maximum Tensile stress (N)
1	5035.59187
2	9276.59199
3	17890.01226
4	8070.02559

Figure 87. Tensile test results of semi-solid forming with vertical pressure die casting samples (Specimen 2: 1st test sample, specimen 3: 2nd test sample, specimen 4: 3rd test sample and specimen 1 is a failed sample.).

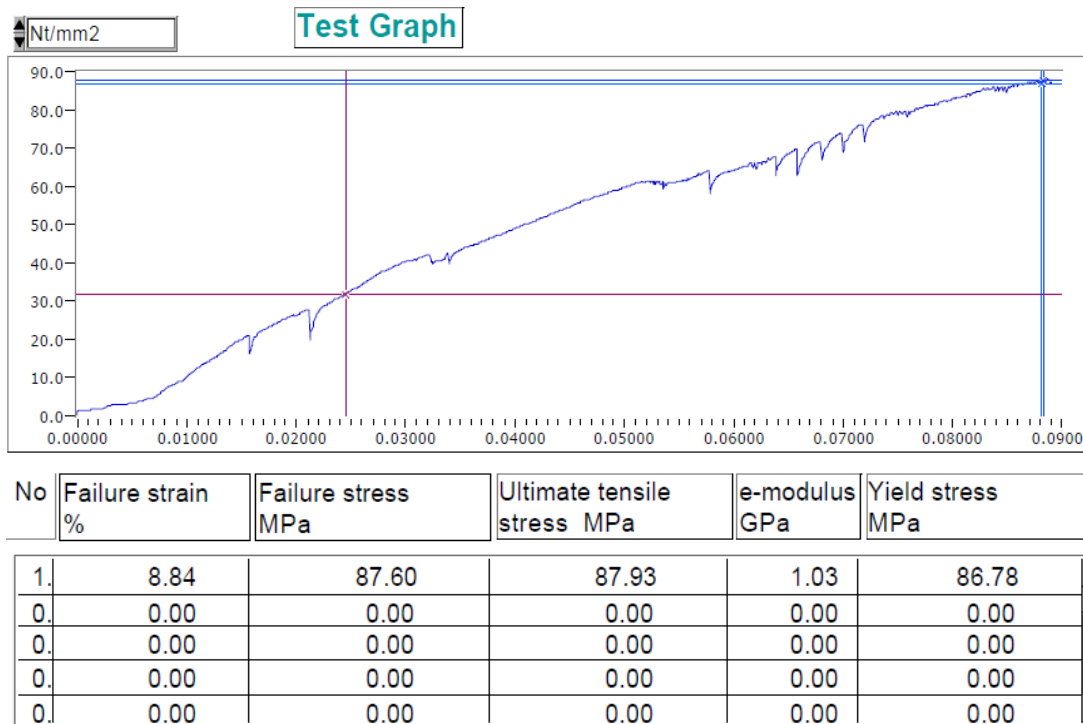


Figure 88. Tensile test result of sand casting specimen.

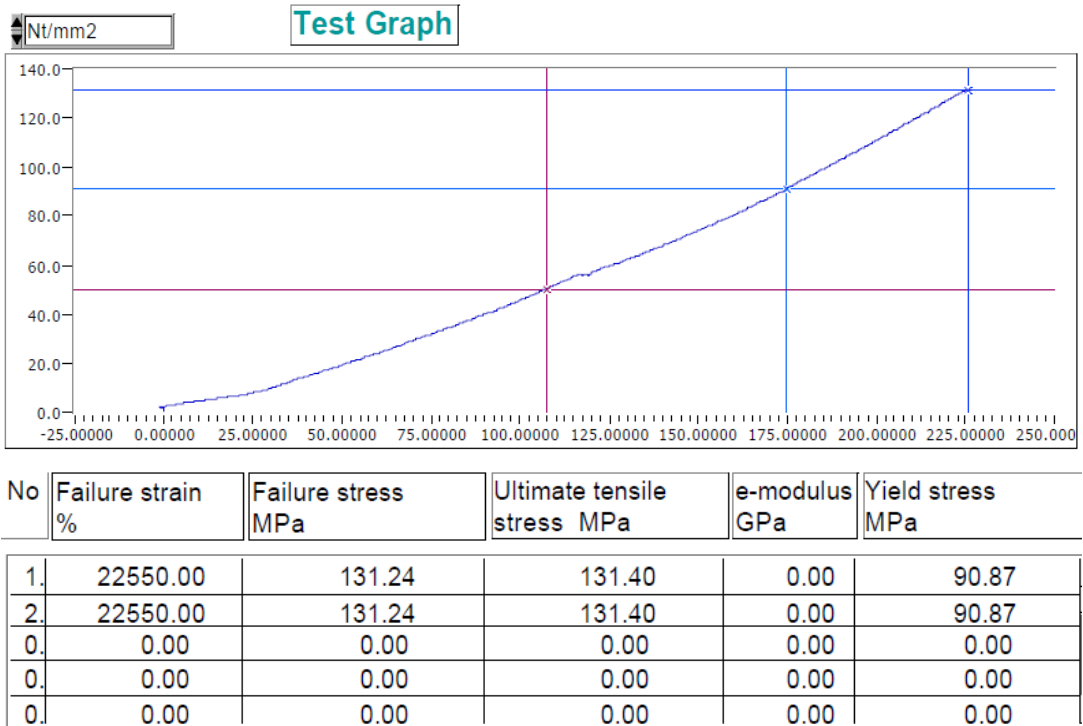


Figure 89. Tensile test result of sand casting with Al5TiB additive specimen.

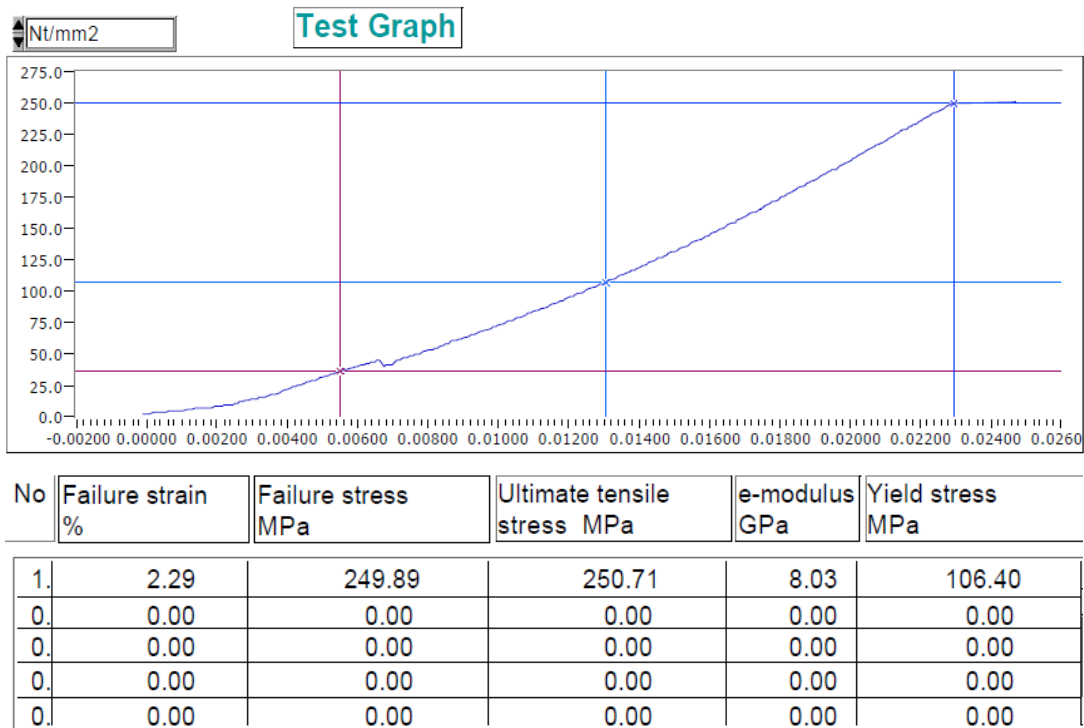
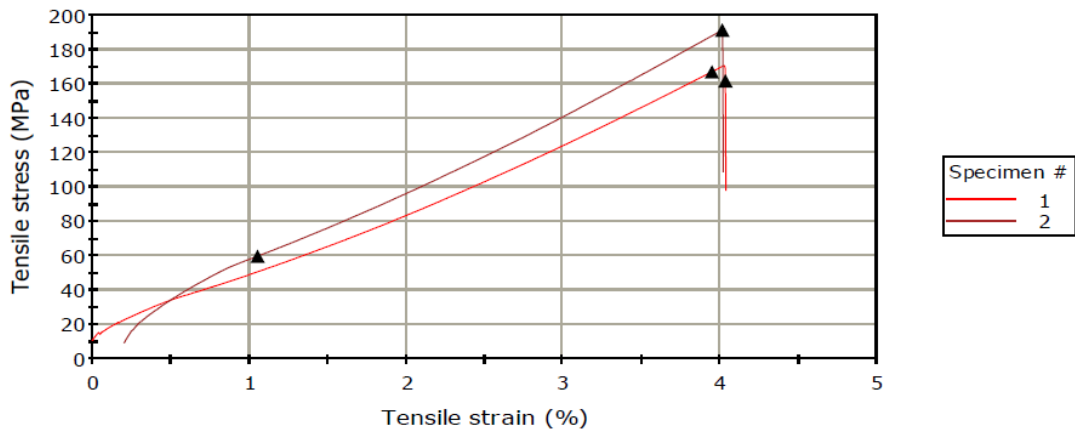


Figure 90. Tensile test result of vacuum assisted gravity die casting experiment specimen.

Specimen 1 to 2



	Tensile stress at Break (Standard) (MPa)	Tensile strain at Break (Standard) (%)	Modulus (Automatic Young's) (MPa)
1	168.59008	4.03101	4621.48630
2	191.13559	3.80969	7191.39197

	Load at Tensile Strength (N)	Tensile stress at Tensile Strength (MPa)	Tensile stress at Yield (Offset 0.2 %) (MPa)
1	23191.76793	166.99143	161.68986
2	26544.91067	191.13559	59.97738

Figure 91. Tensile test results of gravity die casting experiment specimen.

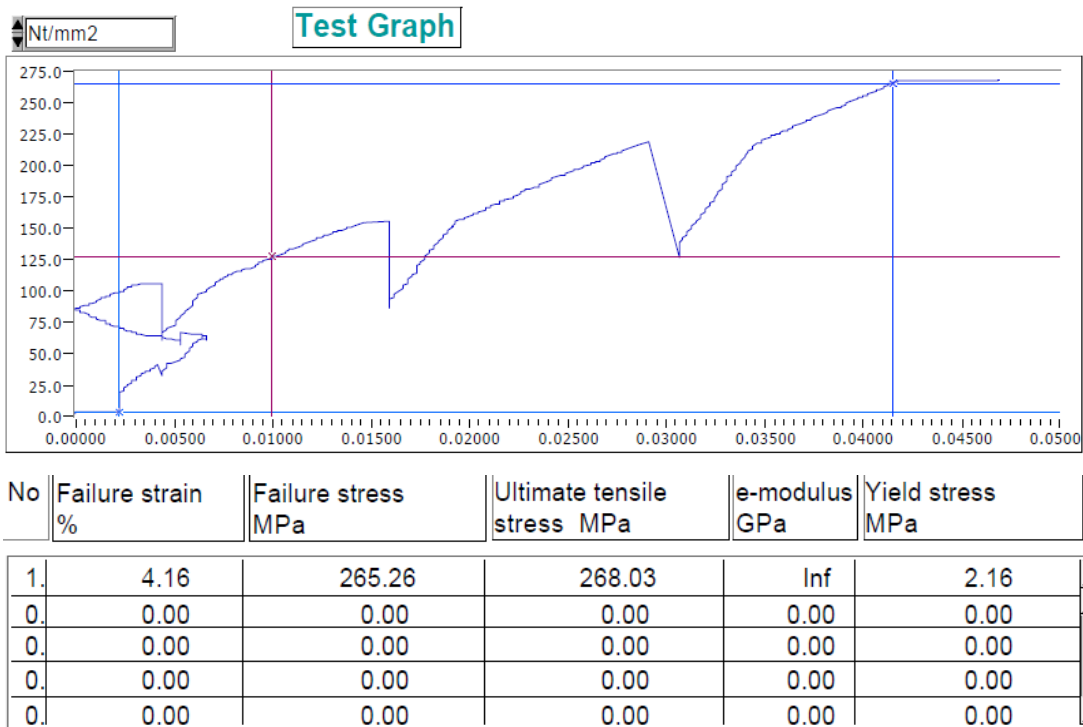


Figure 92. Tensile test results of semi-solid injection molding experiment 1st of extr. 7075 specimen.

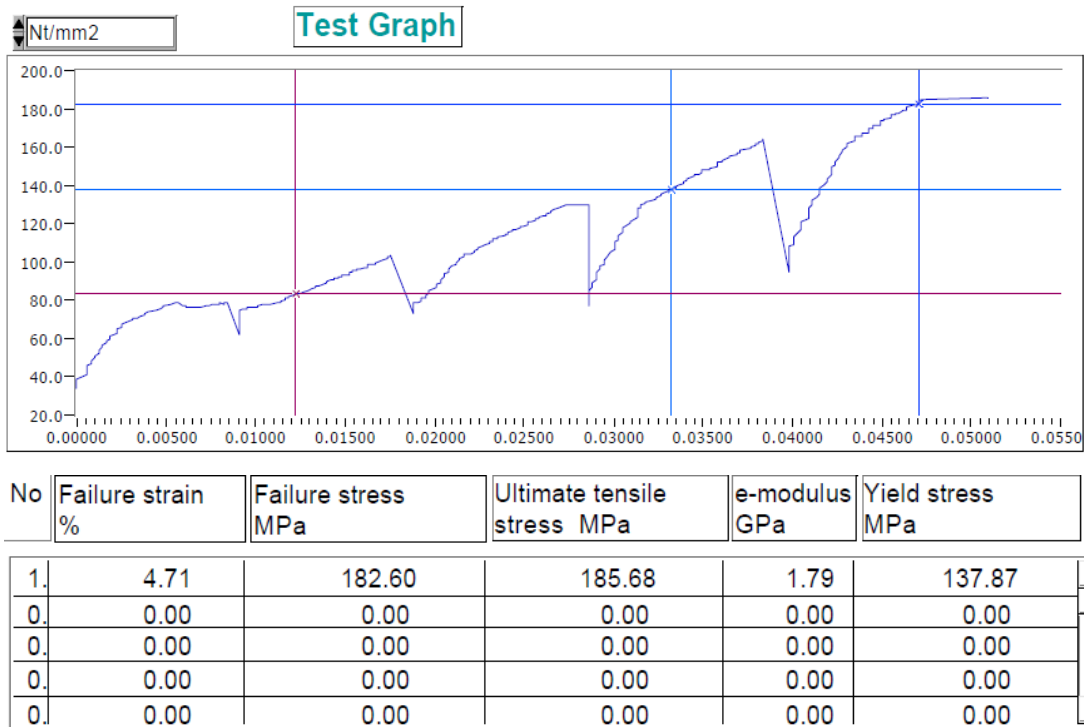


Figure 9310. Tensile test results of semi-solid injection molding experiment 2nd of extr. 7075 specimen.

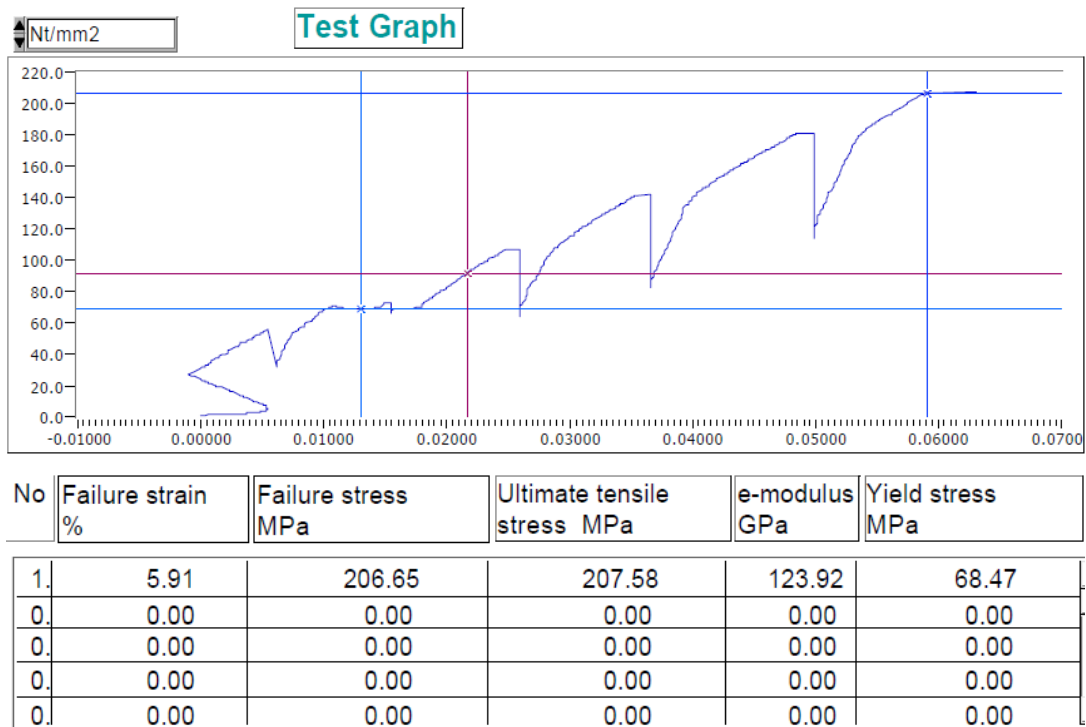


Figure 94. Tensile test results of semi-solid injection molding experiment 6th of mod. 7075 specimen.

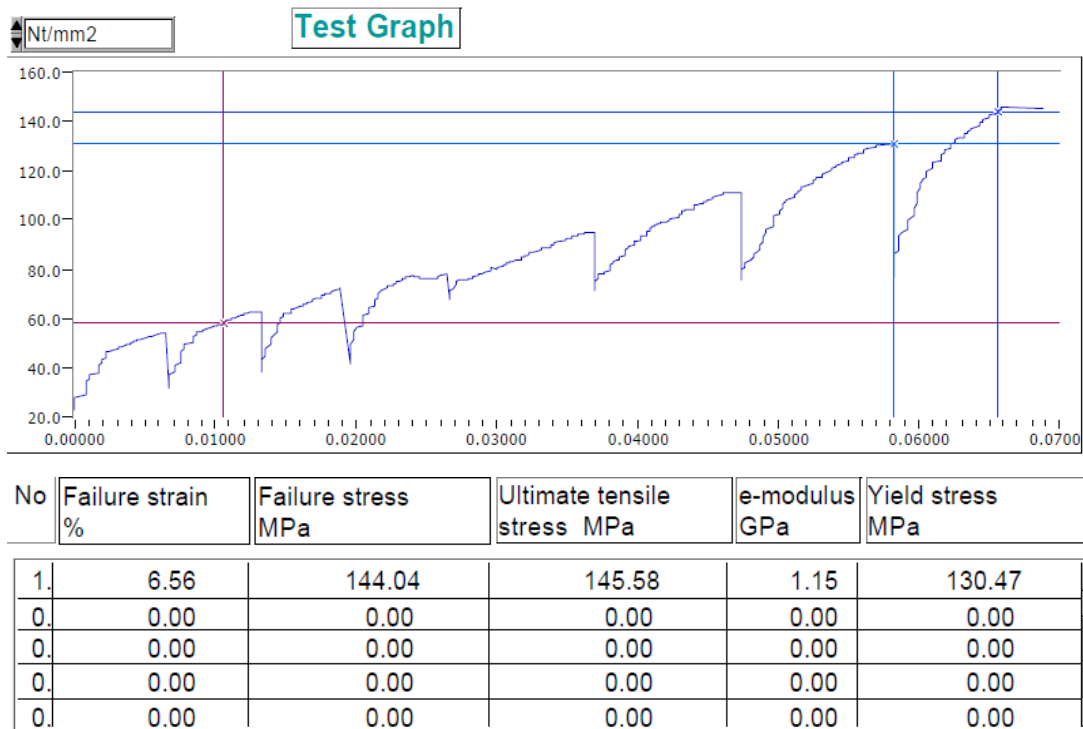


Figure 9512. Tensile test results of semi-solid injection molding experiment 1st of mod. 7075 specimen.

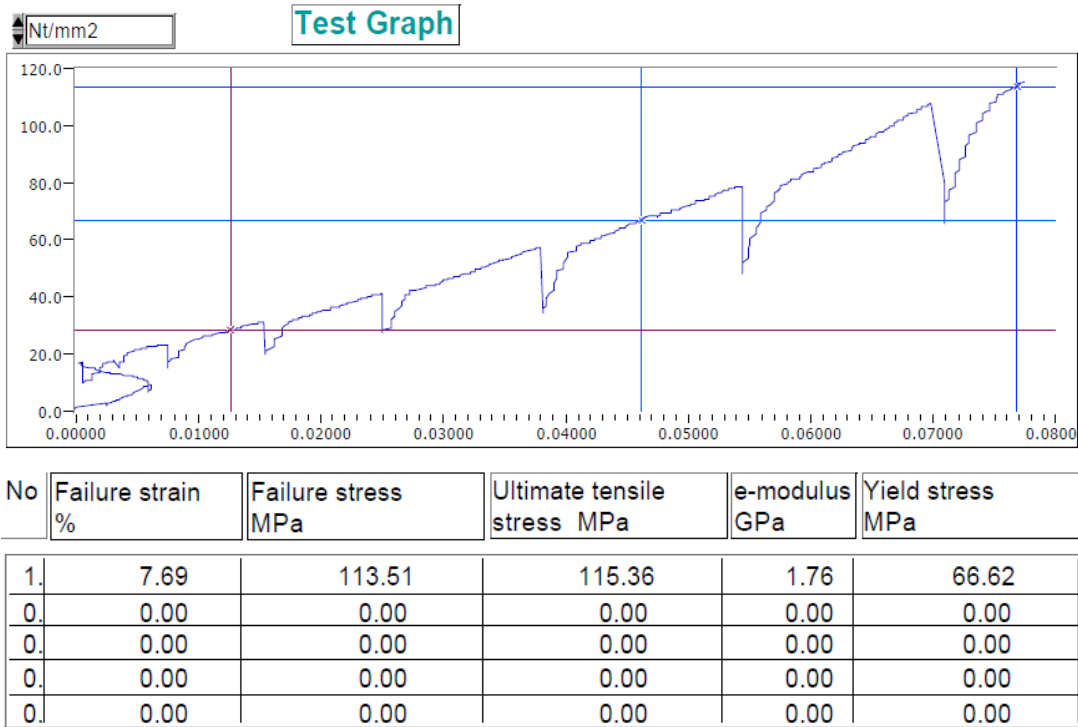


Figure 96. Tensile test results of semi-solid injection molding experiment 2nd of mod. 7075 specimen.

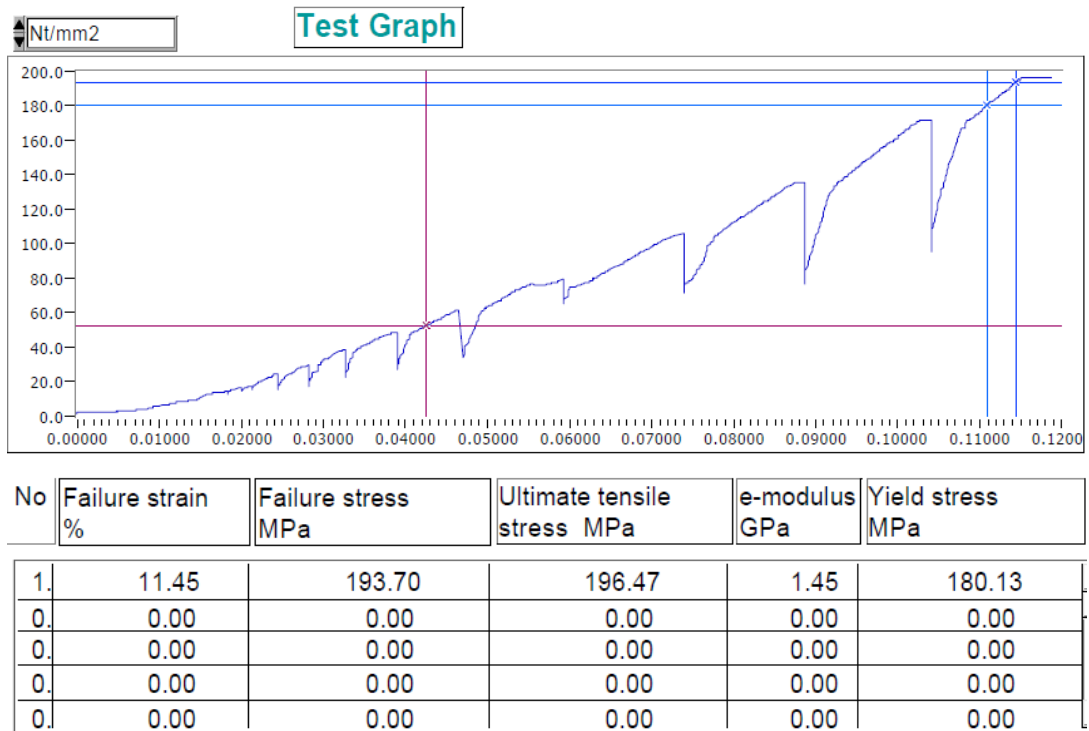


Figure 97. Tensile test results of semi-solid injection molding experiment 3rd of mod. 7075 specimen.

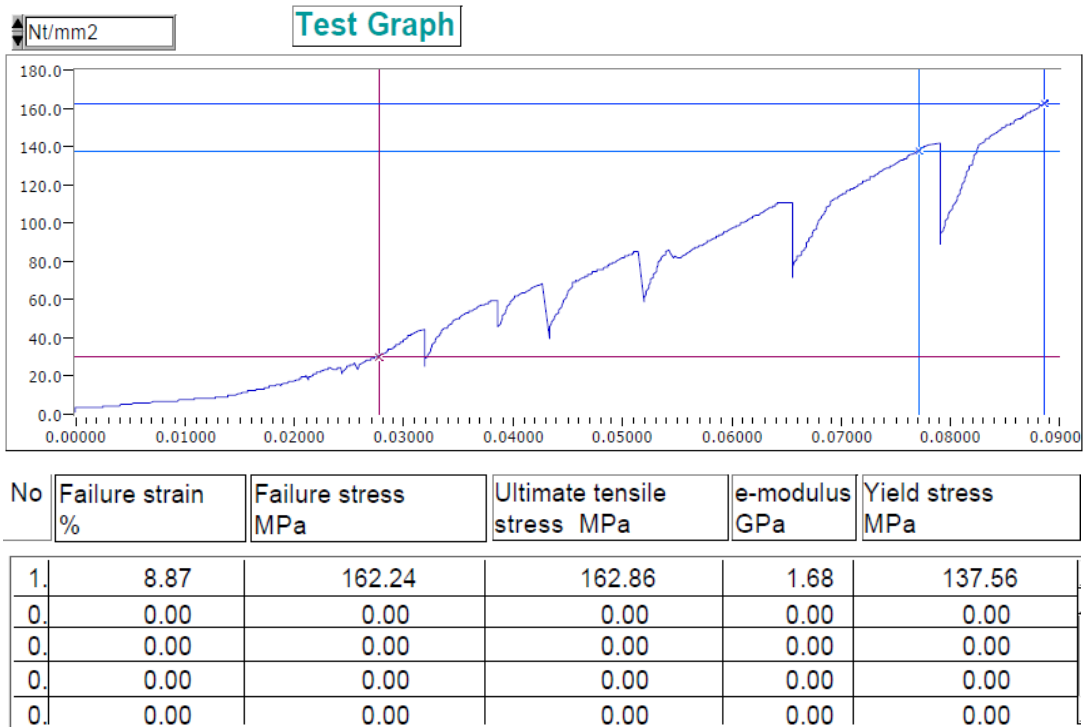


Figure 9815. Tensile test results of semi-solid injection molding experiment 4th of mod. 7075 specimen.

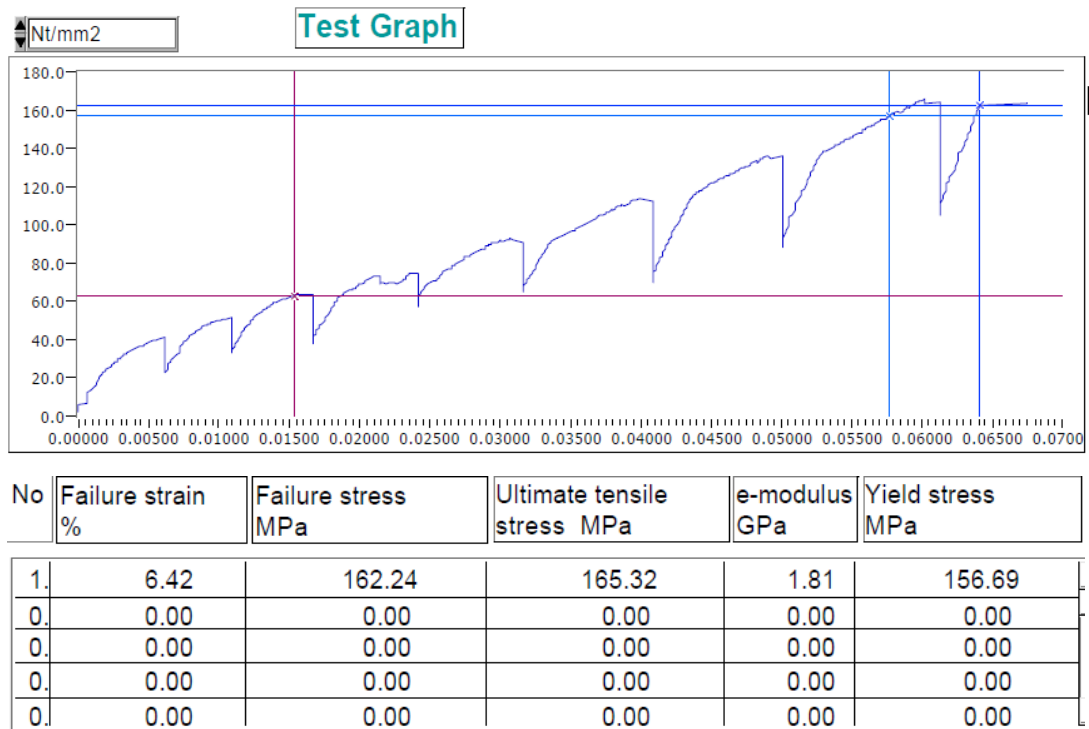
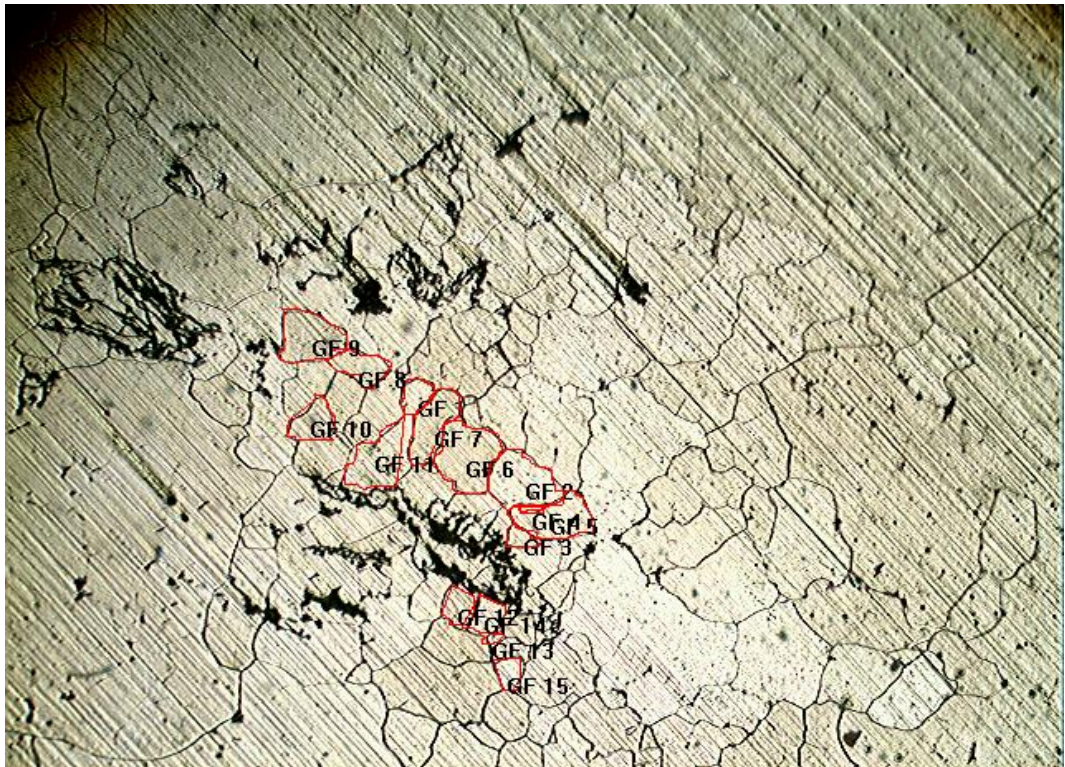


Figure 99. Tensile test results of semi-solid injection molding experiment 5th of mod. 7075 specimen.

APPENDIX B

GRAIN SIZE ANALYSIS



Field	Avrg. Intercept No	Avrg. Dia.(mm)	Avrg Grain Area(mm)	Avrg Grain No
GF 1	1034.598214Micron	30.950000Micron	6.5MicronSqr	1220.000000Micron
GF 2	3873.883929Micron	52.100000Micron	5.0MicronSqr	3440.000000Micron
GF 3	639.508929Micron	21.900000Micron	7.5MicronSqr	608.500000Micron
GF 4	190.848214Micron	13.000000Micron	9.0MicronSqr	215.000000Micron
GF 5	3073.660714Micron	52.100000Micron	5.0MicronSqr	3440.000000Micron
GF 6	4643.973214Micron	61.950000Micron	4.5MicronSqr	4865.000000Micron
GF 7	2986.607143Micron	52.100000Micron	5.0MicronSqr	3440.000000Micron

Figure 100. Grain size analysis of squeeze casting sample.

GF 8	1811.383929Micron	36.800000Micron	6.0MicronSqr	1725.000000Micron
GF 9	3405.133929Micron	52.100000Micron	5.0MicronSqr	3440.000000Micron
GF 10	1811.383929Micron	36.800000Micron	6.0MicronSqr	1725.000000Micron
GF 11	3287.946429Micron	52.100000Micron	5.0MicronSqr	3440.000000Micron
GF 12	1118.303571Micron	30.950000Micron	6.5MicronSqr	1220.000000Micron
GF 13	190.848214Micron	13.000000Micron	9.0MicronSqr	215.000000Micron
GF 14	1359.375000Micron	30.950000Micron	6.5MicronSqr	1220.000000Micron
GF 15	833.705357Micron	26.850000Micron	7.0MicronSqr	861.500000Micron

Figure B.1. (Continued)



Field	Avrg. Intercept No	Avrg. Dia.(mm)	Avrg Grain Area(mm)	Avrg Grain No
GF 2	2681.91964 Micron	43.800000Micron	5.5MicronSqr	2435.000000Micron
GF 3	1617.187500Micron	36.800000Micron	6.0MicronSqr	1725.000000Micron

Figure 101. Grain size analysis of vacuum assisted die casting sample.

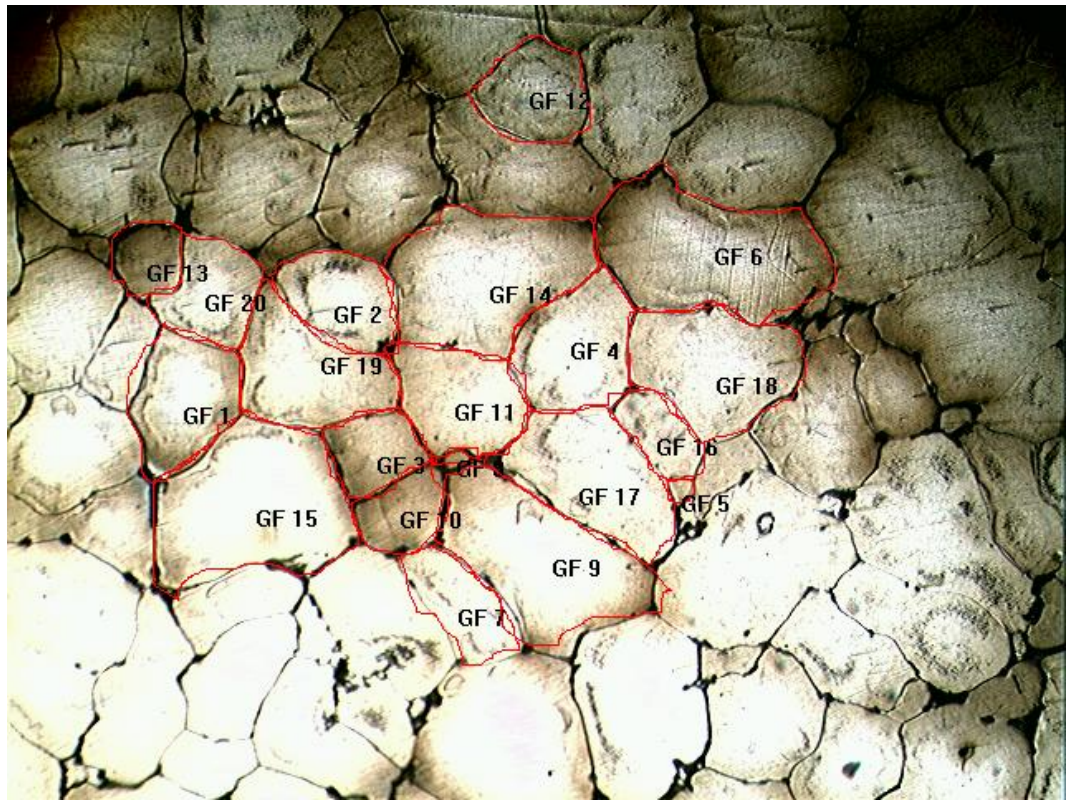
GF 4	3254.464286Micron	52.100000Micron	5.0MicronSqr	3440.000000Micron
GF 5	1419.642857Micron	30.950000Micron	6.5MicronSqr	1220.000000Micron
GF 6	1643.973214Micron	36.800000Micron	6.0MicronSqr	1725.000000Micron
GF 7	2189.732143Micron	43.800000Micron	5.5MicronSqr	2435.000000Micron
GF 8	3016.741071Micron	52.100000Micron	5.0MicronSqr	3440.000000Micron
GF 9	2434.151786Micron	43.800000Micron	5.5MicronSqr	2435.000000Micron
GF 10	4175.223214Micron	61.950000Micron	4.5MicronSqr	4865.000000Micron
GF 11	683.035714Micron	21.900000Micron	7.5MicronSqr	608.500000Micron
GF 12	231.026786Micron	13.000000Micron	9.0MicronSqr	215.000000Micron
GF 13	492.187500Micron	18.400000Micron	8.0MicronSqr	430.000000Micron
GF 14	1935.267857Micron	36.800000Micron	6.0MicronSqr	1725.000000Micron
GF 15	1727.678571Micron	36.800000Micron	6.0MicronSqr	1725.000000Micron
GF 16	2333.705357Micron	43.800000Micron	5.5MicronSqr	2435.000000Micron

Figure B.2. (Continued).



Field	Avrg. Intercept No	Avrg. Dia.(mm)	Avrg Grain Area(mm)	Avrg Grain No
GF 1	4834.821429Micron	61.950000Micron	4.5MicronSqr	4865.000000Micron
GF 2	6518.973214Micron	73.650000Micron	4.0MicronSqr	6880.000000Micron
GF 3	662.946429Micron	21.900000Micron	7.5MicronSqr	608.500000Micron
GF 4	2186.383929Micron	43.800000Micron	5.5MicronSqr	2435.000000Micron
GF 5	1185.267857Micron	30.950000Micron	6.5MicronSqr	1220.000000Micron
GF 6	2973.214286Micron	52.100000Micron	5.0MicronSqr	3440.000000Micron
GF 7	438.616071Micron	18.400000Micron	8.0MicronSqr	430.000000Micron
GF 8	2250.000000Micron	43.800000Micron	5.5MicronSqr	2435.000000Micron
GF 9	1309.151786Micron	30.950000Micron	6.5MicronSqr	1220.000000Micron
GF 10	984.375000Micron	26.850000Micron	7.0MicronSqr	861.500000Micron
GF 11	2768.973214Micron	43.800000Micron	5.5MicronSqr	2435.000000Micron
GF 12	1181.919643Micron	30.950000Micron	6.5MicronSqr	1220.000000Micron
GF 13	518.973214Micron	21.900000Micron	7.5MicronSqr	608.500000Micron
GF 14	475.446429Micron	18.400000Micron	8.0MicronSqr	430.000000Micron
GF 15	2651.785714Micron	43.800000Micron	5.5MicronSqr	2435.000000Micron
GF 16	924.107143Micron	26.850000Micron	7.0MicronSqr	861.500000Micron
GF 17	2404.017857Micron	43.800000Micron	5.5MicronSqr	2435.000000Micron
GF 18	6087.053571Micron	73.650000Micron	4.0MicronSqr	6880.000000Micron
GF 19	4486.607143Micron	61.950000Micron	4.5MicronSqr	4865.000000Micron
GF 20	4978.794643Micron	61.950000Micron	4.5MicronSqr	4865.000000Micron

Figure 102. Grain size analysis of gravity die casting sample.

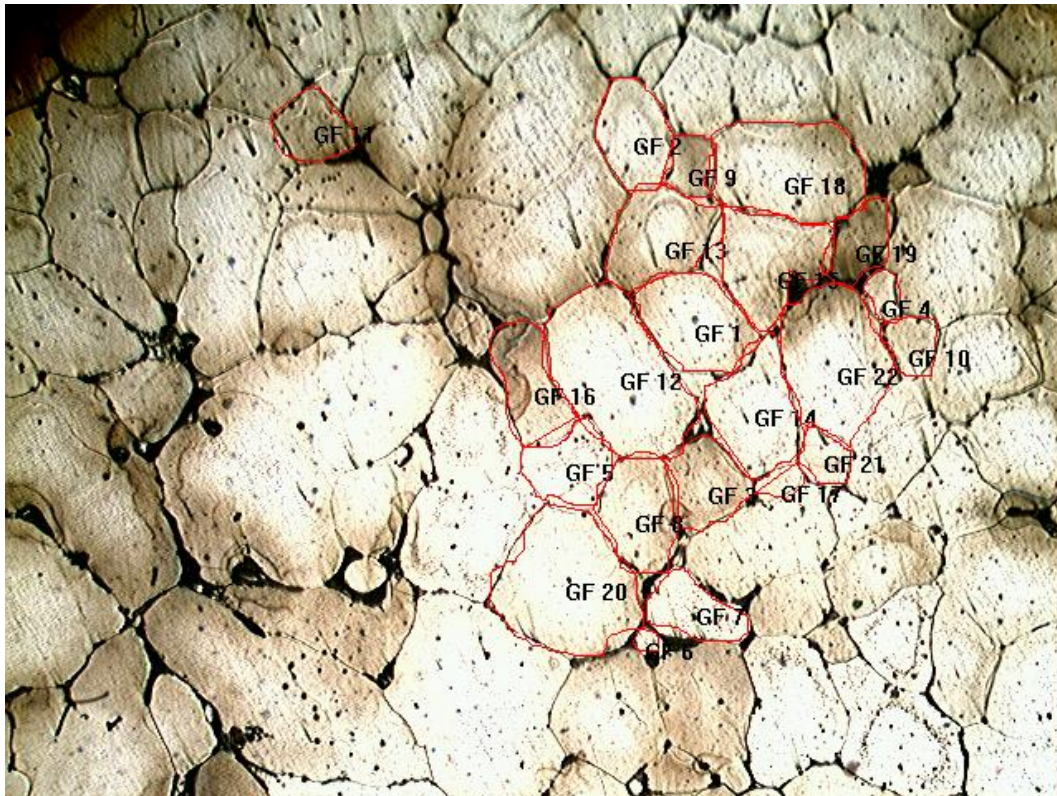


Field	Avrg. Intercept No	Avrg. Dia.(mm)	Avrg Grain Area(mm)	Avrg Grain No
GF 1	14842.633929Micron	104.100000Micron	3.0MicronSqr	13750.000000Micron
GF 2	11608.258929Micron	104.100000Micron	3.0MicronSqr	13750.000000Micron
GF 3	8055.803571Micron	73.650000Micron	4.0MicronSqr	6880.000000Micron
GF 4	15914.062500Micron	104.100000Micron	3.0MicronSqr	13750.000000Micron
GF 5	683.035714Micron	21.900000Micron	7.5MicronSqr	608.500000Micron
GF 6	30030.133929Micron	147.250000Micron	2.0MicronSqr	27550.000000Micron
GF 7	8902.901786Micron	87.550000Micron	3.5MicronSqr	9730.000000Micron
GF 8	659.598214Micron	21.900000Micron	7.5MicronSqr	608.500000Micron
GF 9	27110.491071Micron	147.250000Micron	2.0MicronSqr	27550.000000Micron
GF 10	7088.169643Micron	73.650000Micron	4.0MicronSqr	6880.000000Micron
GF 11	14621.651786Micron	104.100000Micron	3.0MicronSqr	13750.000000Micron
GF 12	11162.946429Micron	87.550000Micron	3.5MicronSqr	9730.000000Micron
GF 13	5601.562500Micron	61.950000Micron	4.5MicronSqr	4865.000000Micron
GF 14	27689.732143Micron	147.250000Micron	2.0MicronSqr	27550.000000Micron
GF 15	30991.071429Micron	147.250000Micron	2.0MicronSqr	27550.000000Micron

Figure 103. Grain size analysis of sand casting sample.

GF 16	6020.089286Micron	73.650000Micron	4.0MicronSqr	6880.000000Micron
GF 17	20045.758929Micron	123.800000Micron	2.5MicronSqr	19450.000000Micron
GF 18	20708.705357Micron	123.800000Micron	2.5MicronSqr	19450.000000Micron
GF 19	17531.250000Micron	123.800000Micron	2.5MicronSqr	19450.000000Micron
GF 20	10295.758929Micron	87.550000Micron	3.5MicronSqr	9730.000000Micron

Figure B.4. (Continued).

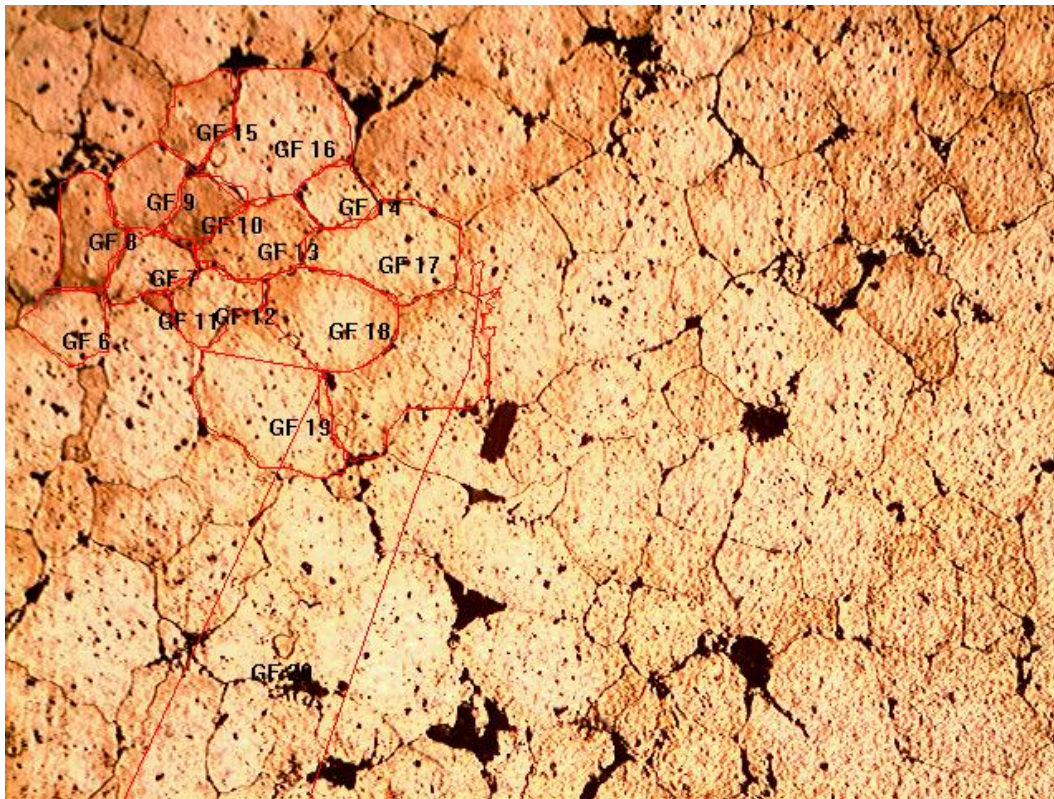


Field	Avrg. Intercept No	Avrg. Dia.(mm)	Avrg Grain Area(mm)	Avrg Grain No
GF 1	10463.169643Micron	87.550000Micron	3.5MicronSqr	9730.000000Micron
GF 2	7955.357143Micron	73.650000Micron	4.0MicronSqr	6880.000000Micron
GF 3	6883.928571Micron	73.650000Micron	4.0MicronSqr	6880.000000Micron
GF 4	1664.062500Micron	36.800000Micron	6.0MicronSqr	1725.000000Micron
GF 5	6331.473214Micron	73.650000Micron	4.0MicronSqr	6880.000000Micron
GF 6	518.973214Micron	21.900000Micron	7.5MicronSqr	608.500000Micron

Figure 104. Grain size analysis of sand casting with Al5TiB additive sample.

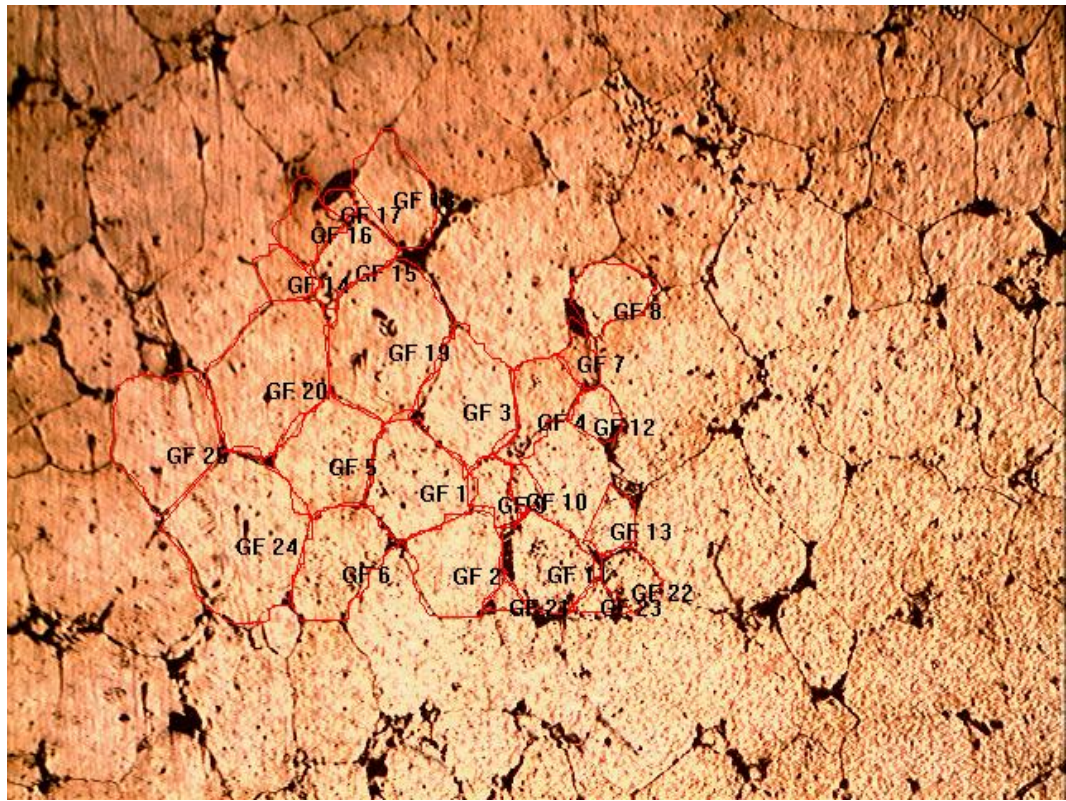
GF 7	5357.142857Micron	61.950000Micron	4.5MicronSqr	4865.000000Micron
GF 8	9164.062500Micron	87.550000Micron	3.5MicronSqr	9730.000000Micron
GF 9	3324.776786Micron	52.100000Micron	5.0MicronSqr	3440.000000Micron
GF 10	3254.464286Micron	52.100000Micron	5.0MicronSqr	3440.000000Micron
GF 11	5116.071429Micron	61.950000Micron	4.5MicronSqr	4865.000000Micron
GF 12	21529.017857Micron	123.800000Micron	2.5MicronSqr	19450.000000Micron
GF 13	10376.116071Micron	87.550000Micron	3.5MicronSqr	9730.000000Micron
GF 14	10767.857143Micron	87.550000Micron	3.5MicronSqr	9730.000000Micron
GF 15	11169.642857Micron	87.550000Micron	3.5MicronSqr	9730.000000Micron
GF 16	7808.035714Micron	73.650000Micron	4.0MicronSqr	6880.000000Micron
GF 17	1024.553571Micron	30.950000Micron	6.5MicronSqr	1220.000000Micron
GF 18	16677.455357Micron	123.800000Micron	2.5MicronSqr	19450.000000Micron
GF 19	4895.089286Micron	61.950000Micron	4.5MicronSqr	4865.000000Micron
GF 20	19312.500000Micron	123.800000Micron	2.5MicronSqr	19450.000000Micron
GF 21	2514.508929Micron	43.800000Micron	5.5MicronSqr	2435.000000Micron
GF 22	15803.571429Micron	104.100000Micron	3.0MicronSqr	13750.000000Micron

Figure B.5. (Continued).



Field	Avrg, Intercept No	Avrg, Dia,(mm)	Avrg Grain Area(mm)	Avrg Grain No
GF 1	5574.78	61.95	4.50	4865.00
GF 2	8691.96	87.55	3.50	9730.00
GF 3	8162.95	87.55	3.50	9730.00
GF 6	5812.50	73.65	4.00	6880.00
GF 7	5809.15	73.65	4.00	6880.00
GF 8	7386.16	73.65	4.00	6880.00
GF 9	6522.32	73.65	4.00	6880.00
GF 10	4898.44	61.95	4.50	4865.00
GF 11	542.41	21.90	7.50	608.50
GF 12	5822.54	73.65	4.00	6880.00
GF 13	8179.69	87.55	3.50	9730.00
GF 14	4546.88	61.95	4.50	4865.00
GF 15	5949.78	73.65	4.00	6880.00
GF 16	17531.25	123.80	2.50	19450.00

Figure 105. Grain size analysis of mechanical stirred SIMA sample.



Field	Avrg, Intercept No	Avrg, Dia,(mm)	Avrg Grain Area(mm)	Avrg Grain No
GF 1	11092.6	87.55	3.5	9730
GF 2	9277.9	87.55	3.5	9730
GF 3	11939.7	104.1	3	13750
GF 4	6231	73.65	4	6880
GF 5	10195.3	87.55	3.5	9730
GF 6	9890.6	87.55	3.5	9730
GF 7	2089.2	43.8	5.5	2435
GF 8	5005.5	61.95	4.5	4865
GF 9	3154	52.1	5	3440
GF 10	1366	30.95	6.5	1220
GF 11	8350.4	87.55	3.5	9730
GF 12	2377.2	43.8	5.5	2435
GF 13	2725.4	43.8	5.5	2435
GF 14	2789	43.8	5.5	2435
GF 15	5393.9	61.95	4.5	4865

Figure 106. Grain size analysis of ultrasonic stirred SIMA sample.

GF 16	4272.3	61.95	4.5	4865
GF 17	847	26.85	7	861.5
GF 18	7349.3	73.65	4	6880
GF 19	17641.7	123.8	2.5	19450
GF 20	16808	123.8	2.5	19450
GF 21	887.2	26.85	7	861.5
GF 22	3234.3	52.1	5	3440
GF 23	1376.1	30.95	6.5	1220
GF 24	20842.6	123.8	2.5	19450
GF 25	13841.5	104.1	3	13750

Figure B.7. (Continued).

APPENDIX C

MATHLAB ALGORITHM

- “New variable” from workspace
- Insert cooling curve data into this variable file (T vs. t), let’s name it “A”
- Start → Toolboxes → Curve Fitting → Curve Fitting Tool
- Data;
 - Data Sets;
 - Y Data → Choose “A”
 - X Data → Choose none
 - Create Data Set
 - Smooth;
 - Original Data Set: “A”
 - Method: Moving Average
 - Span: Odd number greater than 0 and less than or equal to the length of X. (It can be preferred as 5 or 11.)
 - Create smoothed data set
 - Close
- Fitting;
 - New Fit → Choose “Data Set” as A(smooth)
 - Type of fit : Smoothing Spline
 - Apply
 - Close
- Analysis;
 - Fit to analyze : Fit 1 (A)

- Analyze at $X_i = 1:1:?$
 - ✓ Evaluate fix at X_i
 - ✓ Prediction and confidence bounds : None
 - ✓ 1st derivative at X_i
 - Apply
 - Save to workspace
 - Close
- In workspace, double click your “analysisresults1”, open “dydx” file and copy data
- Click new variable and paste data here. Rename the file as “dTdt”
- Start → Toolboxes → Curve Fitting → Curve Fitting Tool
- Data;
- Data Sets;
 - Y Data → Choose “dTdt”
 - X Data → Choose “none”
 - Create Data Set
 - Smooth;
 - Original Data Set: “dTdt”
 - Method: Moving Average
 - Span: Odd number greater than 0 and less than or equal to the length of X. (It can be preferred as 5 or 11.)
 - Create smoothed data set
 - Close
- Exclude;
- Exclusion Rule Name: Z
 - Select Data Set: dTdt(smooth)
 - Exclude graphically: Exclude data between liquidus and solidus points by selecting
- or

- Exclude sections: Exclude data between liquidus and solidus points by entering time data on X.
- Create exclusion rule
- Close
- Fitting;
 - New Fit
 - Data Set: dTdt(smooth)
 - Exclusion Rule: Z
 - Type of fit : Polynomial → Cubic Polynomial
 - Apply
 - Close
- Analysis;
 - Fit to analyze : Fit 1 (A)
 - Analyze at $X_i = 1:1:?$
 - ✓ Evaluate fix at X_i
 - ✓ Prediction and confidence bounds : None
 - Apply
 - Save to workspace
 - Close
- In workspace, double click your “analysisresults2”, open “yfit” file and copy data
- Click new variable and paste data here. Rename the file as “baseline”
- Start → Toolboxes → Curve Fitting → Curve Fitting Tool
- Data;
 - Data Sets;
 - Y Data → Choose “baseline”
 - X Data → Choose “none”
 - Create Data Set
 - Smooth;
 - Original Data Set: “baseline”

- Method: Moving Average
- Span: Odd number greater than 0 and less than or equal to the length of X. (It can be preferred as 5 or 11.)
- Create smoothed data set
- Close

➤ Fitting;

- New Fit
- Data Set: baseline(smooth)
- Type of fit : Smoothing Spline
- Apply
- Close

➤ Analysis;

- Fit to analyze : Fit 1 (baseline)
- Analyze at $X_i = 1:1:?$
 - ✓ Evaluate fix at X_i
 - ✓ Prediction and confidence bounds : None
 - ✓ Integrate to X_i
 - ✓ Start from min (X_i)
- Apply
- Save to workspace
- Close

➤ Start → Toolboxes → Curve Fitting → Curve Fitting Tool

➤ Data;

- Data Sets;
 - Y Data → Choose “dTdt”
 - X Data → Choose “none”
 - Create Data Set
- Smooth;
 - Original Data Set: “dTdt”

- Method: Moving Average
 - Span: Odd number greater than 0 and less than or equal to the length of X. (It can be preferred as 5 or 11.)
 - Create smoothed data set
 - Close
- Fitting;
 - New Fit
 - Data Set: dTdt(smooth)
 - Type of fit : Smoothing Spline
 - Apply
 - Close
- Analysis;
 - Fit to analyze : Fit 1 (dTdt)
 - Analyze at $X_i = 1:1:?$
 - ✓ Evaluate fix at X_i
 - ✓ Prediction and confidence bounds : None
 - ✓ Integrate to X_i
 - ✓ Start from min (X_i)
 - Apply
 - Save to workspace
 - Close
- In workspace, double click your “analysisresults3”, open “integral” file and copy data to an excel sheet. This is your baseline integral data.
- In workspace, double click your “analysisresults4”, open “integral” file and copy data to an excel sheet. This is your dT/dt integral data.
- Subtract baseline integral data from dT/dt integral data. Take data between solidus and liquidus. Then add each data to the next one at the end row you have to have sum of all data. In the last stage, divide each data with the sum of all data. Therefore, solid fraction vs. time graph could be obtained. The

time can be replaced with the corresponding temperature value for having a solid fraction vs. temperature graph.